DESIGN METHODS FOR REMOTELY POWERED UNMANNED AERIAL VEHICLES

A Thesis

presented to

the Faculty of California Polytechnic State University,

San Luis Obispo

In Partial Fulfillment

of the Requirements for the Degree

Master of Science in Aerospace Engineering

by

William Beaman Howe

March 2015

© 2015

William Beaman Howe

ALL RIGHTS RESERVED

COMMITTEE MEMBERSHIP

TITLE:	Design Methods for Remotely Powered Unmanned Aerial Vehicles
AUTHOR:	William Beaman Howe
DATE SUBMITTED:	March 2015
COMMITTEE CHAIR:	Eric Mehiel, Ph.D. Associate Professor of Aerospace Engineering
COMMITTEE MEMBER:	John S. Dunning, Ph.D. Associate Researcher of Electrical Engineering
COMMITTEE MEMBER:	Kira Abercromby, Ph.D. Assistant Professor of Aerospace Engineering
COMMITTEE MEMBER:	Bruce R. Wright Lecturer of Aerospace Engineering
COMMITTEE MEMBER:	Daniel J. Wait, M.S. Lecturer of Aerospace Engineering

ABSTRACT

Design Methods for Remotely Powered Unmanned Aerial Vehicles

William Beaman Howe

A method for sizing remotely powered unmanned aerial vehicles is presented to augment the conventional design process. This method allows for unconventionally powered aircraft to become options in trade studies during the initial design phase. A design matrix is created that shows where, and if, a remotely powered vehicle fits within the design space. For given range and power requirements, the design matrix uses historical data to determine whether an internal combustion or electrical system would be most appropriate. Trends in the historical data show that the break in the design space between the two systems is around 30 miles and 1 kW. Electrical systems are broken into subcategories of onboard energy sources and remote power sources. For this work, only batteries were considered as an onboard energy source, but both lasers and microwaves were considered for remote power transmission methods. The conventional sizing method is adjusted to so that it is based on energy consumption, instead of fuel consumption. Using the manner in which microwaves and laser propagate through the atmosphere, the weight fraction of a receiving apparatus is estimated. This is then used with the sizing method to determine the gross takeoff weight of the vehicle. This new sizing method is used to compare battery systems, microwave systems, and laser systems.

TABLE OF CONTENTS

Page

LIST OF TABLES viii

LIST OF FIGURES ix

CHAPTER

1. Introduction 1

1.1 Purpose 1

1.2 Background 1

1.2.1 Wireless Energy Transfer 3

1.2.2 Unmanned Aerial Vehicles 4

1.2.3 Remote Powered Aviation 5

1.3 Economic Demand 6

2. Design Methods: Developing a Design Matrix 10

2.1 Aircraft Sizing 11

2.2 Mission Profile 13

2.3 Modifying Breguet Range Equation 16

3. Combustion versus Electric 18

3.1 Energy Densities 20

3.2 System Efficiencies and Weight 22

4. Wireless Energy Transfer Methods 30

4.1 Microwaves 30

4.1.1 Transmitting Microwaves 30

4.1.2 Microwave Propagation 32
4.1.3 Receiving Microwaves 36
4.2 Lasers 41
4.2.1 Transmitting Laser 41
4.2.2 Laser Propagation 43
4.2.3 Receiving Laser Power 55
5. Remote Power Vehicle Sizing 58
5.1 Sizing Vehicle with Microwaves 60
5.1.1 Patch Antenna System Weight 60
5.1.2 Microwave Receiver Weight Fraction 63
5.2 Sizing Vehicle with Lasers 66
5.2.1 Laser Receiver: Flat Panel PV Array 66
5.2.2 Laser Receiver: PV Array on Turret 68
5.2.3 Laser Receiver Weight Fraction 70
5.2.4 Comparison of Flat Panel and Turret 74
5.3 Microwave versus Laser Systems 76
5.3.1 Efficiency Comparison 76
5.3.2 Sizing Comparison 77
5.3.3 Surveillance Area 81
5.4 Hybrid Systems 82
5.4.1 Augmented versus Non-Augmented systems 82
5.4.2 Comparison of Hybrid, Battery, and Remote Systems 83
6. Conclusion 86

6.1 Design Methods in Use 86

6.1.1 Concept of Operations 86

6.1.2 Constraints 89

6.1.3 Example Sizing 93

6.2 Process Overview 97

6.3 Conclusion 98

REFERENCES 101

APPENDICES 104

A: UAV Data 104

B: Plots of Electric and Combustion Systems 112

LIST OF TABLES

Table Page

Table 1. Comparison of electric and combustion motors. 23

Table 2. Currently available laser technologies.[30] 41

Table 3. Validation of the sizing code used for battery-powered vehicle. 81

Table 4. Requirements of Raven's mission. 88

Table 5. Determining factors for a combustion vs. electric system 89

LIST OF FIGURES

Figure Page

Figure 1. Aircraft force diagram. 2

Figure 2. Image of SHARP aircraft. [8]..... 6

Figure 3. US spending on UAVs since 1998. [11] 7

Figure 4. Current UAVs in use, categorized by range. 8

Figure 5. Breakdown of unmanned aerial systems. 10

Figure 6. Example of a constraint diagram. [16] 11

Figure 7. Historical regression correlating the empty weight fraction to the takeoff weight. Where Wo is equivalent to $WTOGW$ [17]..... 13

Figure 8. Possible mission for remotely powered vehicles (a) in contact for constant power or (b) in contact only to charge battery. 14

Figure 9. Mission profiles for (a) only one power method and (b) a combination of powering methods. 15

Figure 10. Historical data comparing the weight of the vehicle to the range. 18

Figure 11. Historical data comparing weight of the vehicle to the max power available. 19

Figure 12. Energy densities of different types of batteries. [19] 20

Figure 13. Comparison of efficiencies of different types of motors with respect to horse power.[21] 21

Figure 14. Motor and engine historical regression based on peak power output. 24

Figure 15. Historical data to determine a correlation between the weight of the engine and the weight of the muffler or ignition. 25

Figure 16. Historical regression depicting the correlation between the motor power and the current draw. 26

Figure 17. Regression relating the weight of the speed controller to the continuous current draw. 27

Figure 18. Historical regression relating the peak power output of a combustion engine to its volume. 28

Figure 19. Historical Regression relating the weight of a motor and speed controller to their respective volumes. 29

Figure 20. a) Attenuation due to molecular oxygen for distances of 5 km and inf. b) Attenuation due to water vapor for various water vapor densities and heights. 33

Figure 21. Total atmospheric attenuation. 34

Figure 22. Controus of power (W) received with varying frequency and distance. Part (a) is for horizontal path and part (b) is for vertical path. 35

Figure 23. Contours of power received (W) with a constant receiver diameter of 0.1m: (a) 5 m diameter transmitter, P_t=20 kW, and f =2.54 GHz (b) 10 m diameter transmitter (c) P_t=40 kW (d) f=28 GHz. 36

Figure 24. Gain radiation pattern for a parabolic antenna. [27] 37

Figure 25. Optimization of a Yagi antenna gain.[28] 38

Figure 26. Yagi antenna radiation patterns.[29] 39

Figure 27. Transforming wing structure into a Yagi antenna. 39

Figure 28. Gain patterns for a patch antenna. [29] 40

Figure 29. Various models of the index of refraction.[35] 45

Figure 30. Experimental and calculated results for $r0$ values for a laser with λ = 847 nm and d_l = 0.4 m. The red dots are the superimposed calculated values.[36] 46

Figure 31. Beam spreading due to turbulence, in μrad, with B = 15, d_l =1 m, and λ = 1,060 nm. 47

Figure 32. Contours of a modeled laser profile (a) without blooming and (b) with blooming. [38] 48

Figure 33. Beam spreading due to blooming, in μrad. 50

Figure 34. Extinction coefficient as a function of altitude, λ = 850 nm and 1,060 nm. [30] 51

Figure 35. Intensity at the receiver in kW/m^2 from a 10 kW laser, with B = 15, d_l =1 m, and λ = 1,060 nm at standard clear conditions. 52

Figure 36. Maximum incident power at the vehicle in kW, assuming receiver is sized to match the spot size, with a 10 kW laser, with B = 15, d_l =1 m, and λ = 1,060 nm. 53

Figure 37. Intensity results from Mason using a 10 kW laser, with B = 15, d_l =1 m, and λ = 1,060 nm at standard clear conditions. [30] 54

Figure 38. Conversion efficiencies of several different photovoltaic materials. [30] 55

Figure 39. Photovoltaic efficiency for a Spectrolab CDO-100 solar cell. [30] 56

Figure 40. Contours of the area of the beam spot for a range of altitudes and distances in m^2. 56

Figure 41. Three scenarios for battery sizing: (a) battery provides all power or (b) battery is augmented with laser power. 58

Figure 42. Patch antenna used for weight model. 60

Figure 43. Gain patterns for patch antenna. 62

Figure 44. Historical data of how the weight of a converter is affected by the max power output. 62

Figure 45. Plots of the W_{TOGW} (a) P_t = 20 kW and f = 5 GHz (b) P_t = 20 kW and $d_{t,micro}$ = 65 ft (c) f = 5 GHz and $d_{t,micro}$ = 65 ft 65

Figure 46. Power Received using a flat panel, assuming panel sized to spot size. Using a 10 kW laser, with B = 15, d_l =1 m, η_{rec}=0.25, and λ = 1,060 nm at standard clear conditions. 67

Figure 47. 360 degree gimbaled turret. 68

Figure 48. Historical regression showing how the weight of the turret is related to the diameter. 69

Figure 49. Dimensioned side view of turret. 70

Figure 50. Contours of W_{TOGW} with respect to distance and various laser parameters (a) B = 10, η_{rec}= 0.25, d_l = 0.3 ft (b) B= 10, $P_{t,las}$ = 20 kW, d_l = 0.3 ft (c) B = 10, $P_{t,las}$ = 20 kW, η_{rec} = 0.25 (d) $P_{t,las}$ = 20 kW, η_{rec}= 0.25, d_l = 0.3 ft 73

Figure 51. Required transmitted power in order to power the UAV. 74

Figure 52. A comparison of how the turret reduces the receiver weight ratio. Solid lines represent just a panel and the dotted lines represent the turret. 75

Figure 53. Comparison of the weight fractions for the turret and a panel. 75

Figure 54. A comparison of the efficiencies of a microwave powered and laser powered system. The microwave system has three different cases: a

vehicle with two patch antenna, five patch antenna, and ten patch antenna. 76

Figure 55. (a) Shows how the estimated takeoff weight of remotely powered vehicles changes with the down range sizing distance. For the laser powered vehicle: B = 10, $P_{t,las}$ = 20 kW, η_{rec} = 0.25; and for the microwave powered vehicle: $P_{t,micro}$ = 20 kW, d_l = 20 m. (b) Shows how the estimated takeoff weight of a battery powered vehicle changes with endurance. 77

Figure 56. Sizing comparison of remote power UAVs and battery powered UAVs..... 78

Figure 57. Analysis of plot comparing remotely powered vehicles with battery powered vehicles. 79

Figure 58. Doubling the transmitted power of both remote systems, and doubling the microwave transmitter diameter. 80

Figure 59. Plot of hybrid remote-battery powered systems, with a down range requirement of 7 miles. 82

Figure 60. Comparison of remotely powered, hybrid, and battery powered system. 84

Figure 61. Contours of the growth factor while varying the downrange sizing value and the payload weight..... 85

Figure 62. The design process flow. 86

Figure 63. Range of different unmanned aerial systems over a map of Iraq: (a) short range (b) mid-range and (c) long range. [11] 87

Figure 64. Constrain diagram using Raven requirements..... 92

Figure 65. Information flow diagram of sizing code. 93

Figure 66. Cross section of the S1223 airfoil.[45] 94

Figure 67. Lift curve and drag polar of the S1223 airfoil. 94

Figure 68. Comparing battery powered system, with different laser powered systems. 95

Figure 69. Comparison of battery powered system and system using both batteries and lasers. 97

1. Introduction

1.1 Purpose

The purpose of this work is to develop techniques to design a remotely powered UAV. Most design techniques are based around a vehicle that is either gas or electric powered. Because of this, these methods do not work for an aircraft that is powered by an external source. In order to develop a design method for externally powered vehicles, various ways in which a vehicle could be remotely powered were studied.

To accomplish the goals of this study, a literature review of wireless energy transfer was performed. From this, appropriate methods of energy transfer for aircraft were determined. These were determined to either be microwaves or lasers. Models of how the energy is transferred between a ground station and the aircraft were then researched. These models included the effects of the atmosphere and efficiencies of the respective methods. Using these models, the size of the receiving components on the aircraft can be estimated. Incorporating this into conventional aircraft sizing methods allows for total weight estimations for a remotely powered vehicle.

The motivation for this work comes from an initial NASA grant to study electrically powered vehicles. Initial research showed that current energy storage capabilities are a major limiting factor for electric aviation. Wireless power was viewed as a way to remove the limitations presented by onboard power.

1.2 Background

Weight is the biggest consideration when designing an aircraft. Figure 1 shows a force diagram of a plane. In order to fly, an aircraft must use lift and thrust to overcome

the weight and drag of the vehicle. So, in the design process, the weight of the vehicle sets requirements for the lift and thrust.

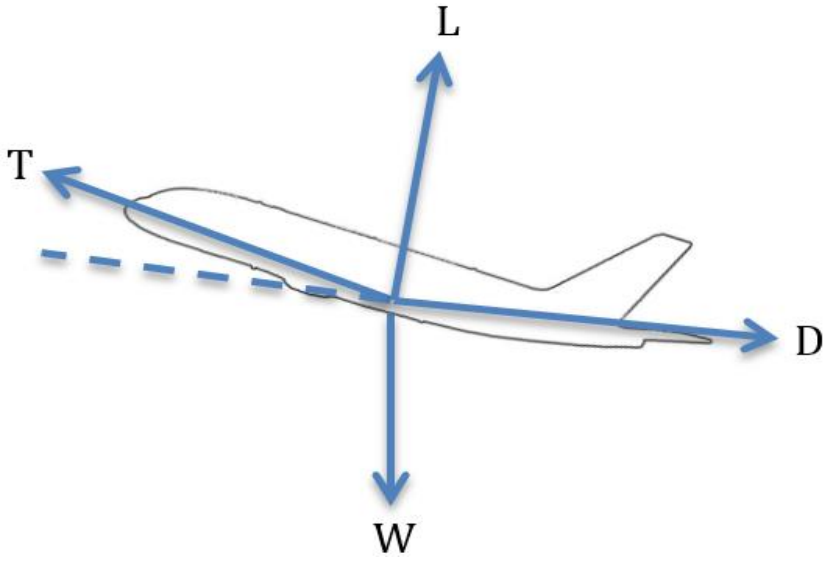

Figure 1. Aircraft force diagram.

The problem with conventional power sources is that the aircraft is limited by the amount of energy it can store onboard. It therefore has a set period it can fly, which is dependent upon the amount of energy it has stored and the fuel consumption. In order to increase the mission parameters, the amount of energy stored onboard needs to be increased. When increasing the amount of energy stored, in the form of fuel or batteries, the weight of the vehicle increases. This in turn increases the lift and/or thrust required.

The benefit to powering an aircraft remotely is that it removes the limit placed on a vehicle by onboard energy storage. This comes at a price though, as the vehicle can only by powered while it is within range of the power transmitter. However, while the vehicle is within this range, it is theoretically possible to have infinite endurance without a massive weight increase. This is obviously an attractive concept, and it’s actually been around for quite some time.

1.2.1 Wireless Energy Transfer

The concept of wireless energy transfer has been around since the time of Nikola Tesla. Tesla conducted experiments as early as the 1890s. In 1898 Tesla successfully demonstrated how a light bulb could be powered from 30 miles away through microwaves. He was a great proponent for the concept, and his work eventually led him to the idea of ionizing the upper atmosphere, thereby allowing it to conduct electricity. In this era, study of wireless power transfer flourished. There were regular contests at fairs to see who could make an electric engine run from the farthest distance away. After a while research for wireless power died off due to lack of funding, with many theories surrounding the fall. [1]

The next major advancement applicable to this field came with the invention of the Yagi antenna in the 1928. This was the first creation of a high gain, highly direction antenna. While the concept was created by the Japanese scientists Shintaro Uda and Hidetsugu Yagi, Americans and their European allies were the ones that put it into wide spread use. The Japanese did not realize the concept for the technology actually came from their own work until interrogating prisoners of war during World War II. [2]

William Brown was the first recorded person to use the advances in microwave technology for remote power transfer. In 1964 he successfully powered a small remote controlled helicopter on CBS news using microwaves. Also around this time Peter Glaser wrote a paper, proposing collecting solar energy in space and beaming it down to earth through microwaves. This is recognized as the first paper of its kind. One square kilometer of solar cells in space collects enough energy to power the entire United States. Because of this, beamed solar energy is considered the ultimate goal of wireless energy transfer. Whether this is truly feasible or not is yet to be determined.

Around the same time as Brown, Theodore Maiman was doing work that would advance wireless power technology. Maiman invented the laser in 1960 [3], however, it was not until a 1993 study by Jet Propulsion Laboratories that lasers were considered as a means for long-range power transmission. [4] Since then numerous programs have advanced upon this research. In 2009, LaserMotive successfully transmitted 1 kW of power over 100 km, winning the NASA Power Beaming competition.

1.2.2 Unmanned Aerial Vehicles

This work is mostly concerned with the design of UAVs as their value is growing exponentially. UAVs have been around for quite some time, and their history actually starts before the Wright brothers. War kites used in the Spanish-American War could be considered the first use of unmanned aerial vehicles. In 1898 Corporal William Eddy place a camera on a kite and flew it up into the air. He had attached a long string to the shutter, so that he could manually take the pictures. He used these kites to take hundreds of pictures of enemy positions. These are credited as the first wartime surveillance photos in history. [5]

The next major step came in World War II by the Germans. In order to prevent the risk of losing pilots trying to bomb England, German engineers came up with the V-1 Buzz Bomb. It consisted of a warhead with an attached pulsejet, which gave it its signature buzz. The V-1 Buzz Bomb was designed to fly 150 miles before dropping their 2,000 lb warhead. It could not be controlled once it had been launched, but since they knew where it needed to fly they just pointed it in the appropriate direction. [6]

In response to the Buzz Bombs, the American Air Force converted several of their Liberators and B17s to be remotely controlled through video guidance systems. They were

unable to make the aircrafts takeoff while remotely controlled, so pilots would handle the takeoff and then bailout over the North Sea where they would then be picked up. The aircraft would then be remotely controlled to its target destination. These were usually used against the heavily guarded Buzz Bomb factories.

Since then, UAVs have advanced immensely. There are currently hundreds of different types of UAVs. The come in a variety of shapes and sizes, all depending upon the mission. As funding is poured into UAV research, the types and abilities of the UAVs will increase exponentially. Currently most UAVs are used overseas but recently there has been a push to be able to use UAVs locally. Right now there are very few laws allowing the use of UAVs in domestic airspace, but it is not unreasonable to expect UAVs to be a common sight in the near future.

1.2.3 Remote Powered Aviation

As mentioned before, William Brown was the first person to combine aircraft and wireless power when he powered a RC helicopter using microwaves in 1964. The next major step in came with solar power. In 1974 the AstroFlight Sunrise was the first aircraft to fly powered by solar power. [7] This development created the groundwork for many vehicles to come.

In 1987, microwave powered flight took another advancement in the form of the SHARP, shown in Figure 2. This was planned to be a high altitude relay platform. Only a 1/8 scale model was actually flown, and it required an 80 meters diameter transmitter array. [8] Lack of funding prevent the flight of a full scale prototype. Microwave powered flight did not end there as in 1992 the MILAX was created. It was for a similar purpose and they managed a 40 second flight over 400 meters. [8]

Figure 2. Image of SHARP aircraft. [8]

Laser powered flight's first success came with lightcraft. Lightcraft use highly focused lasers to create plasma on the backside of the vehicle, which expands and creates thrust. [9] In 2003, NASA used lasers to power a small RC airplane. This time, instead of using the lasers as a direct propulsive device, the laser beam was converted to electricity using solar panels, which in turn powered a motor to drive a propeller. Research has expanded on this to the point that, in August of 2012, LaserMotive teamed up with Lockheed Martin and the two of them powered Lockheed Martin's UAV, the Stalker, for 48 hours. [10] With the advance in technology, and the demand for UAVs with more capabilities increases, research will continue to be done on wireless power transfer.

1.3 Economic Demand

For this work it is important to understand why there is the need to develop new design techniques. The demand for UAVs has increased immensely in the past several decades. Part of this can be attributed to the change in the nature of war. With modern warfare existing in urban areas, it is necessary for constant surveillance to separate civilian targets from military ones. The endurance of a manned aircraft can be limited by its human counterpart. UAVs allow for longer endurance and, because they do not need a human

pilot, they can come in a much smaller size. The smaller size also allows for closer surveillance in densely populated areas. Another added benefit of removing the human, and the life support systems necessary, is that it significantly reduces the weight, which, theoretically, reduces the flyaway cost.

Due to these advantages, the U.S. Senate has invested heavily in UAV systems. In 2005 95% of all aircraft in the military were manned, compared to only 59% today. [11] Figure 3 shows a plot of government spending since 1988. This figure shows that spending from 2000 to 2010 has increased over 700%. It should be noted that the y-axis should be in billions not millions. This plot was corrected in the text of the paper.

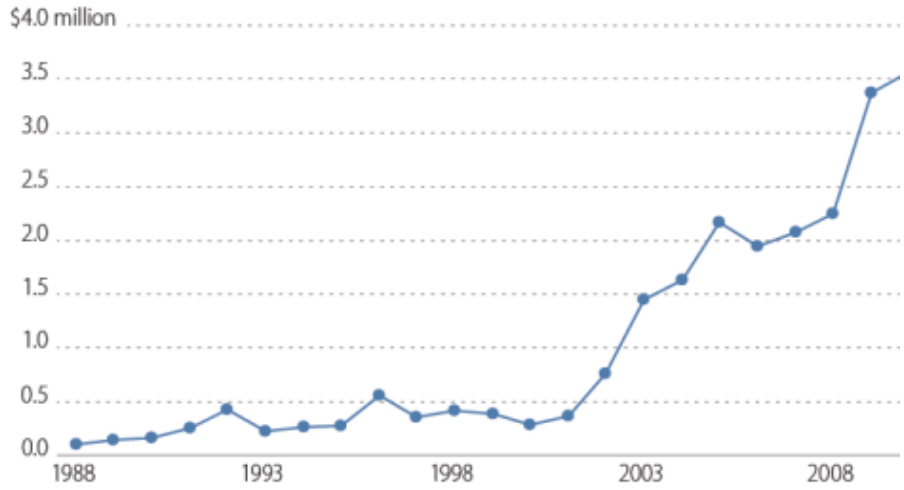

Figure 3. US spending on UAVs since 1998. [11]

Not only have the number of UAVs in use increased, but also the varieties. The U.S. military employs many different types, for many different missions. The vast majority of these tend to be smaller in scale. Figure 4 shows a graph of the number of UAVs in use, for three different range scales. The number of UAVs with a range of less than 10 miles makes up almost 80% of the entire UAV contingent.

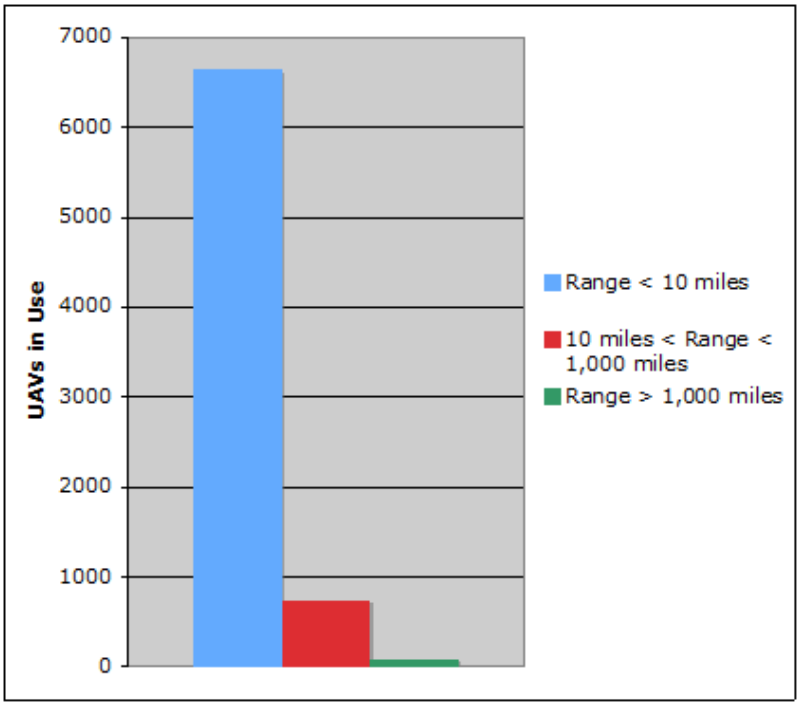

Figure 4. Current UAVs in use, categorized by range.

This shows that not only is there a large demand for UAVs but there especially is a demand for more advanced short-range UAVs. Currently, the military is artificially increasing a UAV system's endurance by using multiple vehicles, and rotating them to maintain constant surveillance. To achieve 30+ hours of endurance for the Raven, 3 separate vehicles are rotated. [12]

Currently the endurance for UAVs is limited by the amount of fuel they can carry or their battery capacity. Efficiencies of fuel-based aircraft are reaching their peak [13], and, while there are advancements that can improve battery life, the current most commonly used battery, lithium-ion, is reaching its theoretical peak as well. [14] Because of this it is necessary to look into new technologies for power UAVs. Remote power may provide the perfect solution to this demand for long endurance, short range UAVs. Remotely powering UAVs takes away the need for new technological advances in onboard

energy storage systems and/or propulsion systems. Remote power already fits within electric aircraft architectures and, since the power source is no longer constrained by the size of the vehicle, there are no necessary advancements in power technology. Using remote power methods to increase the endurance of a single vehicle eliminates the need to cycle multiple vehicles in order to maintain surveillance over a target. Using only one vehicle should reduce the overall cost of the surveillance system.

The intent of this work is to explore the boundaries of remote power capabilities. By determining the range and power capabilities, a design space can be developed. This design space will fit into conventional sizing, and given a specific mission's requirements, will determine if remote power is an appropriate option.

2. Design Methods: Developing a Design Matrix

When designing a remotely power UAS, it is important to determine what design space it would exist in with respect to current systems. Determining this design space will give an idea of the mission requirements at which a remotely powered UAV will be cost effective with respect to its conventional counterparts. However, since current design methods do not apply to remotely powered vehicles, new techniques will need to be developed. In this paper, a design matrix is developed that will assist in determining when a remotely powered vehicle will be comparable to an electric or combustion one.

The design matrix is created by splitting aircraft designs into two major categories: combustion powered and electrically powered. Subsets of combustion-powered aircraft will not be considered for this thesis. Electrically powered aircraft are then broken into two categories as well: battery powered and remotely powered. There are other options for electrically powered, such as fuel cells, but these will be ignored for this work, since they do not have significant historical data. The remotely powered set can then be separated into laser or microwave powered. This breakdown is shown in Figure 5.

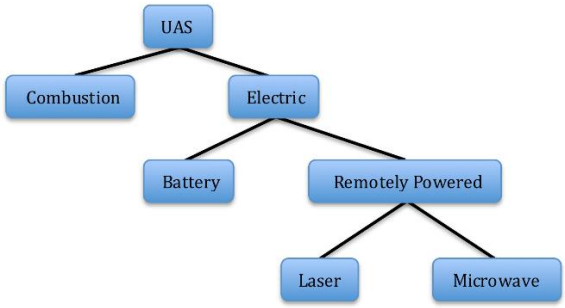

Figure 5. Breakdown of unmanned aerial systems.

2.1 Aircraft Sizing

Two of the most important parts of the design process are the aircraft sizing and the constraint diagram. The constraint diagram uses the mission requirements to develop a design space that the vehicle will need to fall in, and the aircraft sizing gives an estimated weight of the vehicle. An example of a constraint diagram is shown in Figure 6. The estimated weight can be used, along with the constraint diagram, in order to determine factors such as the power requirements, the planform area, and cost [15], among others.

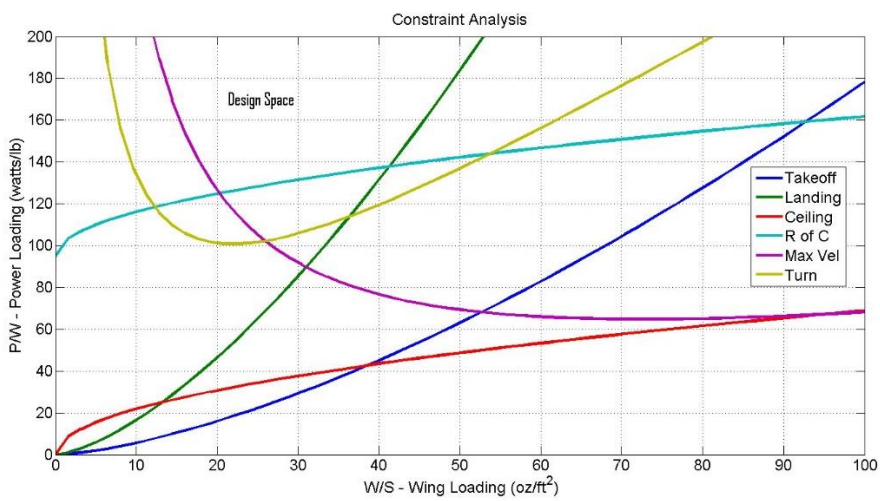

Figure 6. Example of a constraint diagram. [16]

As stated before, aircraft sizing is the process of estimating the takeoff gross weight of the vehicle. Conventional aircraft sizing comes from an iterative method to solve for the gross-takeoff weight. The method is derived from the basic equation for the weight of the aircraft

$$W_{TOGW} = W_P + W_{af} + W_{OES} + W_{pay} + W_m \tag{1}$$

where W_{TOGW} is the takeoff weight of the aircraft, W_P is the propulsion system weight, W_{af} is the weight of the airframe, W_{EOS} is the weight of the onboard energy source, W_{pay}

is the payload weight, and W_m is miscellaneous weight. This can be simplified by combining several of the terms, resulting in

$$W_{TOGW} = W_e + W_{OES} + W_P + W_{pay} \tag{2}$$

where W_e is the empty weight of the aircraft, and is a combination of the airframe weight and miscellaneous weight. In most cases, the weight of the onboard energy source is represented as the fuel weight, W_f. The fuel weight faction is then found by rearranging the Berguet range equation. Since this work is also considering vehicles that do not use fuel, W_{OES} is used as a term to account for however the energy is provided. This includes vehicles that use batteries, fuel, are remotely powered, or any combination of those.

Due to the way in which systems are coupled, conventional sizing methods rearrange Equation (2) to solve for the takeoff gross weight in a different way.

$$W_{TOGW} = \frac{W_{pay}}{1 - \frac{W_e}{W_{TOGW}} - \frac{W_{OES}}{W_{TOGW}} - \frac{W_P}{W_{TOGW}}} \tag{3}$$

The value of the W_{pay} depends on the mission that is being designed for, and $\frac{W_{OES}}{W_{TOGW}}$, called the energy weight fraction, is dependent upon the energy required to perform the mission. The empty weight fraction, $\frac{W_e}{W_{TOGW}}$, and propulsion weight fraction, $\frac{W_P}{W_{TOGW}}$, come from historical data, with the empty weight fraction based on the takeoff gross weight and the propulsion weight fraction based on the power to weight ratio.

The empty weight fraction is highly dependent upon the type of vehicle. Historical data for multiple different types of vehicles are found in Figure 7. The empty weight fraction used in this work is found using data for short range UAVs. This results in an empty weight fraction that is a function of the gross-takeoff weight.

$$\frac{W_e}{W_{TOGW}} = 0.916{W_{TOGW}}^{-0.0795} \tag{4}$$

Because the empty weight fraction is dependent upon the takeoff weight of the vehicle, the problem needs an iterative solver to find the solution.

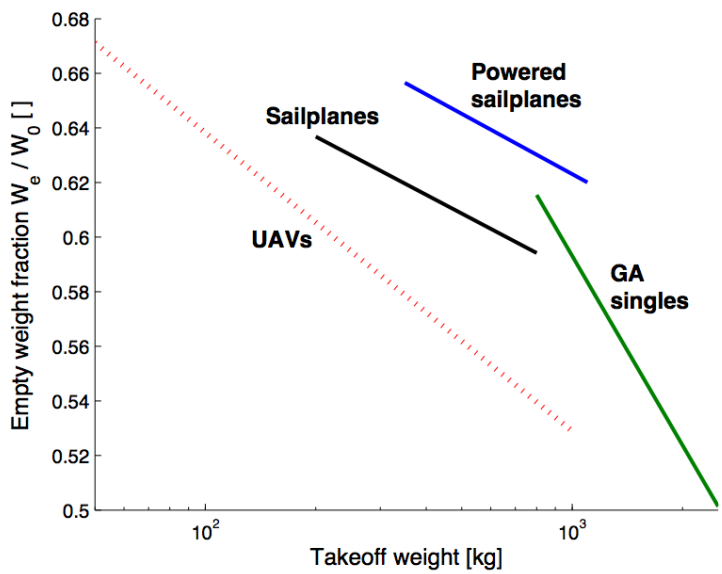

Figure 7. Historical regression correlating the empty weight fraction to the takeoff weight. Where W_o is equivalent to W_{TOGW} [17]

This data is based on current UAVs, which consists mostly of combustion powered systems. Due to this, the equation for the empty weight fraction does not directly apply to electrical and remotely powered systems. However, since the goal of aircraft sizing is to get an estimated weight, this is considered a reasonable estimate with which to use.

2.2 Mission Profile

In order to perform the aircraft sizing, it is necessary to understand the mission profile. In conventional design methods, the mission profile is used to determine the fuel weight fraction at takeoff. This is done by working backwards along the mission and determining the fuel weight fraction for each leg. These are then combined into the total fuel weight fraction. When using electrical systems, it is necessary to determine the amount

of energy consumed during each leg. For battery systems, the W_{OES} can be estimated by using current battery energy densities. For remote power it gets more complicated because the amount of power being provided fluctuates throughout the mission.

With remote power and battery power being considered as subsets of electrical systems, the mission profile for electrical systems can vary from being completely remotely powered, to completely battery powered, and any variation in between. This is depicted in Figure 8 below.

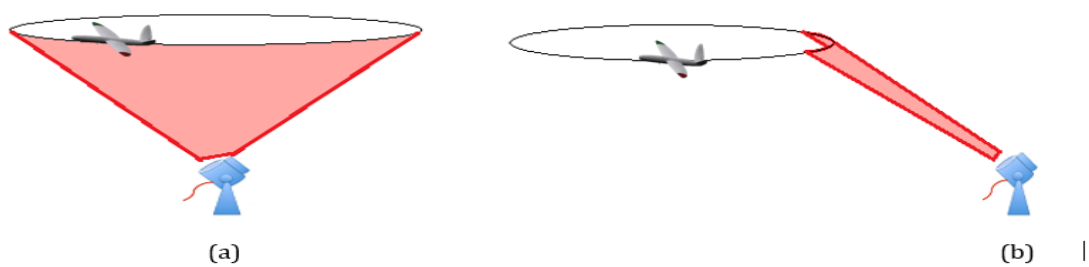

Figure 8. Possible mission for remotely powered vehicles (a) in contact for constant power or (b) in contact only to charge battery.

There are benefits to both possible mission versions. The first one provides constant power the entire time, thereby reducing the necessary battery mass. It also reduces the battery cycles, for which a battery only has a finite amount. The second case, however, provides a greater range but at the cost of a greater battery mass. The extra battery life allows the vehicle to be partially separated from the range restrictions of the transmitter. The degree to which the vehicle could be dependent upon the transmitter varies depending upon the mission. This becomes an optimization problem as it is dependent upon the total range, the power able to be output from the remote power transmitter, and the point at which the vehicle switches from remote to battery power. The results are completely dependent upon the mission requirements.

A mission profile was created to compare the different methods. This can be seen below in Figure 9. Part (a) depicts the mission profile when only one powering method is used, such as combustion, battery, or remote power only. The mission consists of three parts. The first part is a climb to cruise altitude, the second part is a cruise to some distance R and back, and the third part is the descent.

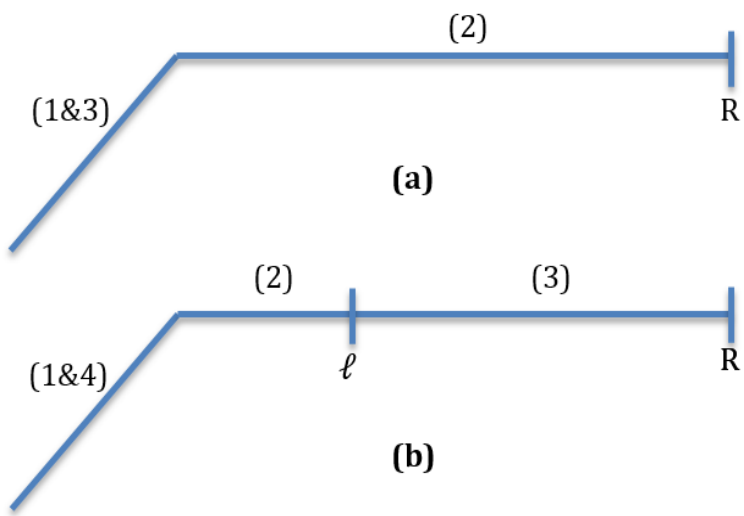

Figure 9. Mission profiles for (a) only one power method and (b) a combination of powering methods.

There is no takeoff leg because it is assumed that the vehicle is hand launched. For landing, it is assumed that the UAV goes into a deep stall to bleed of as much energy as possible as it falls to the ground. Part (b) is for the case where part of the mission is remotely power and part of the mission is powered by battery. The first leg is a climb using battery power. Once it reaches cruising altitude, it switches to remote power where it then flies out to some distance ℓ that the receiver has been sized to. During the second leg, the excess power from the laser is used to recharge the battery from the climb. For the third leg, the UAV uses battery power to fly to distance R and back.

2.3 Modifying Breguet Range Equation

As mentioned before, for a vehicle equipped with a combustion-propulsion system, the Breguet range equation is used to determine the fuel weight fraction for each mission leg. Since this does not apply to electric vehicles, a new way of determining the energy consumed during each leg was developed. This was done using the equation for the specific excess energy

$$Ps = \left(\frac{P_{leg}}{W_{TOGW}}\right)\frac{\eta_{prop}\eta_{motor}\eta_{sc}\alpha}{\beta} - \frac{F_D}{W_{TOGW}}\frac{v}{\beta} \tag{5}$$

where P_{leg} is the power draw from the specific leg, β is the vehicle weight fraction with respect to the gross takeoff weight, α is an efficiency lapse due to altitude. The drag force to takeoff weight is found from

$$\frac{F_D}{W_{TOGW}} = \frac{C_D \rho v^2}{2\beta}\frac{1}{(W_{TOGW}/S)} \tag{6}$$

where C_D is the coefficient of drag and ρ is the density of air. The coefficient of drag is determine through a drag buildup that will be discussed more in section *6.1.2 Constraints*. Rearranging Eq. (5) to solve for mission leg power weight fraction results in the following.

$$\left(\frac{P_{leg}}{W_{TOGW}}\right) = \left(Ps + \frac{F_D}{W_{TOGW}}\frac{v}{\beta}\right)\left(\frac{\beta}{\eta_{prop}\eta_{motor}\eta_{sc}\alpha}\right) \tag{7}$$

Integrating the right side of the equation, with respect to time, gives the specific energy.

$$\left(\frac{E_{leg}}{W_{TOGW}}\right) = \int\left[\left(Ps + \frac{F_D}{W_{TOGW}}\frac{v}{\beta}\right)\left(\frac{\beta}{\eta_{prop}\eta_{motor}\eta_{sc}\alpha}\right)\right]dt \tag{8}$$

The specific excess power within the equation is modified to reflect the type of leg. For a cruise leg, the equation is simplified as the specific excess power is zero. Two types of climbing legs to consider are constant speed climbs and constant Mach climbs. For a constant speed climb, the change in time is equal to the change in height, divided by the

rate of climb. Since the specific excess power is equal to the rate of climb, and the rate of climb is equal to the speed multiplied by the sine of the path angle, the equation can be rearranged.

$$\left(\frac{E_{leg}}{W_{TO}}\right) = \int \left[\left(1 + \frac{F_D}{W_{TOGW}} \frac{1}{\beta \sin(\theta)}\right)\left(\frac{\beta}{\eta_{prop}\eta_{motor}\eta_{sc}\alpha}\right)\right] dh \tag{9}$$

Similar changes can be made for the constant Mach climb. However, it must be noted that the speed of sound is not constant with altitude. This results in

$$\left(\frac{E_{leg}}{W_{TO}}\right) = \int \left[\left(a + \frac{F_D}{W_{TOGW}} \frac{a}{\beta \sin(\theta)}\right)\left(\frac{\beta}{\eta_{prop}\eta_{motor}\eta_{sc}\alpha}\right)\right] d\left(\frac{h}{a}\right) \tag{10}$$

where a is the speed of sound.

The equation for an acceleration leg is developed using the fact that specific excess power is equal to the change in energy height with respect to time. Substituting this into Eq. (8) and accounting for no altitude change gives a time dependent approach.

$$\left(\frac{E_{leg}}{W_{TO}}\right) = \int \left[\left(\frac{1}{2g}\left(v_f^2 - v_i^2\right) + \frac{F_D}{W_{TOGW}} \frac{v}{\beta}\right)\left(\frac{\beta}{\eta_{prop}\eta_{motor}\eta_{sc}\alpha}\right)\right] dt \tag{11}$$

Adding up the specific energy of each leg gives the total energy required to run the propulsion system throughout the mission. This is beneficial for sizing both the battery and remote powered vehicles.

3. Combustion versus Electric

The first step in developing the design matrix is to compare current combustion and electrical systems. In order to determine how combustion powered vehicles and electrically powered ones are divided, historical data was analyzed. It can be estimated that the weight of the vehicle is equal to some function of the range, power, and payload requirements as designated by the mission or

$$W_{TOGW} = f\left(R, P, W_{pay}\right) \tag{12}$$

where R is the range, P is the power, and W_{pay} is the weight of the payload. This was converted into

$$W_{TOGW} - W_{pay} = f(R, P) \tag{13}$$

which allows us to characterize the vehicle weight as only a function of the range and power. This way the weight that is being used is the empty weight of the vehicle plus the weight respective propulsion system.

Figure 10 shows how the weight of the vehicle relates to the designed range. All the UAV data used can be found in the table in *APPENDICES A: UAV Data*.

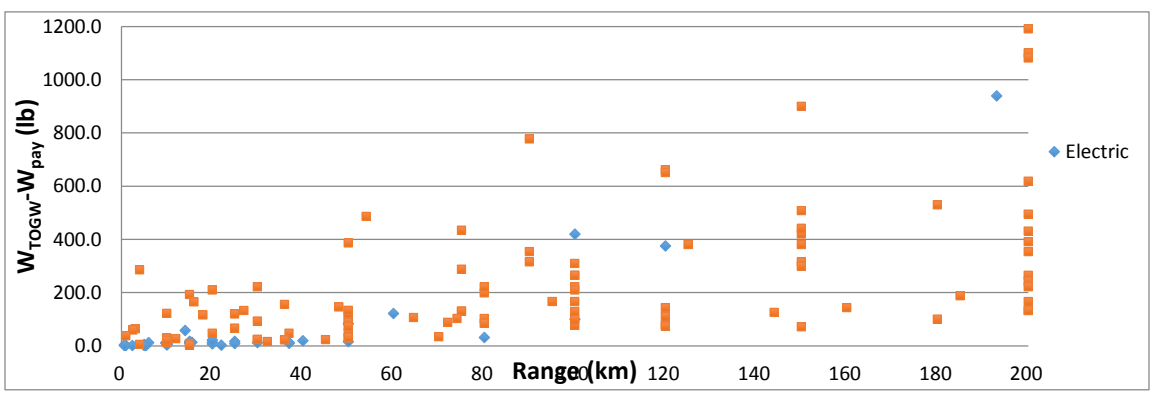

Figure 10. Historical data comparing the weight of the vehicle to the range.

Figure 10 shows that both electrically powered and combustion powered aircraft have overlapping design space with respect to range. The values for the combustion UAVs is very scattered, however, the electrically powered UAVs consistently tend to have less weight at lower ranges. At lower ranges, the electric UAVs tend to have a lower takeoff gross weight minus the payload weight. This trend occurs when the range is less than 50 km, after 50 km the weight of the electrically powered increases dramatically.

Figure 11 shows how the weight of the vehicle relates to the designed power. The power in this case is the maximum shaft power output at sea level. There is less data available on the actual power output of the respective propulsion system than there is range capabilities for UAVs. This is especially true for electrical systems. This is largely due to companies using their own privately made motors. From this plot, it was found that between 500-1000 W is when the combustion power starts to have a lower weight for the same output power. Complete plots for both combustion and electric powered UAVs plotted separately can be found in *B: Plots of Electric and Combustion Systems*.

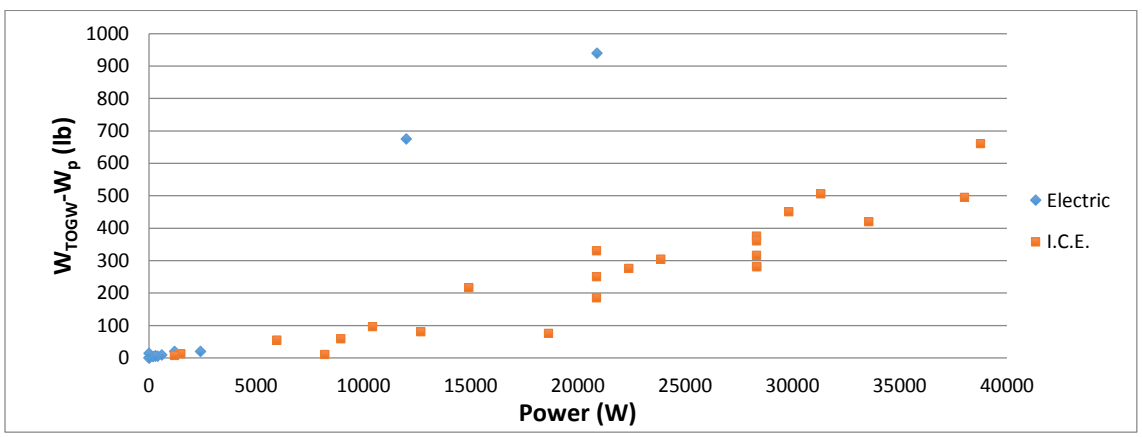

Figure 11. Historical data comparing weight of the vehicle to the max power available.

Using these two figures, a general idea of where the design space for an electrically powered UAV should be. The data is mostly clustered around low power requirements for

the electric vehicles. There were really only two high powered electric vehicles for which data could be obtained. This shows that the design space for an electric powered UAV would exist within a range of less than 50 km and a power requirement of less than 1 kW.

3.1 Energy Densities

To understand why Figure 11 behaves the way it does, it is necessary to look at the energy source and how it is converted into power. For the combustion system, this involves some type of fuel and a combustion engine, and for the electric system, it is a battery and an electric motor. This thesis only considers piston-prop engines for combustion systems in order to ensure similarity between electrical systems.

The best way to compare energy sources is by looking at the energy density. Since we are restricted to piston driven propellers, it is assumed that the combustion system uses conventional gasoline. The energy density varies upon the local atmospheric conditions but at standard day, gasoline has an energy density of around 44 MJ/kg and 31.1 MJ/L. [18] It is harder to give batteries a single energy density, as there are many different types and the values can vary for each type. Figure 12 plots different types of batteries with their respective energy densities.

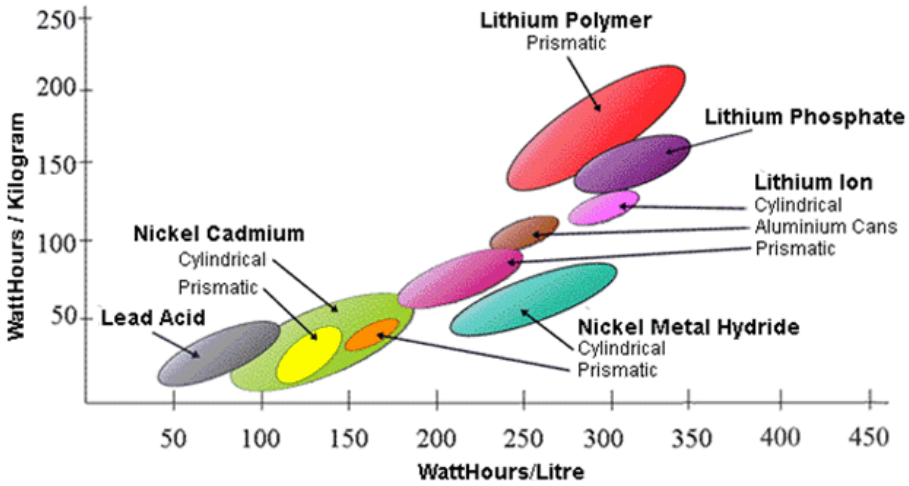

Figure 12. Energy densities of different types of batteries. [19]

Figure 12 shows that currently, the best battery technology in terms of energy density is lithium polymer. These can have energy densities up to about 1 MJ/kg and 1.26 MJ/L. Comparing the values for energy densities, it is obvious that combustion systems have a large advantage due to their energy source. However, it is also important to look at how each system converts the energy into power. Piston engines have been around for a long time and therefore, extensive work has been done to make them as efficient as possible. Piston engines are flawed in the fact that they, theoretically, can only achieve a maximum efficiency of around 40%. [13] Electric motors, on the other hand, have been known to achieve efficiencies up to 90% or higher. [20] This is displayed in Figure 13. When comparing energy densities it is also important to consider the effective energy density. This is the energy when accounting for the efficiencies of the respective systems.

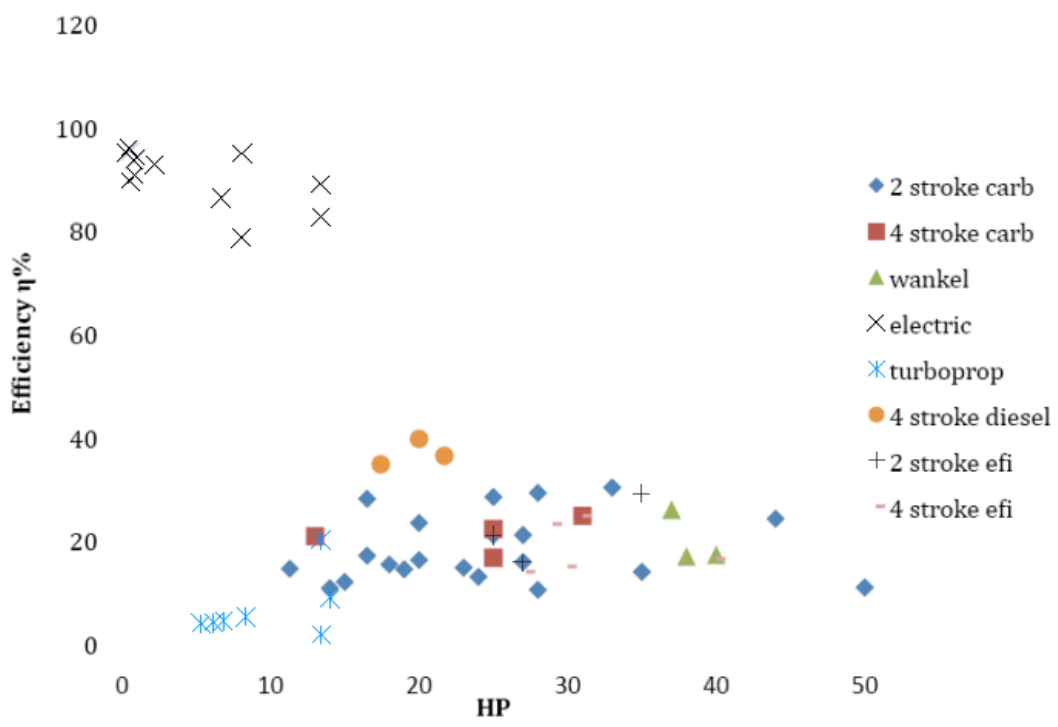

Figure 13. Comparison of efficiencies of different types of motors with respect to horse power. [21]

3.2 System Efficiencies and Weight

As the volume of the energy system decreases, the total energy of the system approaches zero. This can be described mathematically by

$$if\ E = \varrho V\ then\ \lim_{V \to 0} E = 0$$

where ϱ is the energy density and V is the volume. So as the volume decreases the values for the energies of the systems become closer, but the gas system will always have a greater energy. The difference that comes into play is the components of the system, as the system gets smaller.

A system that requires an output power of 800 W for half an hour results in a total necessary energy of 1.44 MJ. In terms of on board storage, this would result in a volume 70 in^3 for a lithium polymer battery or 2.5 in^3 for gasoline. When taking into account the efficiencies of the motor, both these values increase. For a power output of around 800 W two commercially available RC aircraft motors were analyzed, both which put out a maximum of 1500 W. The HC5030-390 electric brushless was used to model the electric system, which has an efficiency of around 80%. The O.S. FT-160 was used for the combustion system. Even though combustion engines have a theoretical value of around 40%, smaller engines have not been advanced as much. According to the manufacturer's specifications, the FT-160 only has an efficiency of 0.09%. Using these efficiencies results in a total energy stored on-board of 1.8 MJ necessary for the electric system and 16 MJ for the combustion system. This translates to volumes of 87 in^3 and 31.5 in^3 respectively and weights of 4 lb [22] and 0.8 lb [23] respectively.

Even considering the efficiencies of the motors, the combustion system still has a lower volume and weight requirements for the energy storage. When comparing the two

engines, the HC5030-390 weighs only 0.9 lb and takes up a volume of 6.5 in^3, while the FT-160 weighs 2.4 lb and takes up a volume of 84 in^3. The combustion system still weighs less but takes up more volume. The combustion still needs a fuel pump, a container to hold the liquid fuel, hoses, and a battery to run the electrical systems of the vehicle. The electrical systems only other major component is a speed controller, which is roughly equivalent in weight to the fuel pump for this size of system. The results are a combustion system that is marginally lighter, but has a greater volume, and an electrical system that is slightly heavier but a smaller volume. Combustion systems also have to deal with movement of the center of gravity as the fuel is burned. So for systems of this size and smaller, electric is usually the appropriate choice due to the ease of use and lower drag due to the smaller volume. This is because most of the mass of an electric system is in energy storage.

Table 1. Comparison of electric and combustion motors.

Motor	Efficiency	Weight (lb)	Energy Weight (lb)	Extras (lb)	System Weight (lb)
HC5030-390	80%	0.9	4.0	0.15	5.05
O.S. FT-160	9%	2.4	0.8	0.85	4.05

Since the propulsion system is the major factor that separates combustion and electrical designs, it is necessary to create estimates of the weight for both types of systems. The two main parts of each system are the electric motor and the combustion engine. Figure 14 shows historical regressions that predict the weight of a motor or an engine based on their peak output power.

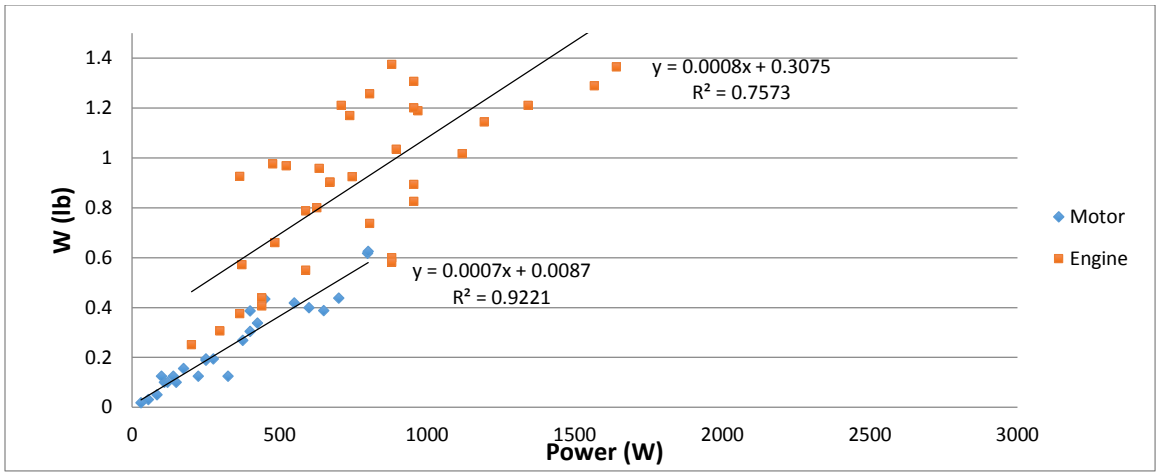

Figure 14. Motor and engine historical regression based on peak power output.

Looking at this figure shows that, for power outputs up to 1 kW, electric motors tend to weigh less. The resulting trend-lines give equations that can be used to estimate the weights of the motor and engine respectively. This is

$$W_{mot} = 0.0007P_{out} + 0.0087 \tag{14}$$

for the motor, where P_{out} is the peak power out, and

$$W_{eng} = 0.0008P_{out} + 0.3075 \tag{15}$$

for the combustion engine.

For the combustion engine, there are three more main parts included into the model: the muffler(s), the electronic ignition, and the regulator pump. Figure 15 shows historical data for the weight of the muffler or ignition with respect to the weight of the engine. From this figure it can be seen that there is a correlation for the weight of the muffle and the weight of the engine, but there is not a correlation between the engine weight and the weight of the ignition.

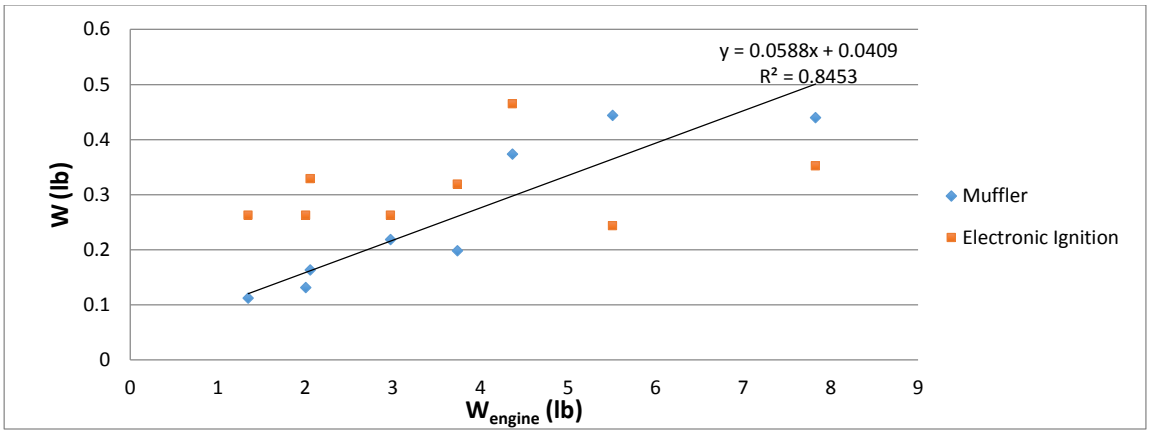

Figure 15. Historical data to determine a correlation between the weight of the engine and the weight of the muffler or ignition.

The weights of the muffler and ignition were also compared to the peak output power of the engine. However, there is a stronger correlation between the weight of the engine and muffler weight, while there was still no correlation for the ignition weight and engine weight. From this figure, the equation for the muffler weight is found to be the following.

$$W_{muf} = 0.0588W_{eng} + 0.0409 \tag{16}$$

Not enough data was found to estimate the weight of a regulator pump. So to model the weight of the pump a Perry VP-40SG regulating pump was used. This is a commercially available pump that is commonly used on RC aircraft. It weighs 0.05 lb and is capable of pumping up to 3.5 Oz/min. This should be enough to handle the requirements for engines within the range of 0 to 1,500 W. Using all of the components, the propulsion system weight for a combustion system is estimated to be

$$W_{P,com} = W_{eng} + W_{muf} + W_{ign} + W_{pump} \tag{17}$$

where W_{ign} and W_{pump} are the weight the ignition and pump and are equal to 0.3 lb and 0.05 lb respectively. The value for the weight of the ignition was chosen to be 0.3 as it is a reasonable estimate looking at the data in Figure 15. Dividing by the takeoff gross weight

and substituting in Eq. (15) and (16) gives the equation for the weight fraction needed in Eq. (3).

$$\frac{W_{P,com}}{W_{TOGW}} = \left[0.0007\left(\frac{P_{out}}{W_{TOGW}}\right) + \frac{0.0087}{W_{TOGW}}\right] + \left[0.0588\frac{W_{eng}}{W_{TOGW}} + \frac{0.0409}{W_{TOGW}}\right] + \frac{W_{ign}}{W_{TOGW}} + \frac{W_{pump}}{W_{TOGW}} \tag{18}$$

Since the weight of the engine is equal to a function of the weight of the power out, this equation can be simplified to

$$\frac{W_{P,com}}{W_{TOGW}} = 0.000741\left(\frac{P_{out}}{W_{TOGW}}\right) + \frac{0.05011}{W_{TOGW}} + \frac{W_{ign}}{W_{TOGW}} + \frac{W_{pump}}{W_{TOGW}} \tag{19}$$

where $\frac{P_{out}}{W_{TOGW}}$ is the power to weight fraction and is found from the constraint diagram.

For electrical system, the only other major component is the speed controller. This acts as the throttle and varies the current depending on what shaft speeds are desired. For the speed controller, the continuous current draw that is desired determines what speed controller is necessary. Depending on how a motor is designed it has a different current draw, so a regression was made to relate the current draw and the power output of the engine. This is shown in Figure 16.

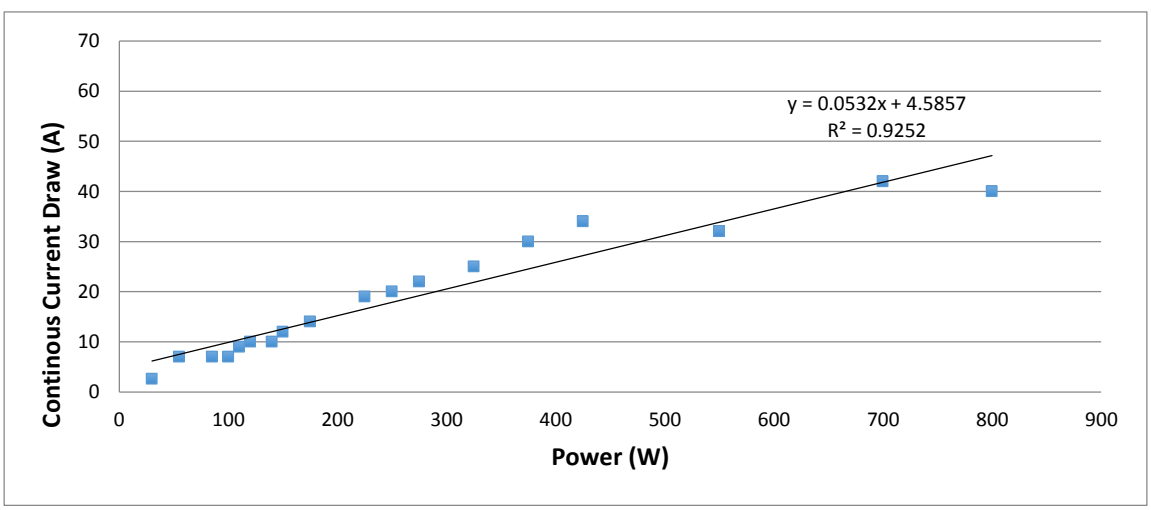

Figure 16. Historical regression depicting the correlation between the motor power and the current draw.

This figures gives an equation for the current draw of the motor.

$$I = 0.0532P_{out} + 4.5857 \tag{20}$$

With the current draw estimated with the relation to the output power, the next step is to relate the output power of the motor to the weight of the speed controller. This is done with the regression shown in Figure 17.

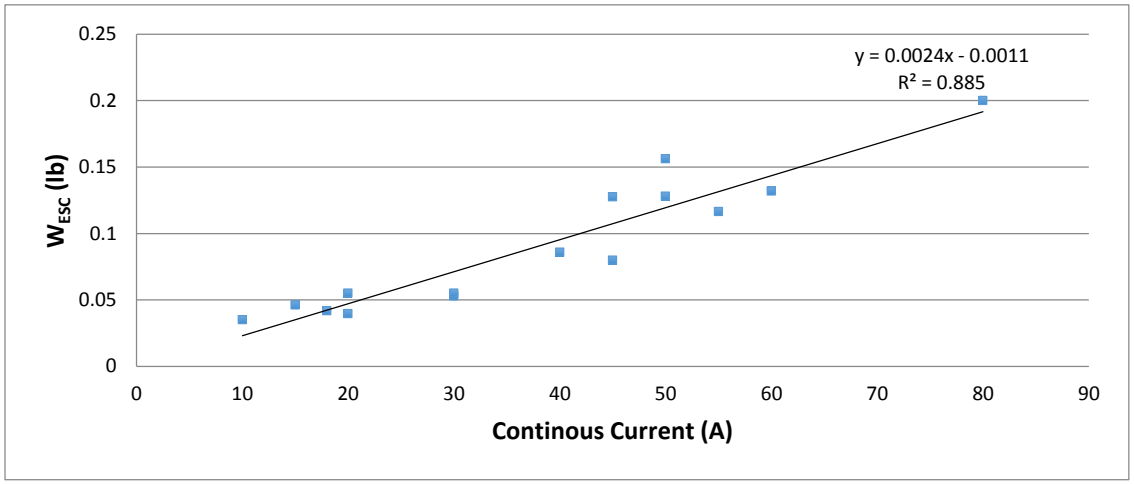

Figure 17. Regression relating the weight of the speed controller to the continuous current draw.

This results in an equation for the speed controller.

$$W_{E.S.C} = 0.0024I - 0.0011 \tag{21}$$

Adding the two components together results in the equation for the propulsive system weight.

$$W_{P,elec} = [0.0009P_{out} + 0.2301\,] + [0.0024I - 0.0011] \tag{22}$$

Substituting in Eq. (20) for the current draw, dividing by the takeoff weight, and simplifying gives the equation for the weight fraction of the electric propulsion system shown below.

$$\frac{W_{P,elec}}{W_{TOGW}} = 0.00102\left(\frac{P_{out}}{W_{TOGW}}\right) + \frac{0.24}{W_{TOGW}} \tag{23}$$

It is also important to consider the volumes of each system, as a greater volume will increase the drag, which requires a more powerful propulsion system, and it will increases the weight of structure. Figure 18 shows the volume of a combustion engine with respect to its peak power output.

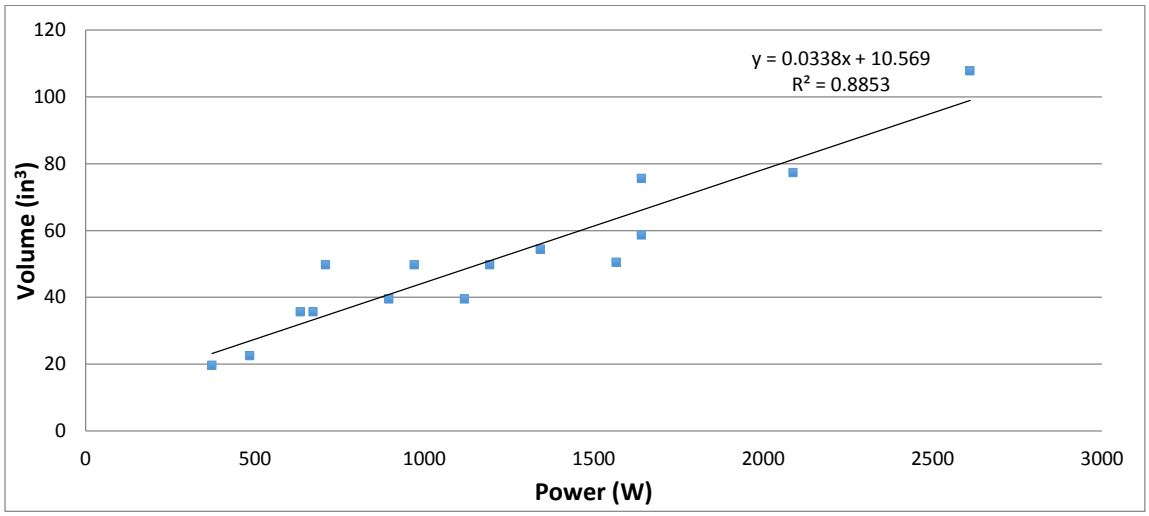

Figure 18. Historical regression relating the peak power output of a combustion engine to its volume.

The volume was related to the output power for combustion engines because it was found to have a better correlation. Since there was no data on the volume of the mufflers or ignition, an extra 10% of the volume of the engine was added. This resulted in an equation for the volume.

$$V_{P,com} = 1.1(0.033P_{out} + 10.569) \tag{24}$$

Figure 19 shows the volume of the motor and the speed controller in relation to their respective weights.

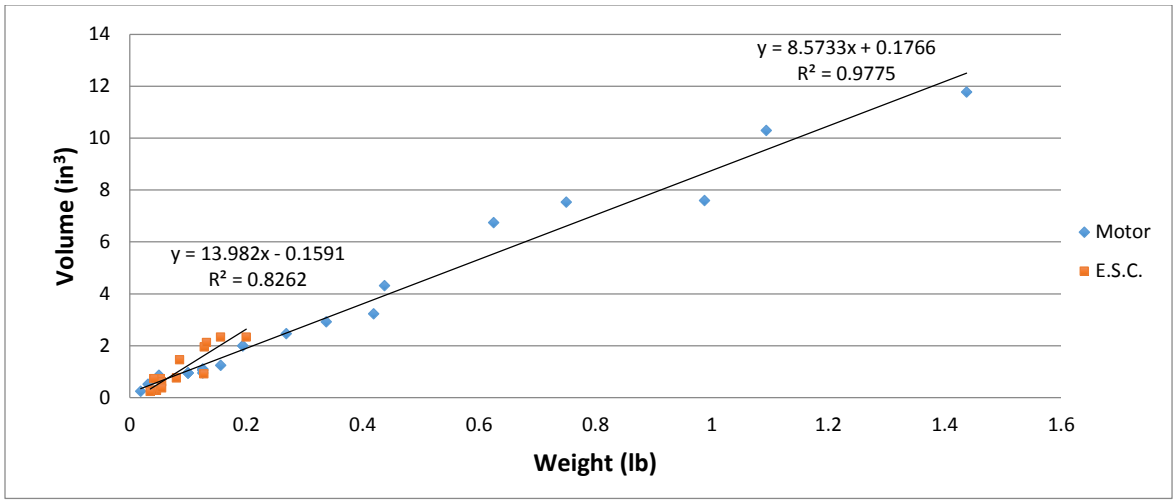

Figure 19. Historical Regression relating the weight of a motor and speed controller to their respective volumes.

Adding the two equations together, substituting in Eq. (14) and (21), and simplifying results in Eq. (25).

$$V_{P,elec} = 0.0078P_{out} + 0.1636 \tag{25}$$

These equations for volume are used in the drag buildup to estimate the surface area of the fuselage. This is shown in section 6.1 Design Methods in Use. From the equations in this section, the propulsion system weight fraction can be estimated for either an electric system or an internal combustion system. Looking at the historical data, it is clearly shown that the components of the electrical system weigh less and are more efficient for lower power requirements. However, this weight benefit is counteracted by the lower energy density of batteries. The volume of each system is then estimated in order to account for the difference in drag. With the weight fraction and volume established, a complete comparison can be made of the two systems, which will be seen more in the following section.

4. Wireless Energy Transfer Methods

Once it is determined that an electrical vehicle is desired, it is necessary to look at how remotely powered vehicles compare with conventional battery powered vehicles. However, before we can compare these two systems, we need to understand how to size a remotely powered UAV, and for that, we need to know how wireless power works.

There are two means of wireless energy transfer: electromagnetic induction and electromagnetic radiation. Electromagnetic induction can be broken into two categories: electrostatic induction and electrodynamic induction. These are just capacitors and inductors respectively. Both of these are near field effects so, even though work is being done to increase their range, they are not really useful for aerial vehicles. Electromagnetic radiation is a much more promising method. Electromagnetic radiation is caused by the movement of charged particles, which releases rays that radiate out from the charged particle element. Electromagnetic radiation is characterized by its wavelength, and for wireless energy transfer the most researched methods use wavelengths within the visible spectrum or microwaves. Going on past research, both microwave emitters and lasers will be considered as possible transfer methods. For this part of paper, the distances will be left in kilometers in order to compare with the results of other works.

4.1 Microwaves

4.1.1 Transmitting Microwaves

Microwaves are convenient because they support high power density and can be directed into narrow beams using high gain antennas, 40 dB. This allows for transmitting over great distances. Transmitting power via microwaves provides problems compared to communication though. Communications signals usually transmit as little power as

possible, generally just enough to be able to separate the signal from the noise. In contrast, when attempting to transfer power, the amount transmitted is dependent upon the power requirements at the receiving end. Microwave transmissions follow the Friis equation, which can be seen below.

$$P_r = \frac{P_t G_t G_r}{L_{fs}} \tag{26}$$

Where P_r is the power received, P_t is the power transmitted, G_r is the gain of the receiver, G_t is the gain of the transmitter, and L_{fs} is the free space loss. The free space loss is the loss in the signal strength over an unobstructed distance. Without increasing the transmitted power, the only way to make microwave power transfer more effective is to increase the gain of the receiver or the transmitter. For this work, only the transmitter will be considered. There are many different types of antennas, the most common for long-range applications being a parabolic antenna. The reason for this being, that they are very directional and can have very large gains. The equation for the gain of a parabolic antenna is found in Eq. (27).

$$G = \left(\frac{\pi d_a}{\lambda}\right)^2 \eta_{an} \tag{27}$$

Where d_a is the diameter of the dish, λ is the wavelength, and η is the aperture efficiency of the antenna. Current technology has the efficiency of the transmission around 85% for dish antennas and 90% for horn antennas. [24] So in order to increase the gain, the diameter of the dish needs to be increased or the wavelength needs to be decreased. Decreasing the wavelength below 10 cm has some negative effects due to atmospheric issues, which will be shown in the next section. Therefore, the only way to increase the gain for use in this work is to increase the diameter.

4.1.2 Microwave Propagation

For microwaves, a range of frequencies from 0.1 GHz to 30 GHz was analyzed. For frequencies less than 3 GHz, propagation theory follows the Friis Equation. The important factor in microwave transmission is the free space loss which is shown below.

$$L_{fs} = \left(\frac{4\pi D}{\lambda}\right)^2 \tag{28}$$

Where D is the distance between the transmitting array and the receiving array, and λ is the wavelength.

With frequencies over 3 GHz, atmospheric absorption becomes a significant factor. This requires another term to be inserted into the Friss equation, which becomes

$$P_r = \frac{P_t G_t G_r}{L_{fs} L_a} \tag{29}$$

where L_a is an atmospheric absorption term. L_a is a complicated term that is dependent upon the makeup of the local atmosphere. For this paper, only oxygen and water vapor will be accounted for.

Since short range UAVs have relatively low maximum altitudes, only a partial path loss needs to be found. Using work from Ho [25], the partial path loss is Eq. (30).

$$L_a = \frac{a_0 H_0}{sin(\theta)}\left(1 - e^{\left(\frac{hsin(\theta)}{H_0}\right)}\right) \tag{30}$$

In these equations, a_0 is the absorption coefficienct, h is the partial atmospheric path, H_0 is the vertical scale height for the respective loss, and θ is the path angle. The oblique path equation is used when the θ is greater than or equal to 5° and less than 90°. The vertical scale height is the distance at which the density of a substance is decreased by a factor of e. This was based on the atmosphere having a mean standard temperature of 273.5 K.

There are two main atmospheric components that contribute to the absorption of microwaves. These are molecular oxygen and water vapor. For oxygen, the specific attenuation dependence is found to be

$$\gamma_{o2} = \left[7.19 \times 10^{-3} + \frac{6.09}{f^2 + 0.227} + \frac{4.81}{(f-57)^2 + 1.50}\right] f^2 \times 10^{-3} \tag{31}$$

where f is the frequency in GHz. For water vapor the specific dependence is

$$\gamma_{o2} = \left[0.067 + \frac{3}{(f-22.3)^2 + 7.3} + \frac{9}{(f-183.3)^2 + 6} + \frac{4.81}{(f-323.8)^2 + 10}\right] f^2 \rho_w \times 10^{-3} \tag{32}$$

where ρ_w is the water vapor density in g/m^3. These attenuation components are in units of dB/km. Ho uses a maximum value of 12 g/m^3 and an average value of 7.5 g/m^3.

The scale height changes depending on the substance. The equivalent scale height of the complete atmosphere is around 8 km. The oxygen equivalent height is less, at only 6 km. The equivalent height for water vapor is found with the following.

$$H_W = 2.2 + \frac{3}{(f-22.3)^2 + 3} + \frac{1}{(f-183.3)^2 + 1} + \frac{4.1}{(f-323.8)^2 + 1} \tag{33}$$

Plots for the respective absorption coefficients can be seen below in Figure 20, and the resulting total attenuation can be seen in

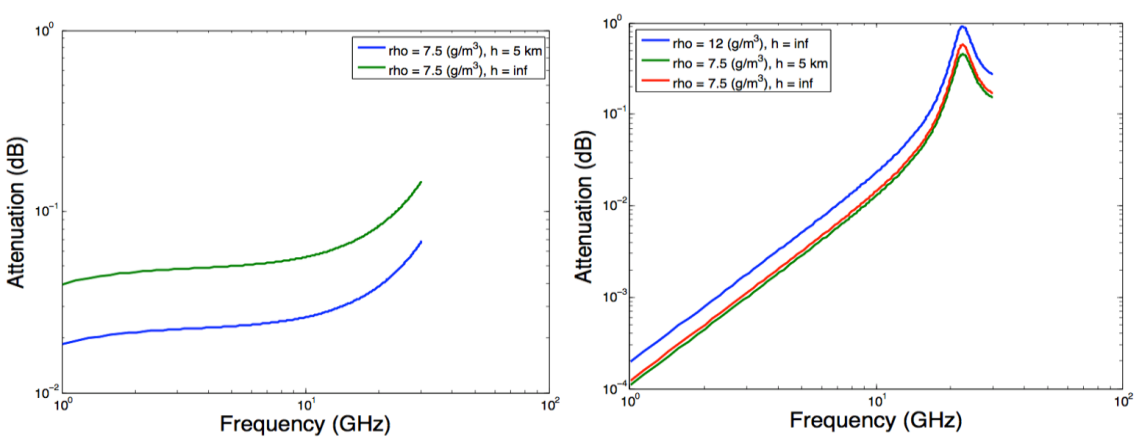

(a) (b)

Figure 20. a) Attenuation due to molecular oxygen for distances of 5 km and inf. b) Attenuation due to water vapor for various water vapor densities and heights.

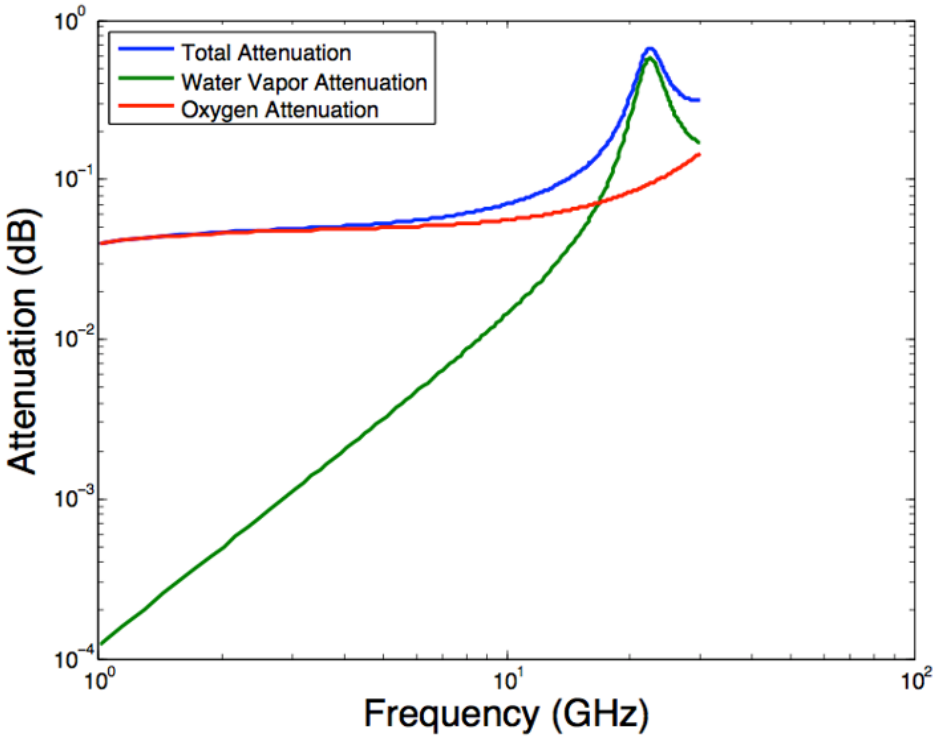

Figure 21. Total atmospheric attenuation.

Applying this to Eq.s (29) and (30) the power at the receiver can be determined. This is plotted in Figure 22 as contours with respect to frequency and distance. The gain for both the transmitter and receiver were modeled as parabolic dishes. The diameter of 5 m was used for the transmitter and 0.1 m for the receiver. A transmitted power of 20 kW was also used. The two plots represent a horizontal path, on the left, and a vertical path, on the right. The atmospheric attenuation is much more pronounced for the horizontal path. For the most part, these plots show that, for the same distance, increasing the frequency results in greater power received. Though for the horizontal path, this is not always true due to the effects of the atmosphere. This major change is due to an absorption line at 22.235 GHz for water vapor. [25]

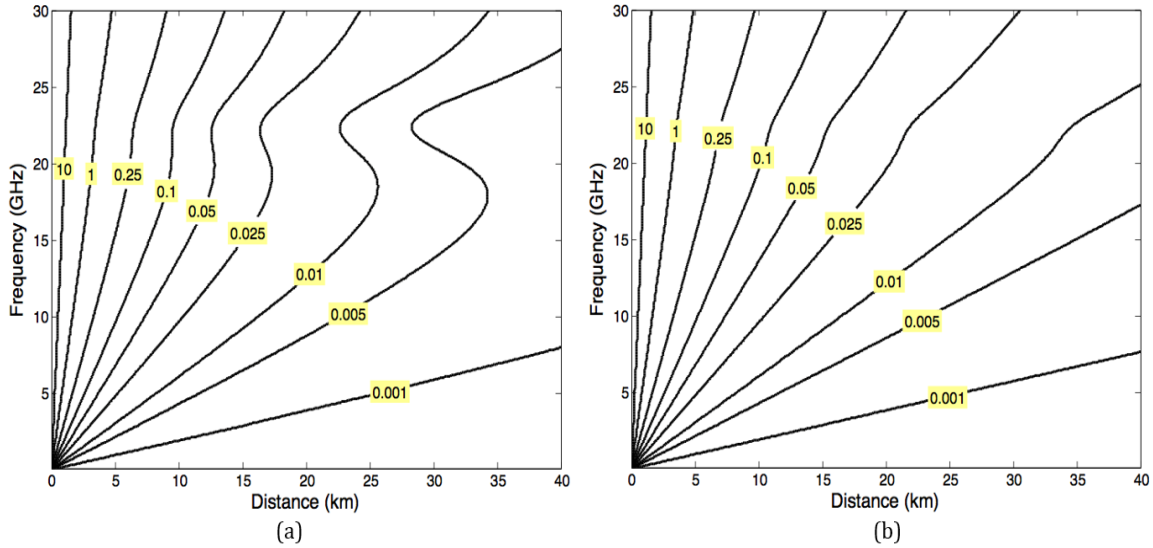

Figure 22. Contours of power (W) received with varying frequency and distance. Part (a) is for horizontal path and part (b) is for vertical path.

Contours of the power received with respect to the downrange distance and the altitude can be seen below in Figure 23. Part (a) is the baseline with a frequency of 2.54 GHz, a transmitter diameter of 5 m, and a transmitted power of 20 kW. The receiver diameter is 0.1 m for all parts. Part (b) increases the transmitter diameter to 10 m, (c) increases the output power to 40 kW, and (d) increases the frequency to 28 GHz.

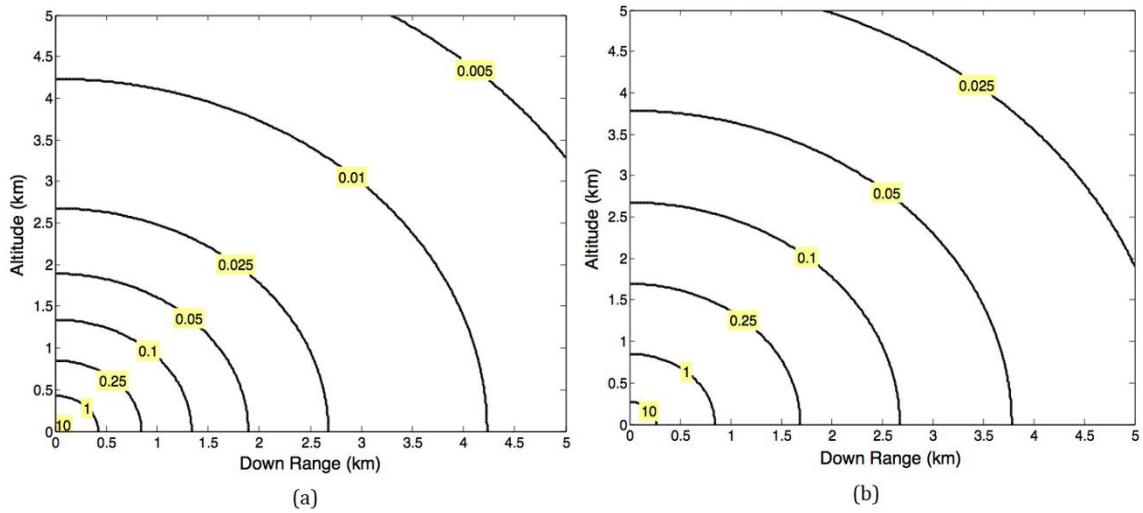

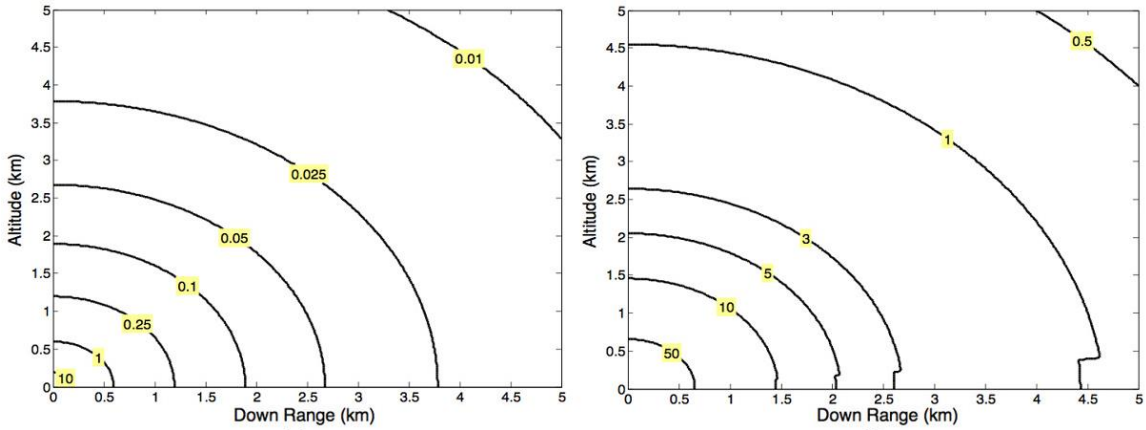

(c) (d)

Figure 23. Contours of power received (W) with a constant receiver diameter of 0.1m: (a) 5 m diameter transmitter, P_t=20 kW, and f =2.54 GHz (b) 10 m diameter transmitter (c) P_t=40 kW (d) f=28 GHz.

While all the changes increased the power received, increasing the frequency had the greatest effect. The sudden change at low altitudes in part (d) is due to the path angle being below 5°. For this part the atmospheric absorption term is assumed to be constant. These plots show very little power can be transmitted over long distances unless the power or antenna area is increased drastically. So it is unlikely that microwaves could be used unless the transmission distance is very close.

4.1.3 Receiving Microwaves

Microwaves are converted back into electricity using a rectenna. This is done by adding a diode to the antenna dipole. The diode converts the alternating current into a direct one. This way, it is very important to have a good antenna in order to receive the maximum amount of power. Current advancements have shown that rectennas are capable of up to 90% efficiencies. [26]

From before, it was shown that changing the receiver gain was one way of increasing or decreasing the efficiency of the power transfer. The size and type of antenna affect the possible gain. Three types of antennas were looked at for this work: a parabolic,

a Yagi, and a patch antenna. A parabolic dish would provide the highest efficiency and gain of the three. Recall that the gain of the parabolic dish is described in Eq. (27) and is proportional to the diameter of the dish squared. The gain pattern for a parabolic dish can be seen Figure 24.

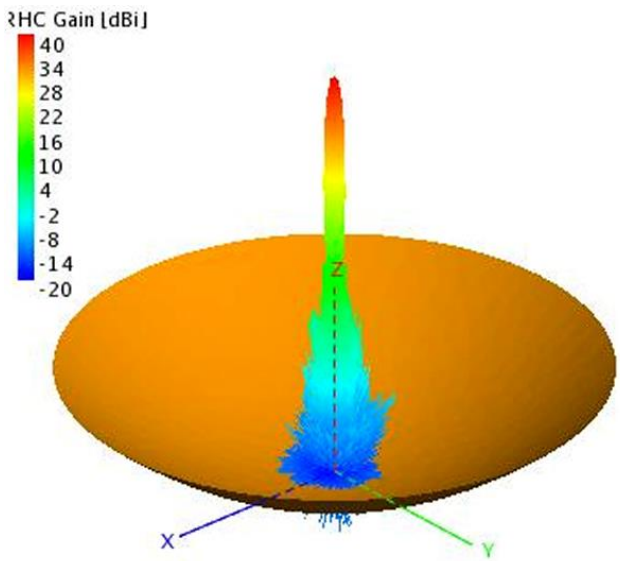

Figure 24. Gain radiation pattern for a parabolic antenna. [27]

In order to achieve a gain of 40 dBi the antenna would have to have a 3 m diameter for a 3 GHz frequency, or a 0.3 m diameter for a 30 GHz frequency. So depending on the transmitting frequency, the dish could become very large. This could be a problem as the geometry might not fit well within the vehicle structure.

The next option is the Yagi antenna. Predicting the gain for a Yagi antenna is more difficult than the parabolic dish. The gain is dependent upon many different factors including the element spacing, the diameter of the elements, the length of the antenna, the operating wavelength, and more. Figure 25 shows the gain with respect to the length of the antenna. Depicted on the graph are antennas using five different spacing values. In order to be applicable to all operating wavelengths, all the distances are normalized by the

wavelength. This plot shows that the achievable gain is oscillatory with respect to the length. Shorter spacing of the elements results in higher frequency oscillations and a lower max gain. This figure shows a maximum gain of around 14 dB for the 0.3λ and 0.4λ at around 10λ long. However, following the oscillatory pattern, it can be surmised that that larger spacing combined with a larger length overall would result in an even higher gain.

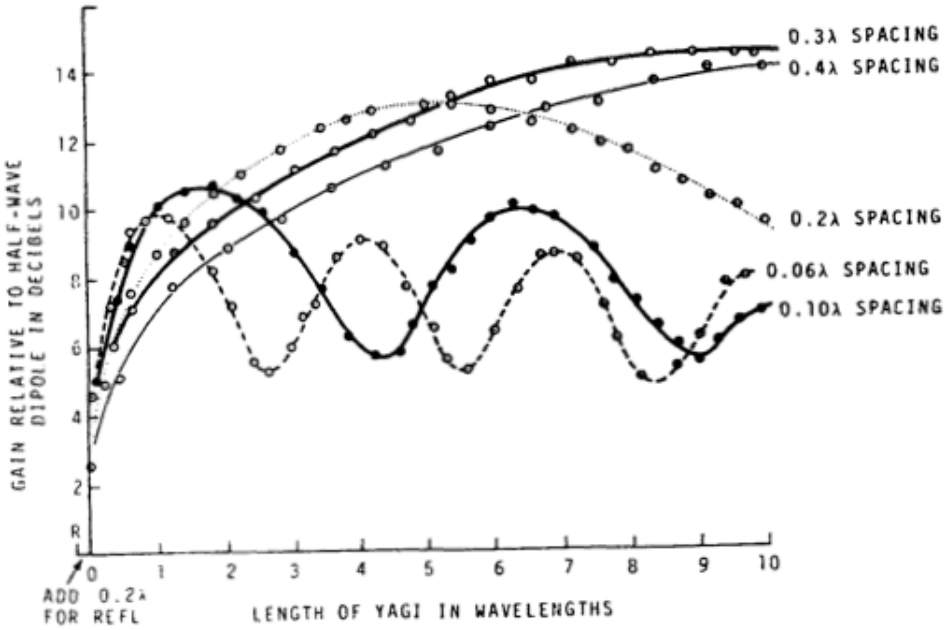

Figure 25. Optimization of a Yagi antenna gain. [28]

To consider what an optimized array would look like, a 3 GHz microwave is considered. As stated before, this plot shows that the max gain occurs when the length is 10λ and the spacing is 0.3λ. A 3 GHz microwave has a wavelength of about 10 cm. This would result in a total array length of 1 meter with elements place every 3 cm. The gain pattern for a Yagi antenna can be seen in Figure 26. This figure shows that the Yagi is less directional than the parabolic antenna.

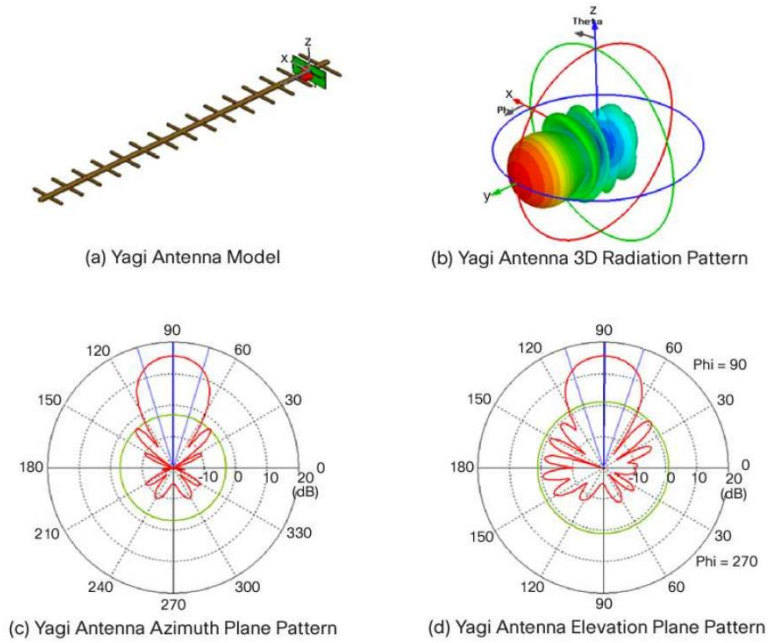

Figure 26. Yagi antenna radiation patterns. [29]

One unconventional idea to fit an antenna into the airframe is to turn the structure of the wings into a Yagi antenna. This idea is depicted in Figure 27. The structure of a wing is already roughly in the shape of a two Yagi antenna back to back. The ribs could be used for the reflector, driven, and director elements. Connecting the antennas in the middle and placing adding in a diode would convert microwave power into DC current.

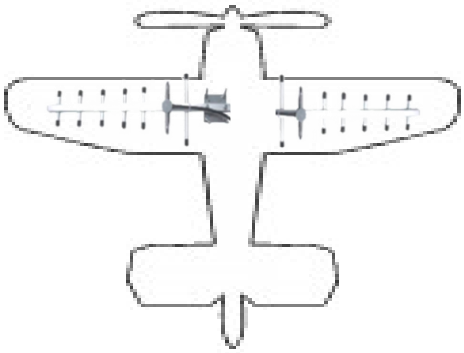

Figure 27. Transforming wing structure into a Yagi antenna.

Even though achieving high gains increases the efficiency, like the Yagi and parabolic antenna do, this can also cause problems. In order to achieve these high gains,

both antennas are very directional. If they are not properly aligned with the transmitting antenna, the gain is severely reduced and the benefits are lost. Unless the antennas are fixed onto turrets, they cannot be expected to maintain alignment. The patch antenna has the benefit as a receiving antenna, in that it is much more omni-directional. Gain patterns for a patch antenna are displayed in Figure 28.

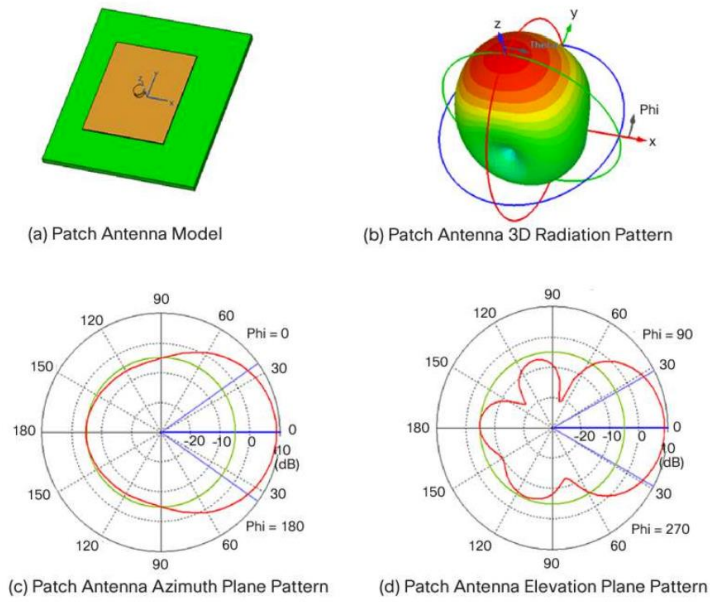

Figure 28. Gain patterns for a patch antenna. [29]

Using a patch antenna increases the ability to receive power when not directly aligned with the transmitter. Also, since they are small, it is possible to place multiple patch antennas on the exterior of the UAV in order to receive more power. Since the distance between the transmitter and the UAV is much greater than the distance between two points on the UAV, it can be assumed that there is no transmitter gain loss due to pointing accuracy. Using two patched antennas with an assumed gain of 0 dBi, results in a total equivalent receiving gain of 2 or 3 dBi. This way the gain can be artificially increased.

4.2 Lasers

4.2.1 Transmitting Laser

The next option to provide power remotely via electromagnetic radiation, is through lasers. The process of converting electricity to light and then back again tends to be inefficient, but lasers benefit from being highly directional with much smaller transmitters. Table 2 shows currently available high power lasers. This table shows that the max efficiency for converting electricity to light is around 50% using the Diode Laser.

Table 2. Currently available laser technologies. [30]

Laser Type	Wavelength, λ (nm)	Efficiency, η	Beam Quality, $B_x \times B_y$	Radiance, R_{source} (W/m²–sr)
Diode, 10 kW	850	50% DC to light	100 × 1.5	1×10^{10}
Spectral beam combining, 25 W	850	25% DC to light	4.5 × 3	2×10^{12}
Thin disk, 8 kW	1,060	25% DC to light	24 × 24	1.2×10^{13}
Thin disk, 25 kW	1,060	25% DC to light	3 × 3	2.4×10^{15}
Fiber, 2 kW	1,060	25% DC to light	1.2 × 1.2	1.2×10^{15}
Fiber, 10 kW	1,060	25% DC to light	15 × 15	4×10^{13}
Fiber, 20 kW	1,060	25% DC to light	35 × 35	1.4×10^{13}
Diode-pumped alkali, 48 W	795	25%–40% DC to light	1.2 × 1.2	6×10^{15}
Chemical oxygen iodine, 1 MW	1,315	300 kJ/kg	1.3 × 1.3	3×10^{17}
Hydrogen fluoride, 1 MW	2,700	150 kJ/kg	2 × 2	3×10^{16}
Deuterium fluoride, 1 MW	3,800	150 kJ/kg	2 × 2	2×10^{16}

SOURCES: Kare (2004), TRUMPF (2008), IPG (2008), Zhdanov, Sell,and Knize (2008), Cathcart (2007).

In order to have a high power transmission, it is important to analyze how a laser beam is actually formed. A Gaussian beam can be characterized by the radius of the beam spot at the transmitter, W_o, and the radius of curvature, F_o. The beam spot radius is defined as the distance at which the beam intensity falls below $1/e^2$ of the maximum on the beam axis [31]. The radius of curvature just describes the forming of the beam. The radius of curvature is used to find the curvature parameter, which is

$$\Theta_0 = 1 - \frac{s}{F_0} \tag{34}$$

where s is a given position down the length of the beam. The curvature parameter describes the radius of curvature of the wave front at some length down the beam [32]. There are

three different cases: when $F_o < 0$, $F_o > 0$, and $F_o = \infty$. These relate to a beam that is divergent, convergent, and collimated respectively. The ideal case is to have a collimated beam, which results in a curvature parameter of 1. This means that the wave front of the beam is perfectly flat. Another important factor is the beam divergence half angle. This is found by

$$\theta = B^2 \frac{\lambda}{\pi W_0} \tag{35}$$

where B is the beam quality. The beam divergence half angle describes how the beam spreads as it propagates. The quality of the beam can be different between the x-axis and y-axis of the beam. This is shown in Table 2 as the B_x and B_y values that are described. The B value itself, is just the root mean square of the x and y quality values. The radius of the beam spot down the path can be found using Eq. (36).

$$W_0 = \frac{W_0}{\left[\left(\frac{kW_0^2}{2F_0}\right)^2 + 1\right]^{1/2}} \tag{36}$$

So if the beam is highly collimated, i.e. $F_o = \infty$, the waist radius will be the same as the beam radius at the aperture.

In order to transfer power over a large distance, it is necessary to consider beam spreading. By reducing the spreading, it is able to minimize the size of the receiving apparatus. When designing a Laser for long distance transmissions, the two important characteristics that can be adjusted are the beam quality and the radius of curvature. Having a very large radius of curvature results in a curvature parameter of 1 and the spot size will be constant along the entire beam. From there, if the spot size is constant, the larger you make the beam waist the less the beam diverges. The desired beam quality is 1. That way

the divergence is only dependent upon beam waist. With these parameters met, high power transfer can be achieved.

4.2.2 Laser Propagation

Similar to microwaves, it is necessary to understand how the beam propagates through the atmosphere. Understanding this will allow for the efficiency of the transfer to be analyzed. Lasers can be directed more efficiently but because they fall within the visible spectrum, they are affected more by particles in the atmosphere. The intensity at the receiver in its simplest form, can be found by

$$I = \frac{\cos(\beta)P_t}{A_{spot}}\eta_a \tag{37}$$

and is in units of Watts per meter squared. By multiplying by a receiver area the incident power at the receiver can be found.

$$P_i = \frac{\cos(\beta)P_t}{A_{spot}}A_{rec}\eta_a \tag{38}$$

Where P_t is the power transmitted, A_{spot} is the spot size at the receiver, A_{rec} is the area of the receiver, η_a is the efficiency of transfer through the atmosphere, and β is the zenith angle. The $\cos(\beta)$ accounts for the power loss due to the incident angle. The efficiency is a term that depends upon the local atmospheric conditions.

The spot size of the receiver depends upon the initial spot size of the laser and the amount the beam spreads along the path. This can be determined by

$$A_{spot} = \pi\left(\frac{d_l + \alpha D}{2}\right)^2 \tag{39}$$

where d_l is the diameter of the beam when leaving the forming optics and α is how much the beam spreads along the path.

The beam spreading has several causes. The model used in this paper comes from work done by Breaux [33]. The total spreading is a combination of linear effects and non-linear effect. The linear effects come in the form of diffraction, turbulence, jitter, and beam wander. Non-linear effects come in the form of blooming. The total spreading is the root mean square of these values, as shown below.

$$\alpha = \sqrt{\sigma_{dif}^2 + \sigma_{turb}^2 + \sigma_{jit}^2 + \sigma_w^2 + \sigma_{bl}^2} \tag{40}$$

Because these beams have a divergence angle of less than 1 rad, the paraxial approximation holds true and therefore these beams are considered diffraction limited. The equation for the spreading due to diffraction is

$$\sigma_{dif}^2 = \left(\frac{m' B \lambda}{d_l}\right)^2 \tag{41}$$

where m' is a characteristic of the beam shape. For this work the beam shape is assumed to have a Gaussian profile that is truncated at $1/e^2$.

Turbulence within that atmosphere can have a twofold effect on beam spreading. It can affect the propagation path of the laser, considered a high-frequency effect, and it can affect the receiver or transmitter, considered a low-frequency effect. The term for spreading due to turbulence accounts for the high-frequency effect.

The atmosphere can be thought of as a large number of lenses that are constantly changing. These changes are brought about by turbulence. As the “lenses” are changed by the turbulence, the beam can be rendered incoherent. This effect is what causes the blurring and twinkling when viewing stars. An important parameter is the index-of-refraction structure constant, which is a measure of the strength of the turbulence. There are many

different ways to determine this value, as shown in Figure 29, but for this work a modified version of the Hufnagel-Valley 5/7 model

$$C_n^2(h) = 8.2 \times 10^{-26} \left(\frac{h}{1000}\right)^{10} X^2 e^{-h/1000} + 2.7 \times 10^{-16} e^{-h/1500} + 1.7 \times 10^{-14} e^{-h/100} \tag{42}$$

was used. In this model χ is the wind correlating factor, and was set to 21. [34] The Hufnagel-Valley 5/7 model estimates the index of refraction structure constant based on the altitude.

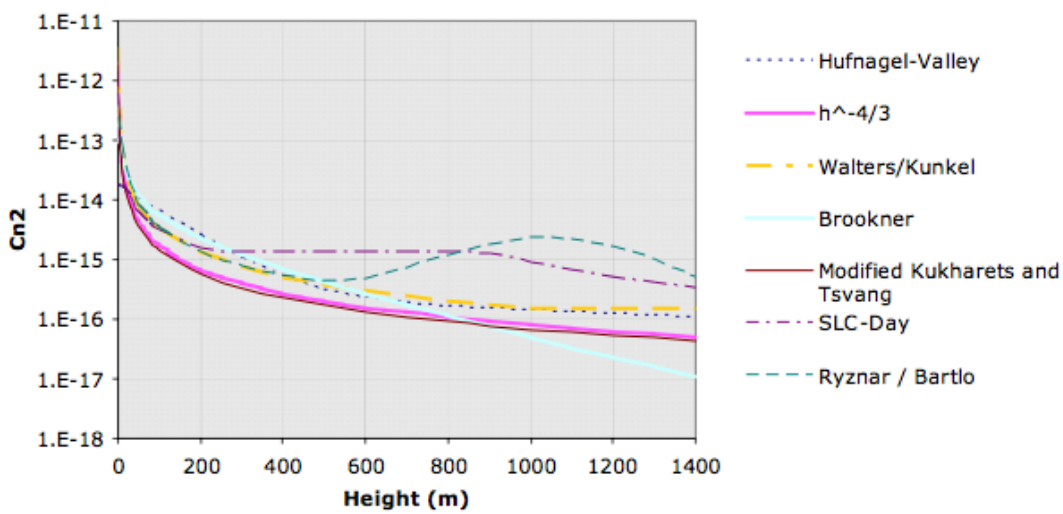

Figure 29. Various models of the index of refraction. [35]

It should be noted that the index of refraction is dependent upon current local atmospheric conditions. These models are based on empirical data, taken at specific locations at a specific time. The index-of-refraction structure constant can then be used to calculate the Fried coherence parameter.

$$r_0 = 2.1 \left[1.45 k^2 \int_0^D C_n^2(s) \left(\frac{D-s}{D}\right) ds \right]^{-5/3} \tag{43}$$

The Fried coherence parameter is a measurement of the length of the "lens" at which the beam remains coherent. Since the index of refraction changes with respect to the altitude, the original equation is modified so that it is now a function of the path length, resulting in

$$C_n^2(D) = 8.2 \times 10^{-26} \left(\frac{Dcos(\beta)}{1000}\right)^{10} X^2 e^{\frac{-Dcos(\beta)}{1000}} + 2.7 \times 10^{-16} e^{\frac{-Dcos(\beta)}{1500}} + 1.7 \times 10^{-14} e^{\frac{-Dcos(\beta)}{100}} \quad (44)$$

which allows for C_n^2 to be integrated with respect to the path length. Figure 30 shows experimental values for the fried parameter. The superimposed red dots represent the Fried parameter calculated using Eq.s (43) and (44).

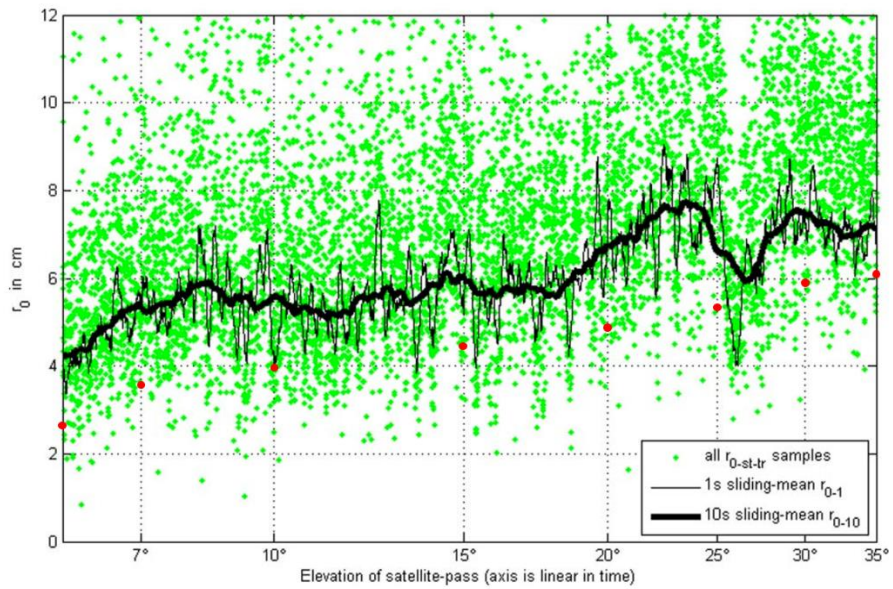

Figure 30. Experimental and calculated results for r_0 values for a laser with λ = 847 nm and d_l = 0.4 m. The red dots are the superimposed calculated values. [36]

Measurements in Figure 30 were taken by using a laser with an 847 nm wavelength and an aperture diameter of 0.4 m. The path was between a ground station and a satellite in a geo-synchronous orbit at 350 km. The variation between the calculated values and the mean experimental values, is due to the difference in the C_n^2 value at ground altitude for the Hufnagel-Valley model and where the data was taken.

The Fried parameter is used to calculate the effects due to turbulence.

$$\sigma_{turb}^2 = \begin{cases} 0.182 \left(\frac{\sigma_{dif}}{B}\right)^2 \left(\frac{d_l}{r_0}\right)^2 & if \left(\frac{d_l}{r_0}\right) < 3.0 \\ \left(\frac{\sigma_{dif}}{B}\right)^2 \left[\left(\frac{d_l}{r_0}\right)^2 - 1.18 \left(\frac{d_l}{r_0}\right)^{5/3}\right] & if \left(\frac{d_l}{r_0}\right) \geq 3.0 \end{cases} \quad (45)$$

Using a laser with a 1 m telescope, a beam quality of 15, and a wavelength of 1060 nm results in Figure 31.

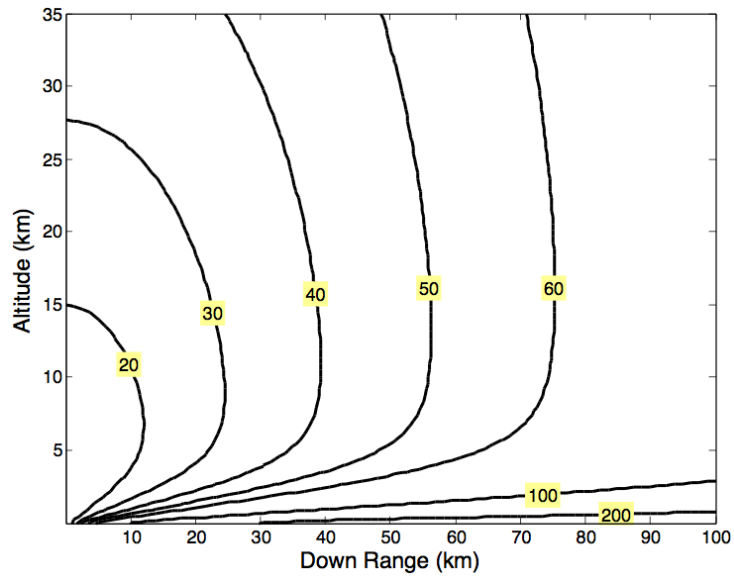

Figure 31. Beam spreading due to turbulence, in *μrad*, with B = 15, d_l =1 m, and λ = 1,060 nm.

Blooming is the self-induced thermal distortion of laser radiation. [37] For lasers with energy densities surpassing 1 MJ/cm^3, the air begins to break down into plasma causing extreme distortion of the radiation. While the lasers studied in this work do not reach this intensity, there is still a small effect do to thermal blooming. Thermal blooming is the result of the laser heating the atmosphere along the propagation path. This results in energy being dispersed into the surrounding atmosphere, thereby reducing the energy at the target. While this loss of energy is a small amount, the heating induces a temperature gradient thereby changing the index of refraction of the local atmosphere. The temperature gradient difference will actually induce turbulence, which will cause further spreading. [38] A comparison of a focal plane without blooming and one with blooming effects is shown in Figure 32.

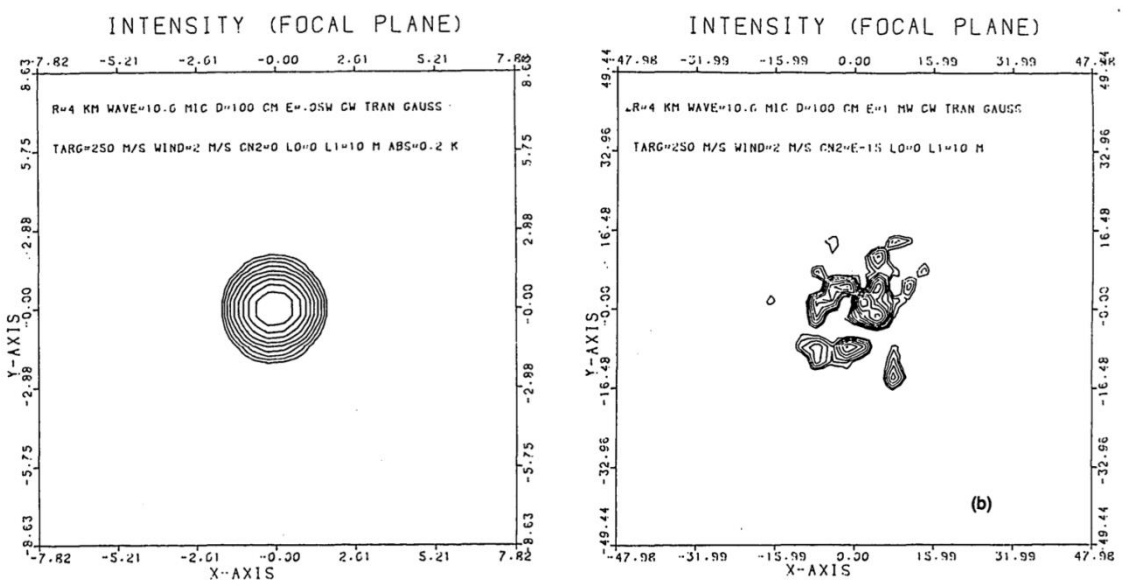

(a) (b)

Figure 32. Contours of a modeled laser profile (a) without blooming and (b) with blooming. [38]

The effect to due to blooming is a function of the beam qualities, the heating process, and the spreading of the beam. The equation for blooming is found to be

$$\sigma_{bl}^2 = C_B'\left(\sigma_{dif}^2 + \sigma_{turb}^2 + \sigma_{jit}^2\right)(\psi_h)^a \tag{46}$$

where C_B' and a are coefficients based on beam shape. The phase integral, ψ_h, is a function that describes the heating phase. The equation for the phase integral is

$$\psi_h = \int_0^1 \frac{N_D N_F e^{-\varepsilon s} dz}{N_Q'(1 + zN_S)\left[(1-z)^2 + \left(\frac{2zN_Q}{N_F}\right)^2\right]^{1/2}} \tag{47}$$

where $z = s/D$, N_S is the slew number, N_F is the Fresnel number, N_D is the distortion number, and N_Q and N_Q' are effective beam qualities. The equations for the parameters are

$$N_S = U_t/U_w \tag{48}$$

$$N_F = (.5\pi d_l^2)/(\lambda D) \tag{49}$$

$$N_D = 2.33 \times 10^{-9}[(P_t D N_A)/(.125 d_l^3 U_w)] \tag{50}$$

$$N_Q = \frac{\left(m^2\sigma_{dif}^2 + \sigma_{turb}^2 + \sigma_{jit}^2\right)^{1/2}}{\sigma_{dif,0}^2 m''} \tag{51}$$

$$N_Q' = \frac{\left(\sigma_{dif}^2 + \sigma_{turb}^2 + \sigma_{jit}^2\right)^{1/2}}{\left(\sigma_{dif}/B\right)} \tag{52}$$

where U_t is the target velocity, U_w is the wind velocity, m and $m''$are beam shape parameters. N_A is the absorption number and is found with

$$N_A = \varpi D \tag{53}$$

where ϖ is the absorption coefficient and is in units of km^{-1}. It was estimated to be around 0.0004 km^{-1}. [30] $\sigma_{dif,0}^2$ is a divergence term and dependent upon the wave length and diameter of the beam.

$$\sigma_{dif,0}^2 = \left(\frac{\lambda}{.5\pi d_l}\right)^2 \tag{54}$$

Figure 33 plots contours of the spreading due to blooming in *μrad*. This was done for a 12 kW laser, with a beam quality of 3, and a wavelength of 1,060 nm and a diameter of 1m. Due to the low intensity of this laser, the effects from blooming are small. Because of this, the term for blooming was just set to zero when modeling the total incident power.

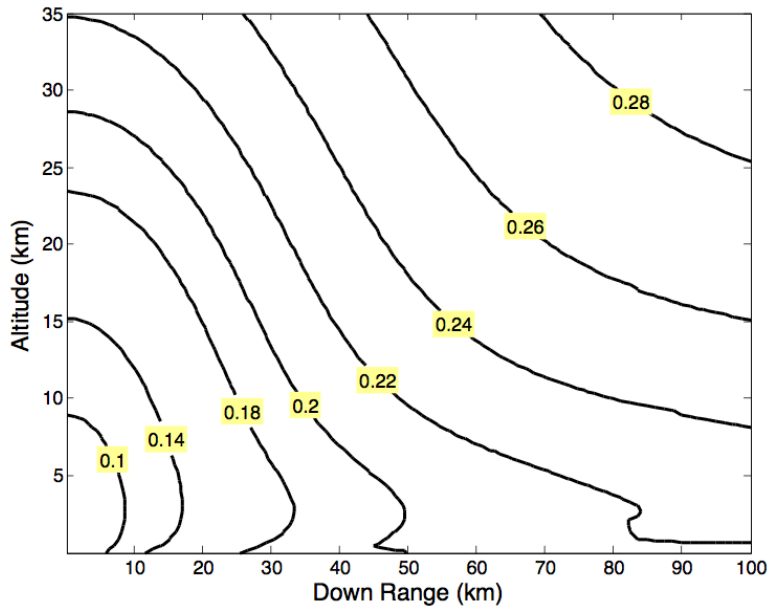

Figure 33. Beam spreading due to blooming, in μrad.

Jitter and wander are effects caused by stabilization and control of the transmitter and receiver. The low frequency effect from turbulence is incorporated into these terms. Placing the laser on an inertially stable platform and having a high pointing accuracy can reduce these terms. An inertially stable platform can reduce very dynamic motion to less than 6 μrad. [39] Since it is difficult to predict the exact mechanics of the transmitter system, the laser model used in this work used a combined value 10 μrad for the spreading due to jitter and beam wander. [30]

The next major part to take account for is the efficiency loss caused by the atmosphere. As stated before, modeling this efficiency loss is complex. Mathematically, the atmospheric attenuation looks like

$$\eta_a = e^{-\varepsilon D} \tag{55}$$

where ε is the attenuation coefficient per unit distance. This coefficient is due to absorption and scattering of the beam within the atmosphere. Elder, Strong, and Langer developed an

empirical model to estimate values for the absorption of the beam. The main parameter is the concentrations of water in the atmosphere. Several different methods have been created to determine the effects of scatter. Scattering is dependent upon the amount, and concentration, of particles in the atmosphere that would get in the way of the beam. A simple way of determining this is by relating the amount of particles present to the visibility of the atmosphere. [40]

Since estimating the visibility and the amount of water in the atmosphere is arbitrary, using experimental data is a much simpler and equivalent way of determining the attenuation coefficients. The atmospheric extinction values come from experimental data taken by Burle Industries. This can be seen in Figure 34. For the laser propagation model, this plot was digitized so that the extinction coefficient could be found for a range of altitudes. So an equation was used in the model that was dependent upon the path length.

$$\eta_a = e^{-\int_0^D \varepsilon ds} \tag{56}$$

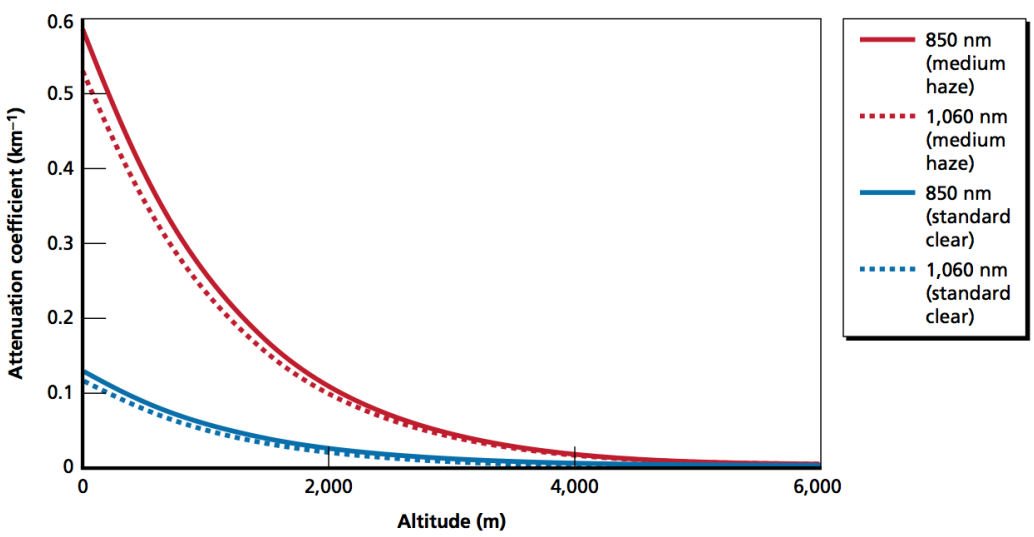

Figure 34. Extinction coefficient as a function of altitude, λ = 850 nm and 1,060 nm. [30]

With all the components understood, it is possible to predict the intensity of the beam at the receiver. Using Eq. (37) and substituting in Eq.s (39), (40),and (56) gives the

equation for intensity shown below. The equation is multiplied by 0.86 because it is assumed that it is a Gaussian beam, where only 86% of the power falls within the angular diameter. [30]

$$I = 0.86 \frac{4cos(\beta)P_t e^{-\int_0^D \varepsilon ds}}{\pi\left(d_l + D\sqrt{\sigma_{dif}^2 + \sigma_{turb}^2 + \sigma_{jit}^2 + \sigma_w^2 + \sigma_{bl}^2}\right)^2} \tag{57}$$

Plotting the results of this equation results in in Figure 35. This plot models a Laser with a wavelength of 1,060 nm, a beam quality of 15, and an aperture diameter of 1 meter. This figure shows that the intensity of the beam is greater closer to the point of origin. Also the intensity falls of much more rapidly in the horizontal direction. This makes sense because according to the Hufnagel-Valley model, the turbulence is stronger closer to the ground. This increases the spreading due to turbulence, as shown in Figure 31. Also the extinction coefficient is greater near the ground.

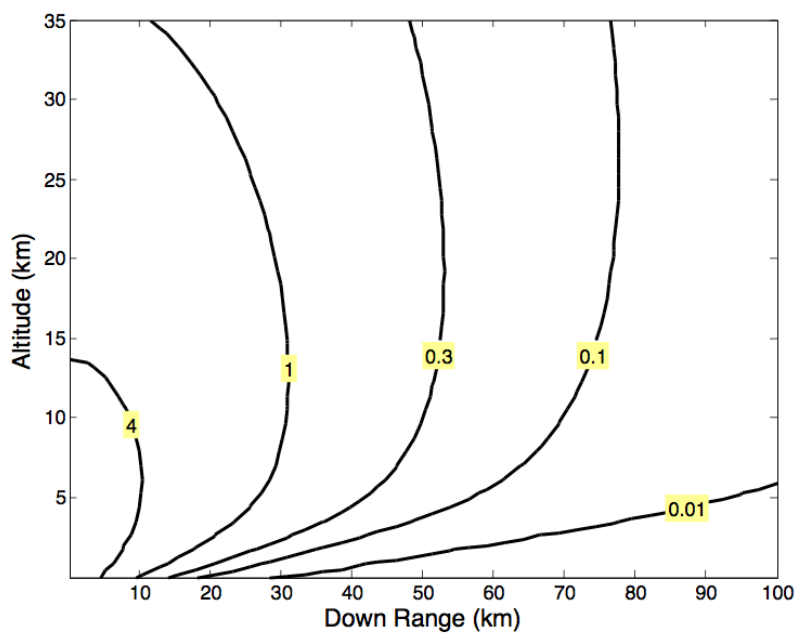

Figure 35. Intensity at the receiver in kW/m^2 from a 10 kW laser, with B = 15, d_l =1 m, and λ = 1,060 nm at standard clear conditions.

As the beam propagates, the beam spot increases in size. To obtain the maximum possible power from the transmitter, the receiver has to be sized to capture all incident power. Multiplying Eq. (57) by Eq. (39) results in the maximum possible power. Figure 36 plots contours of the maximum possible incident power. According to this figure, it is possible to maintain around 4 kW of power out to about 10 km for a horizontal path, and around 7 kW up to 15 km for a vertical path.

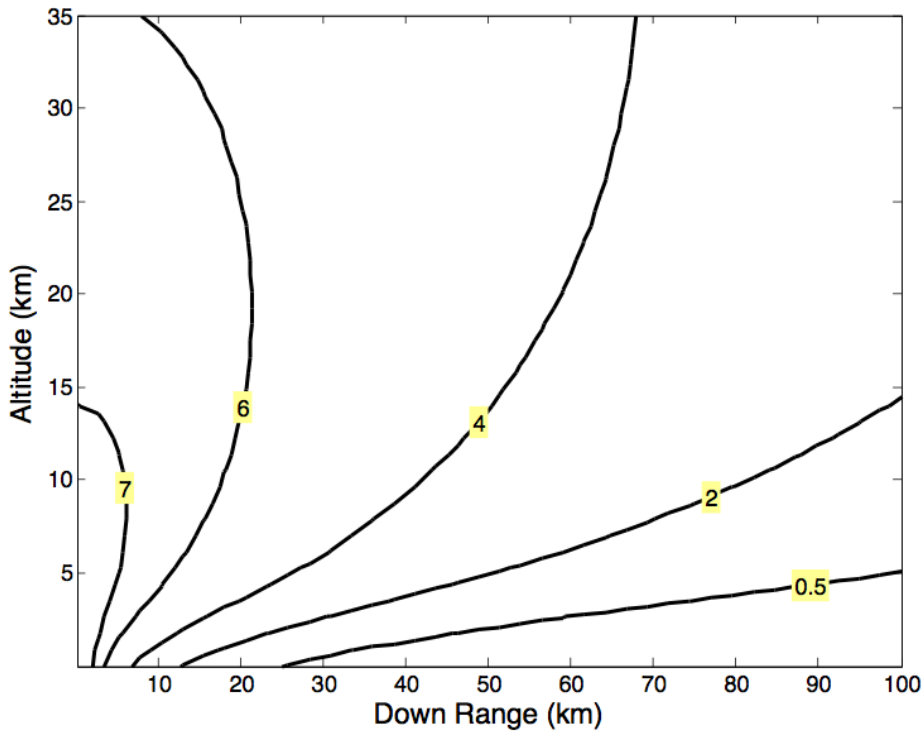

Figure 36. Maximum incident power at the vehicle in kW, assuming receiver is sized to match the spot size, with a 10 kW laser, with B = 15, d_l =1 m, and λ = 1,060 nm.

To determine if these contours are reasonable, Figure 37 show intensity contours with the same parameters as in Figure 35. The figures share the same general idea and are similar in values. However, in Figure 37, a greater intensity is achieved a farther distances. This is due to several key differences in models. For Figure 37, the index-of-refraction structure constant is assumed constant unless within 35° degrees of zenith and a modified

version of the turbulence equation is used. This results in much lower values for spreading due to turbulence. The assumption is also made that the extinction coefficient is constant. In Figure 37 a simplification is made to the equation for the spot size. By assuming the path length is much greater than the aperture diameter, i.e. $D \gg d_l$, Eq. [(39)] can be simplified as shown.

$$A_{spot} = \pi \left(\frac{\alpha D}{2}\right)^2 \tag{58}$$

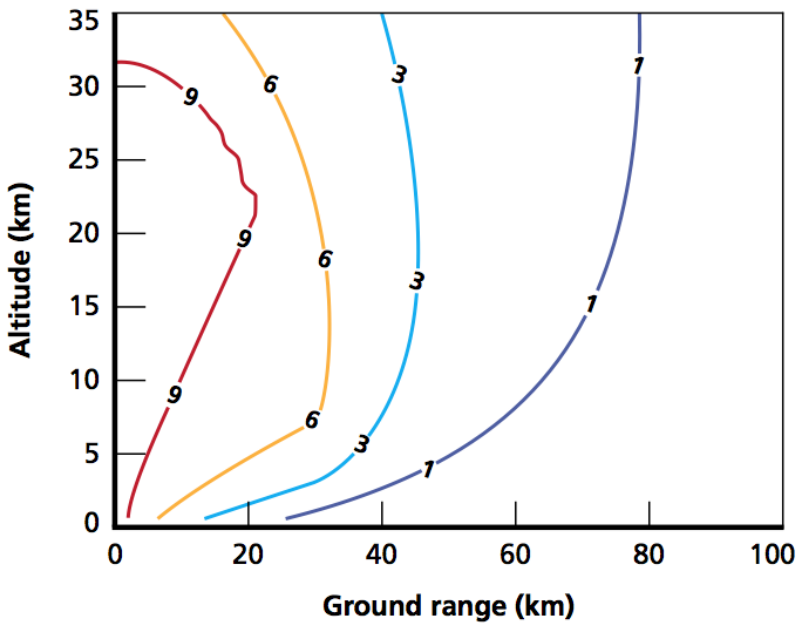

Figure 37. Intensity results from Mason using a 10 kW laser, with B = 15, d_l =1 m, and λ = 1,060 nm at standard clear conditions. [30]

The aforementioned differences make the model used for this work a more conservative estimate of achievable power transfer. While this model is useful for this paper, for a true application of this work it would be beneficial to find a better model. It would be necessary to get statistical data on the atmospheric conditions of the mission location. This would allow for a more accurate model of the absorption coefficient to be

determined. The turbulence and jitter models would also benefit from a more in-depth analysis.

4.2.3 Receiving Laser Power

Energy from a laser is converted back into electricity the same way as collecting solar energy, by using photovoltaic cells. Solar energy is considered inefficient because the max amount of energy converted is usually only around 20% of total incident radiation. Lasers actually have an advantage in that they are only one wavelength. Photovoltaic cells can be tuned to a specific frequency, resulting in higher efficiencies, as shown in Figure 38.

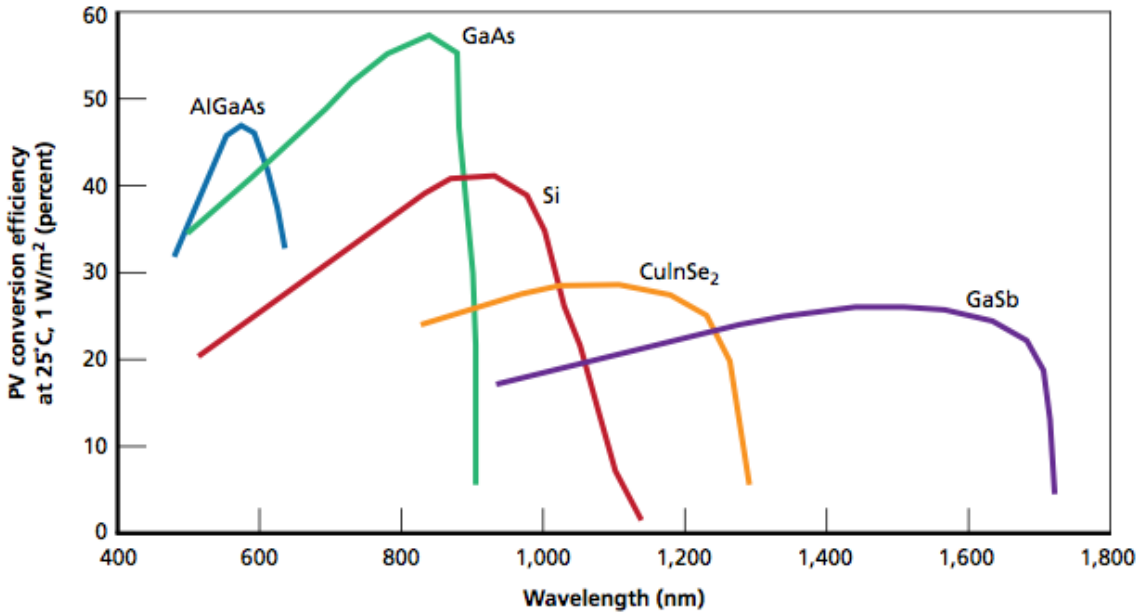

Figure 38. Conversion efficiencies of several different photovoltaic materials. [30]

It's also important to note that the efficiency of photovoltaic cells are not constant. As shown in Figure 39, there is a max efficiency for a photovoltaic cell that depends upon the intensity on the receiver. These cells also have an optimum operating temperature.

Because of how sensitive these cells are, a large amount of energy can be wasted if the optimum conditions are not met.

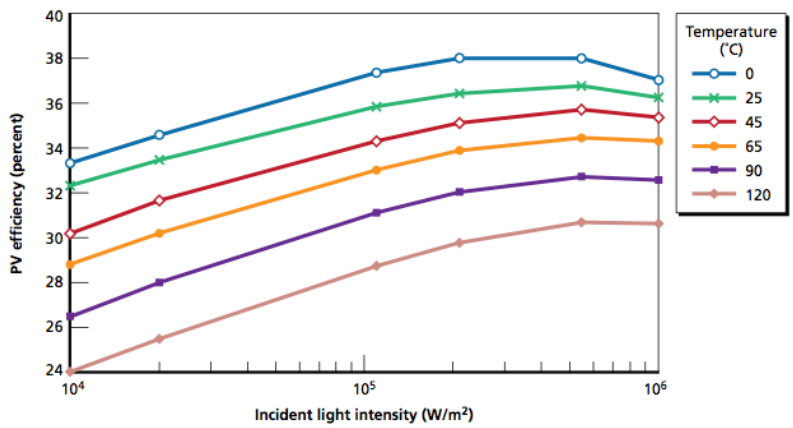

Figure 39. Photovoltaic efficiency for a Spectrolab CDO-100 solar cell. [30]

It has already been determined that, as the beam propagates, the spot size at the receiver increases with distance. Ideally, a receiver would be designed to be the same size as the spot size, at the maximum distance that the mission requires. This way, the maximum amount of power would be transmitted. However, this is not always possible due to size constraints on the vehicle. Figure 40 shows how the area of the spot size changes.

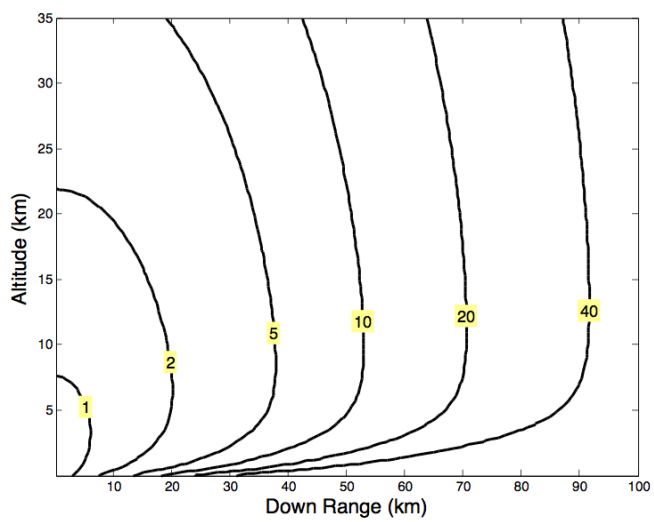

Figure 40. Contours of the area of the beam spot for a range of altitudes and distances in m^2.

This figure shows that the beam spot increases very rapidly down range, especially at low altitudes. Since it would be impossible to build photovoltaic arrays of these sizes on small UAVs, it must be accepted that even more power will be lost at greater path distances.

5. Remote Power Vehicle Sizing

This section is the main focal point of this work, and all the sizing equations were derived by specifically for this paper. For a remotely powered vehicle, the weight fraction of the onboard energy source is broken into the weight fraction of the receiver and the weight fraction of the battery.

$$\frac{W_{OES}}{W_{TOGW}} = \frac{W_{rec}}{W_{TOGW}} + \frac{W_{bat}}{W_{TOGW}} \tag{59}$$

There are three different scenarios for powering remotely powered vehicles. The first is where the vehicle is only solely by a remote source up to some range requirement R. In the second scenario, the vehicle is powered to a distance ℓ that the receiver is sized to, and then a battery provides all the energy to the vehicle out to some distance R. In the last scenario, the transmitter continues to provide power while the battery provides the remaining power necessary. The three scenarios are depicted in Figure 41.

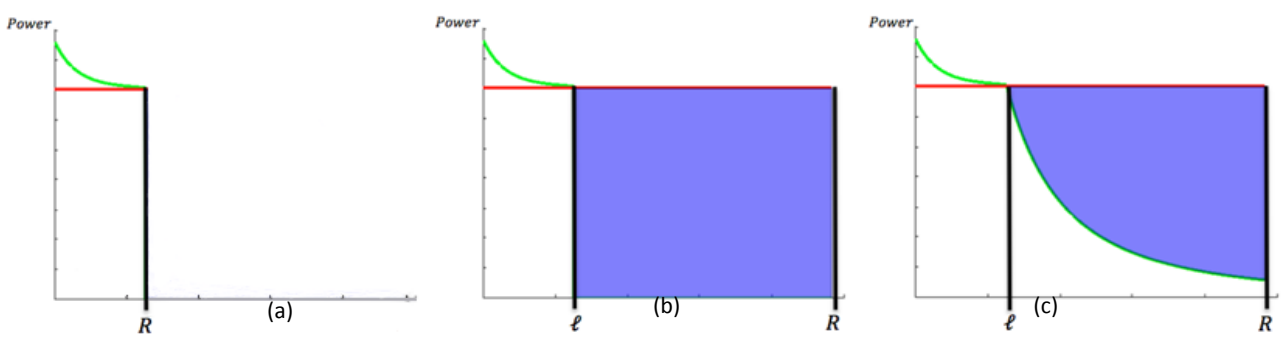

Figure 41. Three scenarios for sizing: (a) laser provides all the power; (b) remotely powered, then only battery powered; or (c) battery is augmented with remote power.

The two most important parameters for sizing an aircraft that is remotely powered, are the total downrange distance from the receiver, R, that the vehicle will go and the downrange distance, ℓ, that the receiver will be sized to. The distance ℓ, is the maximum distance at

which the vehicle can be completely powered remotely. The distance from the transmitter is found from the downrange distance and the altitude.

$$D = \sqrt{\ell^2 + h^2} \tag{60}$$

To determine the battery weight fraction, it is necessary to determine the total specific energy required for the mission. The total specific energy of the mission consists of the energy necessary for the payload, the energy necessary for the downlink, and the energy needed to power the propulsion for any mission leg. This gives

$$\frac{E_{bat}}{W_{TOGW}} = \frac{E_{pay}}{W_{TOGW}} + \frac{E_{com}}{W_{TOGW}} + \sum_{i=1}^{n} \frac{E_{leg,i}}{W_{TOGW}} \tag{61}$$

where n is the number of legs, E_{pay} is the energy required by the payload, E_{com} is the energy required for the communications downlink, and $E_{leg,i}$ is the energy of the *i*th mission leg. The energy of the payload is determined by the power draw of the payload multiplied the time of the mission. Dividing by the takeoff weight gives the weight fraction.

The power necessary to create the downlink can be found using the signal to noise ratio equation. This equation can be transformed to solve for the necessary transmitting power

$$P_{com} = \left(\frac{E}{N}\right) \frac{kT_s(DR)L_l L_a L_{fs} margin}{G_t G_r} \tag{62}$$

where k is the Boltzman constant, $\frac{E}{N}$ is the system noise temperature, DR is the data rate, L_l is the line loss, and $margin$ is a desired gain margin. Integrating this with respect to time and dividing by the takeoff weight creates the energy weight fraction.

The equations for the mission leg energy fractions can be found in section *2.3 Modifying Breguet Range Equation*. Dividing Eq. (61) by the specific energy of the battery type gives the battery weight fraction.

$$\frac{W_{bat}}{W_{TOGW}} = \frac{1}{\varrho}\frac{E_{bat}}{W_{TOGW}} \tag{63}$$

5.1 Sizing Vehicle with Microwaves

5.1.1 Patch Antenna System Weight

From before, a patch antenna will be used to receive the microwaves. In order to estimate the weight, a commercially available antenna is used as a baseline for estimates. The antenna used was an AA-800-6000 Appliqué, as shown in Figure 42. It is 5” long and 2” wide, and the cable is 14.75” long. The entire system only weighs 0.28 oz.

Figure 42. Patch antenna used for weight model.

For design purposes, it is important to understand how adding a receiver would increase the weight of the aircraft. The two components considered are the patch antennas and a DC-DC converter. Because the power received by the panels is not guaranteed to be consistent, a DC-DC converter is necessary to make sure the appropriate voltage is applied to the system. This way the weight of the receiver can be estimated by the following.

$$W_{rec,micro} = W_{patch} + W_{DC} \tag{64}$$

The weight of the patch can be estimated from the area required to receive the necessary amount of power

$$W_{patch} = NW_{pa} \tag{65}$$

where N is the number of patch antennas necessary, and W_{pa} is the weight of each patch and is equal to 0.28 oz. These antennas have an adhesive side so there is no need for any extra equipment in order to mount them.

The number of patches necessary is found by determining the total gain necessary on the receiving end. This is done by adding the power from each antenna together, resulting in

$$P_r = \frac{P_t G_t}{L_{fs} L_a} \left(\sum_{I}^{N} G_{r,i} \right) \tag{66}$$

where m is the number of antennas and $G_{r,i}$ is the receiving gain for each respective antenna. The assumption that the distance between the receiving antennas is much smaller than the distance from the transmitting antenna, allows for the assumption of a constant transmitter gain and that the gains the receivers are approximately the same. Applying this assumption to Eq. (66) and solving for N results in Eq. (67).

$$N = \frac{L_{fs} L_a P_r}{P_t G_t G_r} \tag{67}$$

The gain of the receiving antennas is determined from the gain pattern of the patch antenna used. This is shown in Figure 43.

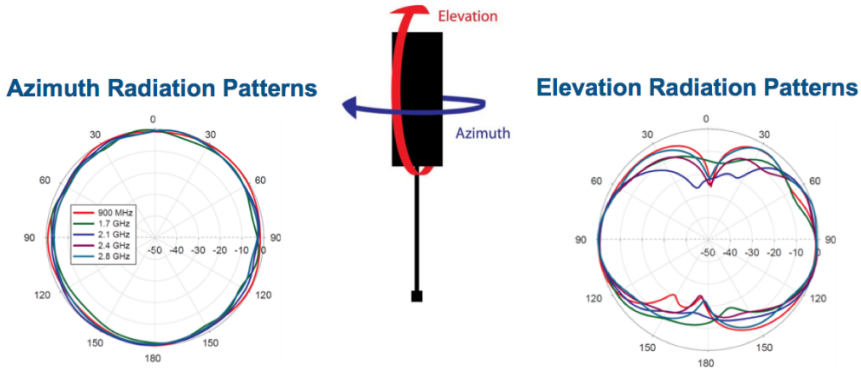

Figure 43. Gain patterns for patch antenna.

By determining the location and orientation of the UAV with respect to the transmitter, the receiver gain can be estimated.

The weight of a DC-DC converter varies substantially depending on the desired requirements. In order to determine a method of estimation, multiple converters were examined and a correlation between the maximum power output and the weight was established. This can be seen in Figure 44.

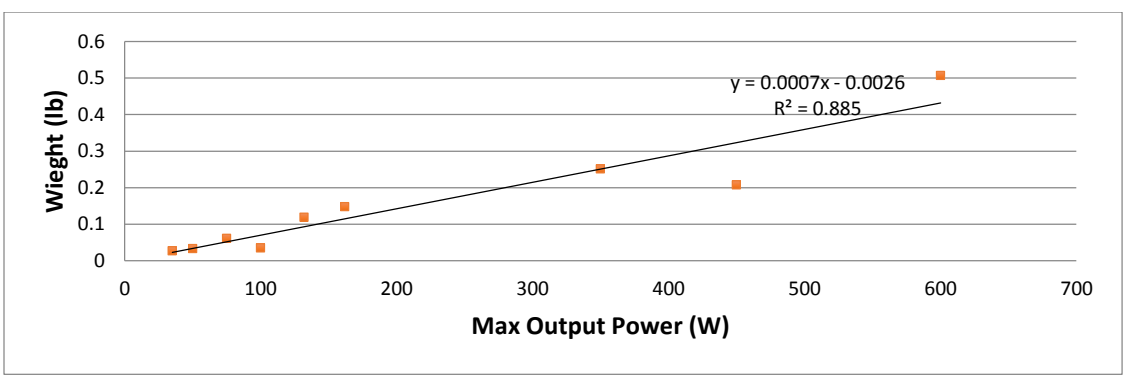

Figure 44. Historical data of how the weight of a converter is affected by the max power output.

Using the linear regression found with the historical data, an estimation of the weight of a DC-DC converter is found to be

$$W_{DC} = 0.0007P_{max} - 0.0026 \tag{68}$$

where P_{max} is the maximum input power to the converter.

5.1.2 Microwave Receiver Weight Fraction

When sizing a remotely powered vehicle, the receiver weight fraction in Eq. (59) is made up of the weight fraction of the patch antennas and the weight fraction of the DC-to-DC converter.

$$\frac{W_{rec}}{W_{TOGW}} = \frac{W_{patch}}{W_{TOGW}} + \frac{W_{DC}}{W_{TOGW}} \tag{69}$$

The first step for sizing a vehicle powered by microwaves is to determine the number of antennas needed to receive the necessary power. Dividing Eq. (67) gives the number of patches to weight ratio.

$$\frac{N}{W_{TOGW}} = \frac{L_{fs}L_a}{P_t G_t G_r}\left(\frac{P_r}{W_{TOGW}}\right) \tag{70}$$

The power received is transformed into the power needed by dividing by the efficiency of the motor, the efficiency of the propeller, and the efficiency of the speed controller.

$$\frac{N}{W_{TOGW}} = \frac{L_{fs}L_a}{P_t G_t G_r \eta_{rec}}\left(\frac{P_n}{W_{TOGW}}\right)\frac{1}{\eta_{prop}\eta_{motor}\eta_{sc}} \tag{71}$$

The power received to weight term is the important part of this equation. This fraction is found by adding Eq.s (7), (62), the power draw of the payload, and dividing the latter two by weight.

$$\frac{P_n}{W_{TOGW}} = \frac{P_{leg}}{W_{TOGW}} + \frac{P_{com}}{W_{TOGW}} + \frac{P_{pay}}{W_{TOGW}} \tag{72}$$

Using Eq. (65) along with Eq. (92) results in the antenna weight fraction.

$$\frac{W_{patch}}{W_{TOGW}} = \frac{N}{W_{TOGW}} W_{pa} \tag{73}$$

It is then necessary to size the battery portion of the mission. For the first case, where the transmitter stops powering once the UAV has passed distance ℓ, the equation for the weight fraction of the battery is the same as Eq. (63). For the second case, it is necessary

to make some adjustments. Now the battery weight fraction is equal to the battery weight fraction minus the weight of a battery that holds the equivalent amount of energy that the microwave provides.

$$\frac{W_{bat,micro}}{W_{TOGW}} = \frac{W_{bat}}{W_{TOGW}} - \frac{W_{MEB}}{W_{TOGW}} \tag{74}$$

Where

$$\frac{W_{MEB}}{W_{TOGW}} = \left(\frac{N}{W_{TOGW}}\right)\frac{P_t G_t \eta_{rec}}{\sigma_{bat}} \int \frac{G_r}{L_{fs} L_a} dt \tag{75}$$

and it should be noted that this work assumes that the battery portion consists of a cruise leg out to distance *R*, and a return cruise leg. Because of this, the change in time is equal to the change in distance divided by the velocity. This changes the microwave equivalent battery weight to

$$\frac{W_{MEB}}{W_{TOGW}} = 2\left(\frac{N}{W_{TOGW}}\right)\frac{P_t G_t \eta_{rec} N}{v \sigma_{bat}} \int_{\ell/v}^{R/v} \frac{G_r}{L_{fs} L_a} ds \tag{76}$$

where s is the down range path distance. When determining the battery weight fraction, Eq. (8) is simplified.

$$\left(\frac{E_{leg}}{W_{TOGW}}\right) = 2\left(\frac{F_D}{W_{TOGW}}\right)\frac{(R-\ell)}{\eta_{prop}\eta_{motor}\eta_{sc}\alpha} \tag{77}$$

This assumes that there is only one mission leg for the battery-powered portion. The factor of two is included to account for the energy for trip out to distance *R* and the trip back.

The next part is to determine the weight fraction of the DC-to-DC converter. In Eq. (68) the DC-DC converter is dependent upon the maximum power put into the converter. Dividing Eq. (68) by the takeoff weight, and assuming that the maximum power received by the converter is two times the maximum power needed, an equation for the weight fraction can be found to be

$$\frac{W_{DC}}{W_{TOGW}} = 0.0001\left(\frac{P}{W_{TOGW}}\right)\frac{1}{\eta_{prop}\eta_{motor}\eta_{sc}} - 0.0026 \tag{78}$$

where $\frac{P}{W_{TOGW}}$ is the power to weight ratio found from a constraint diagram.

With all the weight fractions solved for, it is possible to solve for the takeoff weight given an initial takeoff weight guess. The power to weight ratio can be found from a constraint diagram. The range, velocity, and altitude can all be found from mission requirements. Using an iterative solver, the takeoff weight can be solved for. Figure 45 shows how contours of the takeoff gross weight changes with respect to the sizing distance and various transmitter parameters. For all plots a cruise velocity of 57 ft/s was used, at an altitude of 1000 ft.

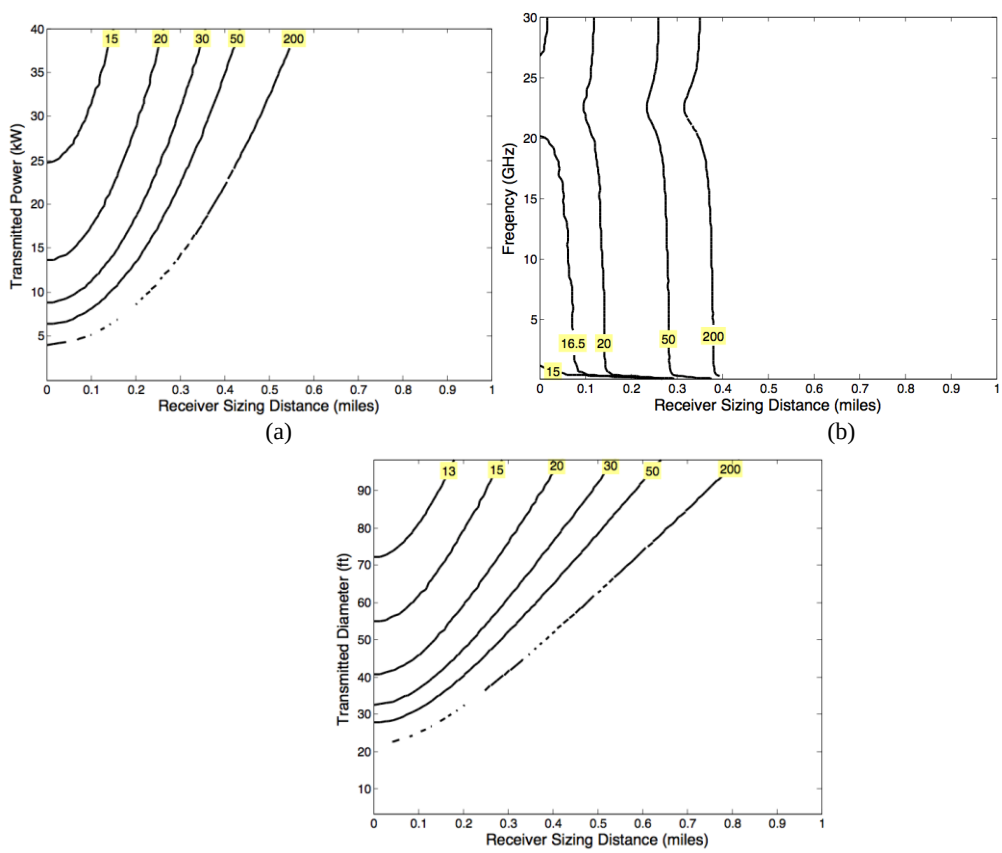

Figure 45. Plots of the W_{TOGW} (a) P_t = 20 kW and f = 5 GHz (b) P_t = 20 kW and $d_{t,micro}$ = 65 ft (c) f = 5 GHz and $d_{t,micro}$ = 65 ft

The contour lines start to break up as the necessary transmitted power to run the UAV becomes greater than the power being transmitted. Increasing the power is a simple way of increasing the sizing distance, and reducing the weight at specific distances. Even with large power outputs, the UAV can only be powered over short distances. This is due to the tendency of microwaves to spread rapidly. Changing the frequency has very little effect on the takeoff gross weight, unless the frequency is within the high absorption band, around 22 GHz.

Increasing the diameter of the transmitter dish, results in a larger transmitter gain. This is allows the vehicles to be sized to greater distance, and decreases the weight at shorter distances. However, this hinges on the ability to have the space, and ability, to create these sizes. These large sizes would rule out the likelihood of using a microwave transmitter.

5.2 Sizing Vehicle with Lasers

5.2.1 Laser Receiver: Flat Panel PV Array

It's already been determined that photovoltaic cells are needed to convert the light energy into electrical energy. This then raises the question of how will the photovoltaic cells be placed on the aircraft. The simplest way to do this is to just place them on them on the bottom of the vehicle, however this causes issues that must be accounted for. Photovoltaic cells only capture energy that comes in normal to the cell plane. So at steady level flight, the total power at the receiver is actually only the power multiplied by the cosine of the zenith angle. To see how this effects the power transmission, Figure 36 was now considered with the $cos(\beta)$ term accounted for. This results in Figure 46. It shows that

this term does not affect the higher altitudes that much, but it comes into play when considering lower altitude operations at large ranges.

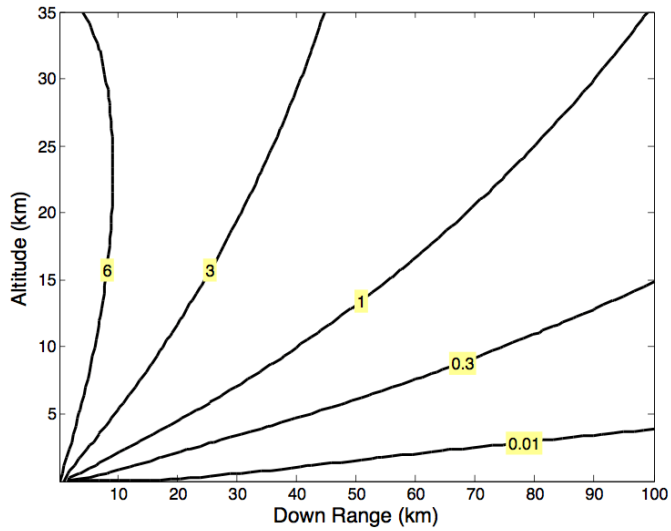

Figure 46. Power Received using a flat panel, assuming panel sized to spot size. Using a 10 kW laser, with B = 15, d_l =1 m, η_{rec}=0.25, and λ = 1,060 nm at standard clear conditions.

Figure 46 only considers the case of steady level flight. If there were to be any pitch angle or roll angle, there would be even more losses. There could also be the case that, due to the orientation of the aircraft, the beam would not be able to reach the receiving array at all.

The equation for the weight of the receiver is the almost identical to the equation for the weight of the receiver when using a patch antenna.

$$W_{rec,las} = W_{pan} + W_{DC} \tag{79}$$

where W_{pan} is the weight of the receiving panel. The weight of the converter is found from Eq. (68) The panel weight can be estimated from the size of the panel and how it is mounted. This results in

$$W_{pan} = A_{rec}\delta\kappa \tag{80}$$

where A_{rec} is the area of the receiver, δ is the weight per area, and κ is a mounting factor. To determine the area necessary, Eq. (38) can be rearranged to solve for A_{rec}. Substituting in Eq. (39), (55), assuming a Gaussian profile, and accounting for the efficiency of the receiving material shows that the area of the receiver can be found from

$$A_{rec} = \frac{\pi(d_l + \alpha D)^2}{3.44e^{-\varepsilon D}\eta_{rec}cos(\beta)}\left(\frac{P_r}{P_t}\right) \tag{81}$$

where η_{rec} is the efficiency of the receiver, P_r is the power received, and P_t is the power transmitted. The power received comes is equal to the incident power, divided by the efficiency of the receiving material.

5.2.2 Laser Receiver: PV Array on Turret

One way to make sure the photovoltaic array is normal to the beam, is to place the array on a turret like the one shown in Figure 47. This would greatly reduce the incident angle of the incoming beam, but there are several drawbacks as well. Adding a turret like this would have a much greater added weight than just the panels themselves. It would also need to stick out of the airframe in order to place the array in the needed position. This would increase the overall drag and therefore require more power. This becomes a tradeoff on whether the added power requirements, due to running the servo motors and weight increase, makes up for the decrease in incident angle.

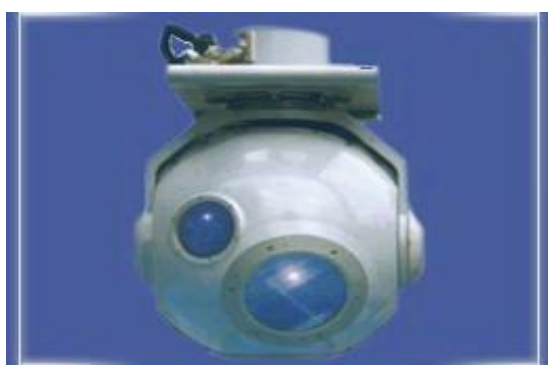

Figure 47. 360 degree gimbaled turret.

Sizing of the turret is similar to that of the panel except now there is an added term for the weight of the turret itself. This is shown in

$$W_{rec} = W_{pan} + W_{DC} + W_{tur} \tag{82}$$

where W_{tur} is the weight of the turret and includes all the motors, servos, and mounting in order to operate it. Like the DC-DC converter, the weight of the turret is estimated through a historical regression shown in Figure 48.

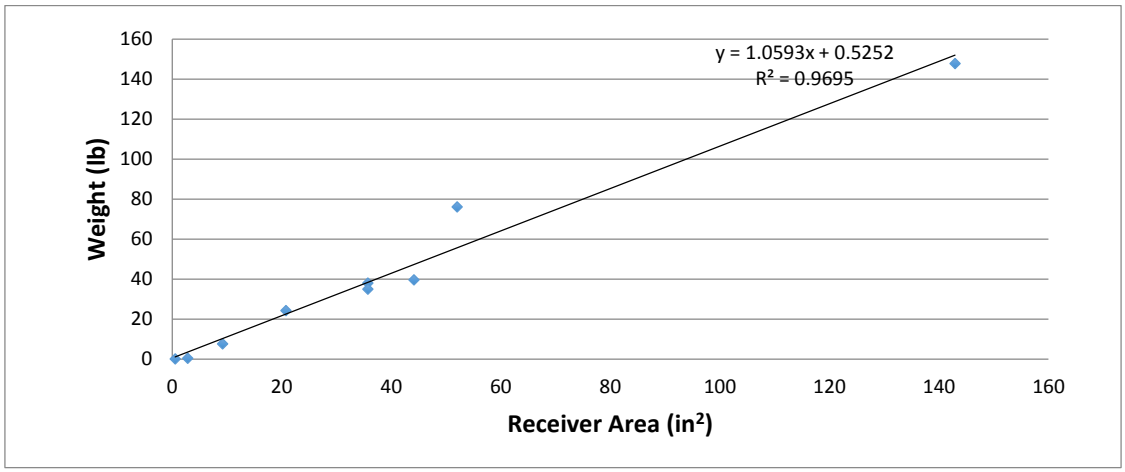

Figure 48. Historical regression showing how the weight of the turret is related to the diameter.

Initially a correlation between the diameter of the turret and the weight is found. The relationship between the diameter of the turret and the diameter of the receiving panel on the turret is found by using Figure 49. It is assumed that the beam will very rarely be horizontal. Therefore, the receiving panel on the turret does not need to be able to reach a perpendicular state. This allows for the size of the turret to be reduced. A minimum ϕ value of 10° is used, that way even of the beam is perfectly horizontal, 98.5% of the power will still be received.

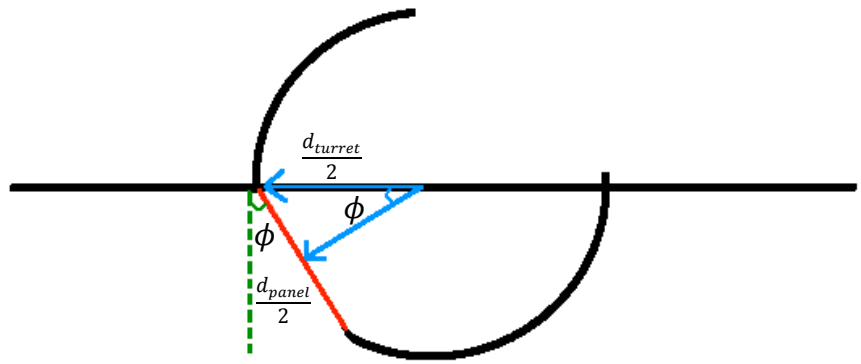

Figure 49. Dimensioned side view of turret.

This ϕ allows for a relationship between the area of the receiving panel and the diameter of the turret to be found. Using the historical regression, the weight function is found.

$$W_{tur} = 1.0593A_{rec} + 0.5252 \tag{83}$$

Equation (81) can be substituted in for the area of the receiver.

5.2.3 Laser Receiver Weight Fraction

The receiver weight fraction for a remotely powered UAV using lasers includes the weight fraction of the receiving panel, the weight fraction of the DC-to-DC converter, and the weight of the turret if one is used.

$$\frac{W_{rec}}{W_{TOGW}} = \frac{W_{pan}}{W_{TOGW}} + \frac{W_{DC}}{W_{TOGW}} + \frac{W_{tur}}{W_{TOGW}} \tag{84}$$

A slightly different approach is taken to sizing a remotely powered vehicle using lasers. Unlike microwaves, for lasers, a receiver can be sized in order to capture all incident laser radiation. This allows for the necessary transmitted power to be calculated. In order to solve for the necessary transmitted power, Eq. (81) is rearranged. The receiver is to be sized so that, at distance ℓ, the size of the receiver is equal to beam spot size. Solving for

the transmitted power, and substituting converting the power received into the power needed the necessary transmitted power.

$$P_t = \frac{P_n}{0.86cos(\beta)e^{-\varepsilon D}\eta_{rec}\eta_{prop}\eta_{motor}\eta_{sc}} \tag{85}$$

Dividing and multiplying by the takeoff gross weight gives

$$P_t = \left(\frac{P_n}{W_{TOGW}}\right)\frac{W_{TOGW}}{0.86cos(\beta)e^{-\varepsilon D}\eta_{rec}\eta_{prop}\eta_{motor}\eta_{sc}} \tag{86}$$

where the power needed weight fraction is found from Eq. (72).

The next step is to solve for the receiver area weight fraction. This is done by taking Eq. (81) and converting the power received to power needed, and substituting in the drag force and velocity. Excluding the initial takeoff weight guess gives Eq. (87).

$$\frac{A_{rec}}{W_{TOGW}} = \left(\frac{P_n}{W_{TOGW}}\right)\frac{A_{spot}}{0.86cos(\beta)e^{-\varepsilon D}\eta_{rec}\eta_{prop}\eta_{motor}\eta_{sc}} \tag{87}$$

Combining this with Eq. (80) gives panel weight fraction of the vehicle.

$$\frac{W_{pan}}{W_{TOGW}} = \frac{A_{rec}}{W_{TOGW}}\delta\kappa \tag{88}$$

The weight fraction for the DC-to-DC converter is the same as Eq. (78) The historical regression for the weight of the turret is dependent on the necessary receiver panel size, so all that needs to be done is divide Eq. (83) by the takeoff weight. This gives

$$\frac{W_{tur}}{W_{TOGW}} = 1.-503\left(\frac{A_{rec}}{W_{TOGW}}\right) + \frac{0.5252}{W_{TOGW}} \tag{89}$$

where $\left(\frac{A_{rec}}{W_{TOGW}}\right)$ is found from Eq. (87). Adding together Eq.s (78), (88), and (89) results in the total weight fraction due to the receiver.

The battery weight fraction equation for a UAV using a laser system is similar to that of one using a microwave system. If the battery portion is not being augmented by

power from the laser, then the battery weight fraction is just as Eq. (63). If the battery portion is being augmented, then the battery weight fraction is

$$\frac{W_{bat,laser}}{W_{TOGW}} = \frac{W_{bat}}{W_{TOGW}} - \frac{W_{LEB}}{W_{TOGW}} \tag{90}$$

where W_{LEB} is the weight of a battery equivalent to in size to the energy provided by the laser.

$$\frac{W_{LEB}}{W_{TOGW}} = \left(\frac{A_{rec}}{W_{TOGW}}\right)\frac{3.44P_t\eta_{rec}}{\pi\sigma_{bat}}\int\frac{cos(\beta)e^{-\varepsilon D}}{(d_l + \alpha D)^2} \tag{91}$$

Using the same mission profile as before, allows for Eq. (77) to be used when solving for the battery weight fraction. This also changes Eq. (91).

$$\frac{W_{LEB}}{W_{TOGW}} = \left(\frac{A_{rec}}{W_{TOGW}}\right)\frac{3.44P_t\eta_{rec}}{V\pi\sigma_{bat}}\int_{\ell/v}^{R/v}\frac{cos(\beta)e^{-\varepsilon D}}{(d_l + \alpha D)^2} \tag{92}$$

Using these equations, and their results, the gross takeoff weight can then be solved for.

Figure 50 shows contours of the gross takeoff weight, with respect to the sizing distance and various sizing parameters. As before, the contours get cut off where the necessary transmitted power is greater than the actual transmitted power. Figure 50 (a) and (b) show how the effects of increasing the transmitted power and increasing the receiving panel efficiency, respectively. These two plots show that, changing the transmitted power and receiving efficiency has the same effect. This is to be expected as the received power is directly related to both the efficiency of the receiver and the power transmitted.

Figure 50 (c) shows that there is an optimum aperture diameter. It is around 0.1-0.2 for small distances, and increases with the sizing distances. This is because, over small distances, the smaller the aperture diameter is, the smaller the initial spot size is smaller.

However, smaller aperture diameters cause greater diffraction as seen in Eq. (41). Overtime they spread more, resulting in larger spot sizes.

Figure 50 (d) shows that better quality beams result in lower weights, which is to be expected. Also the greater the sizing distance, the more important the beam quality is. Just as the aperture diameter, this is due to the diffraction effect. Diffraction is directly related to quality of the beam. For all plots a cruise velocity of 57 ft/s was used, at an altitude of 1000 ft.

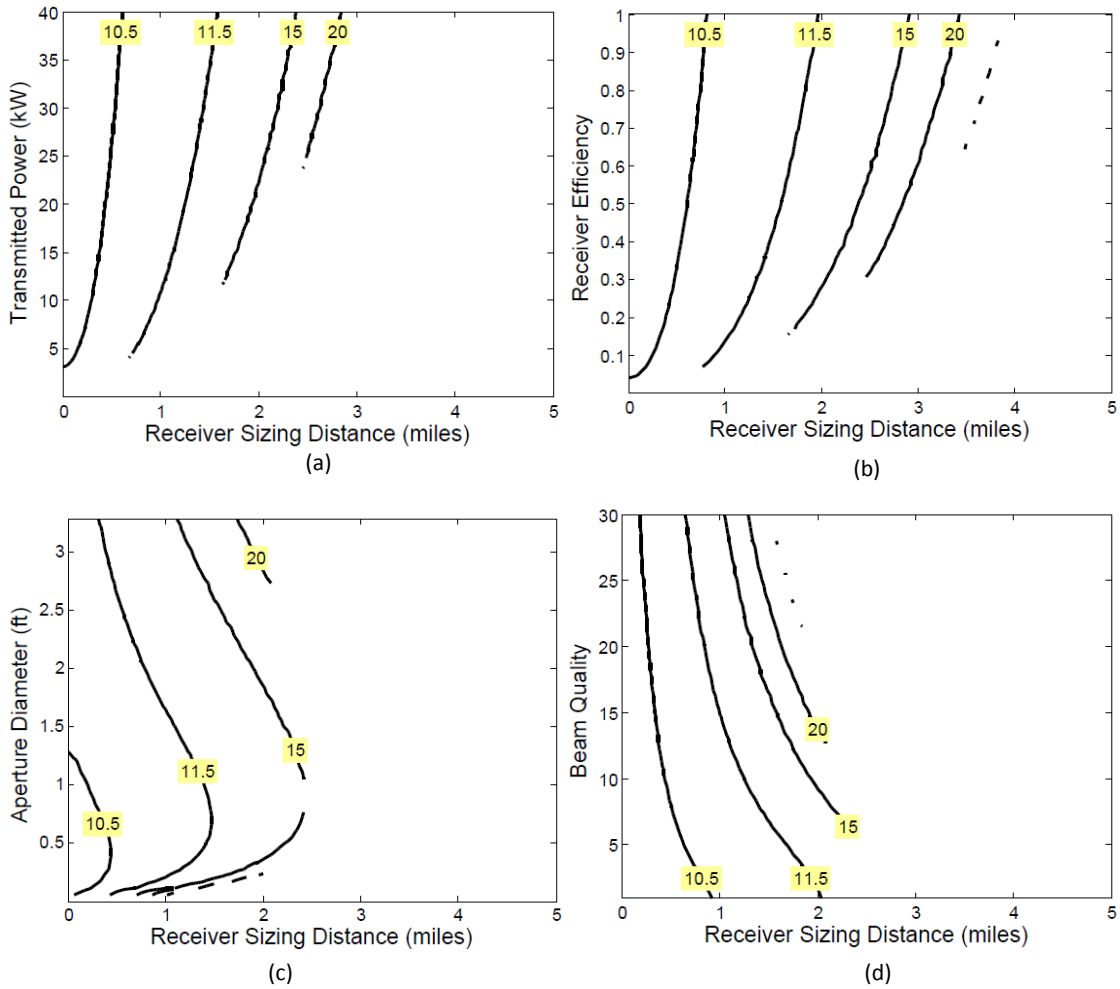

Figure 50. Contours of W_{TOGW} with respect to distance and various laser parameters (a) B = 10, $\eta_{re\ c}$= 0.25, d_l = 0.3 ft (b) B= 10, $P_{t,las}$ = 20 kW, d_l = 0.3 ft (c) B = 10, $P_{t,las}$ = 20 kW, η_{rec} = 0.25 (d) $P_{t,las}$ = 20 kW, η_{rec}= 0.25, d_l = 0.3 ft

Figure 51 shows the required transmitted power that is necessary to power the UAV. The laser is assumed to have a beam quality of 10, an aperture diameter of 0.3 ft, and a receiver efficiency of 25%. For this plot, the receiving panel is sized to be equal to the spot size of the beam. This plot shows that the required transmitted power increases with the downrange distance. As the altitude increases, the required transmitted power actually decreases for this range. This is because as the altitude is increased the incident angle of the beam is reduced, which allows for more energy to be captured.

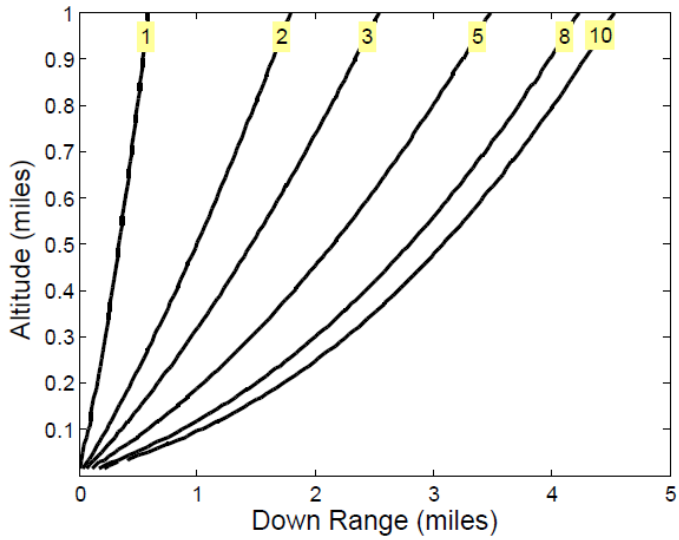

Figure 51. Required transmitted power in order to power the UAV.

5.2.4 Comparison of Flat Panel and Turret

A way to possibly increase the efficiency of the system would be to put the receiving panel on a turret. By using a turret, the incident angle should be reduced to near zero. This would reduce the area of the receiver necessary. Figure 52 shows that adding a turret reduces the receiver area to takeoff weight ratio. The solid lines represent the panel and the dotted lines are using a turret. The three different colors are different excess output powers. As the excess power increases, the receiving area weight fraction decreases.

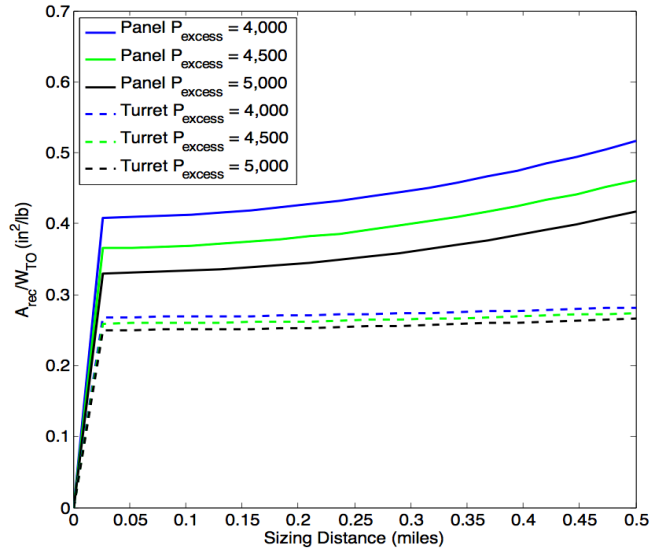

Figure 52. A comparison of how the turret reduces the receiver weight ratio. Solid lines represent just a panel and the dotted lines represent the turret.

While using a turret does reduce the area of the receiver, it is important to determine how adding a turret affects the overall weight of the craft. Figure 53 shows how the weight fractions of the panel and the turret change with the receiving area weight fraction. Because the scale between the two plots are so different, the y-axis for the turret weight fraction is on the left and the y-axis for the panel is on the right.

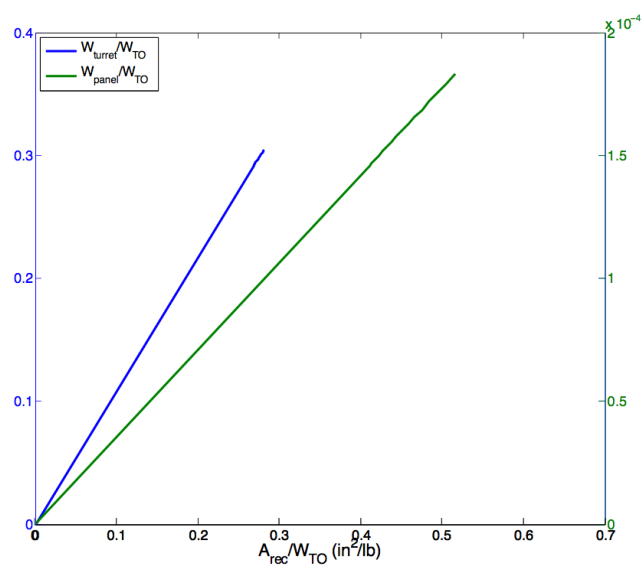

Figure 53. Comparison of the weight fractions for the turret and a panel.

Even though using a turret reduces the incident angle, therefore decreasing the necessary incident area, the weight cost is much greater than that of just the flat panel. Figure 53 only compares the weight fraction of the turret to the weight fraction of a panel. Even though having a turret makes the remote powering process more efficient, it increases the weight so much that it requires a greater output power. This plot shows that just having a flat receiving panel on the fuselage of the vehicle is a better option.

5.3 Microwave versus Laser Systems

5.3.1 Efficiency Comparison

In order to predict how the systems would compare, the efficiencies of each system were determined. This is displayed in Figure 54. This efficiency accounts for converting DC to electromagnetic radiation, the transmission path efficiency, and converting it back to DC. Each case with for the microwave system assumes a transmitter diameter of 30 ft and an altitude of 50 ft.

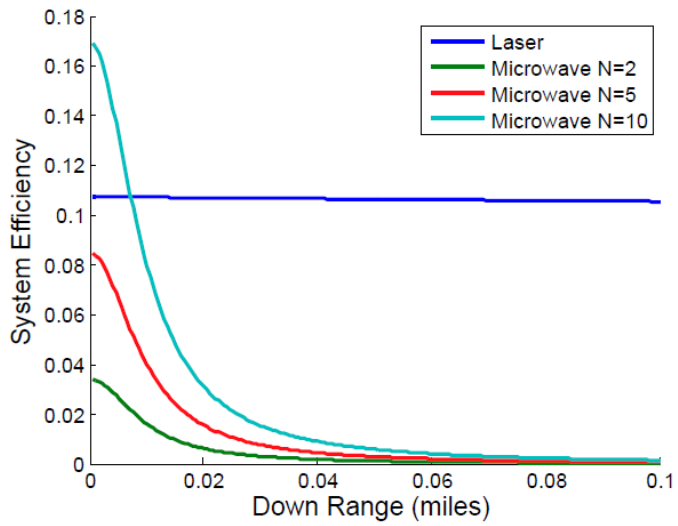

Figure 54. A comparison of the efficiencies of a microwave powered and laser powered system. The microwave system has three different cases: a vehicle with two patch antenna, five patch antenna, and ten patch antenna.

Figure 54 shows that, even though the process of converting DC to microwaves and back again is more efficient than the equivalent process for a laser, the laser system is more efficient, except at extremely close distances and high receiver gains. The microwave system can be made more efficient by increasing the diameter of the transmitter, but this becomes a cost benefit analysis of having of increases the transmitter diameters to extreme sizes.

5.3.2 Sizing Comparison

For this part, only the first scenario depicted in Figure 41 is considered for remotely powered UAVs. It is also important to understand that remotely powered vehicles and battery powered vehicles are highly dependent upon different parameters. The remotely powered vehicle is restricted by distance and the battery powered vehicle is restricted by endurance. Figure 55 (a) shows the comparison of microwave and laser powered vehicles, and (b) shows the battery powered vehicle. It is clear from (a) that the microwave vehicle will always weigh more for these mission parameters.

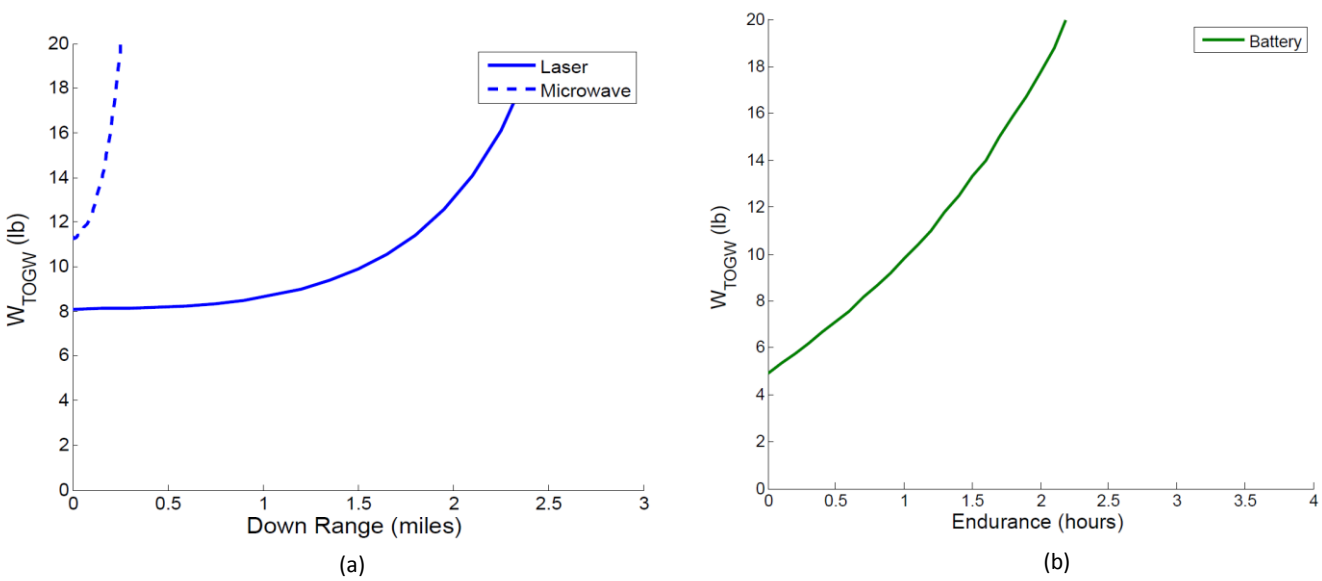

Figure 55. (a) Shows how the estimated takeoff weight of remotely powered vehicles changes with the down range sizing distance. For the laser powered vehicle: B = 10, $P_{t,las}$ = 20 kW, η_{rec} = 0.25; and for the microwave powered vehicle: $P_{t,micro}$ = 20 kW, d_l = 20 m.

(b) Shows how the estimated takeoff weight of a battery powered vehicle changes with endurance.

In order to compare the battery powered vehicle with the remotely powered vehicle, the two plots are superimposed and the Y-axis is set to the same values. The x-axis for the remotely powered vehicles is on the bottom in blue, and the x-axis for the battery powered vehicle is on the top in green. The profile described in section *2.2 Mission Profile* is used for comparison. Using Figure 56 it is possible to extrapolate the mission requirements at which a remotely powered vehicle would be beneficial.

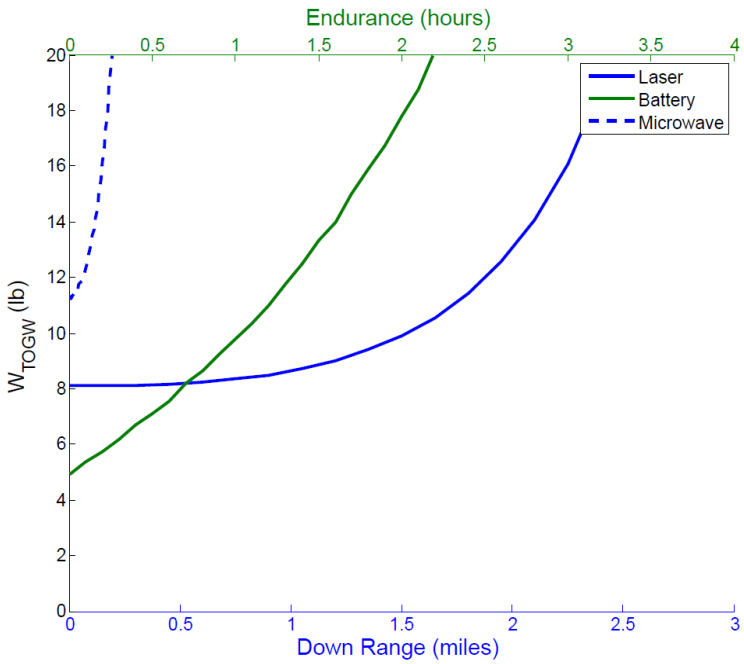

Figure 56. Sizing comparison of remote power UAVs and battery powered UAVs.

Figure 56 illustrates how a battery-powered vehicle will weigh less than either a laser-powered or a microwave-powered vehicle as long as the endurance is less than 0.7 hours. This is determined by getting the minimum weight value for thee remotely powered vehicles, which is around 8 lbs, and endurance value that corresponds a battery powered vehicle of that weight. If the endurance requirement is greater than 0.7 hours, it is possible

to have a have a remotely powered vehicle, with essential unlimited endurance, that would weigh the same, or less, than a battery powered vehicle. This is dependent upon the range requirements though. For example, if the mission requirements call for an endurance of at least 1 hour, unlimited endurance is possible, without increasing the weight, as long as the down range distance is less than 2 miles. In fact, if the down range distance requirement is only 1 mile, then a laser-powered vehicle will weigh less than a battery-powered vehicle.

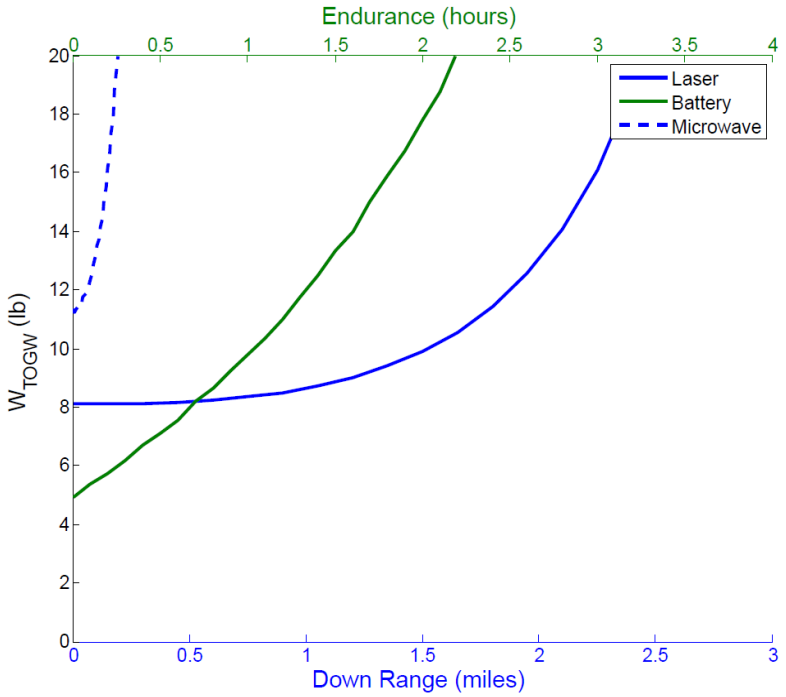

Figure 57. Analysis of plot comparing remotely powered vehicles with battery powered vehicles.

The same pattern follows for microwave-powered when compared with battery-powered, however the microwave-powered vehicle will weigh less as long as the endurance is less than 1.3 hours. The weight of the microwave-powered vehicle increases rapidly with down range distance, so any added endurance benefits are restricted to a very small range of distances.

By making the transmitter and receiver parameters better; such as increasing the transmitted power, have a higher quality laser, better receiving efficiency, or higher transmitter gain; it is possible to increase the range of distances at which there is a weight benefit for using a remotely powered vehicle. In Figure 58 the transmitted power was doubled for both systems, and the transmitter diameter was doubled for the microwave system. The endurance value, at which a battery powered vehicle is always better, stays the same at around 0.7 hours. However, when doing a comparison again of a mission with an endurance requirement of greater than 1 hour, it is possible to have a laser powered vehicle with no weight penalties as long the range requirement is less than 2.5 miles, instead of 2 miles from before.

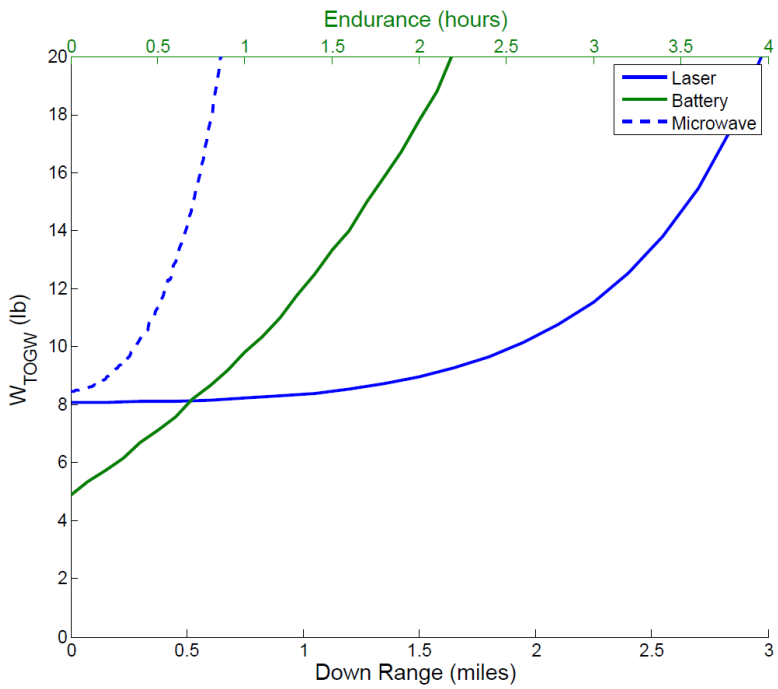

Figure 58. Doubling the transmitted power of both remote systems, and doubling the microwave transmitter diameter.

Table 3 is a validation of the sizing code used to estimate the weight of a battery-powered vehicle given the endurance. Several UAVs were chosen, their mission requirements were used, and the estimated weight was determined.

Table 3. Validation of the sizing code used for battery-powered vehicle.

Vehicle	Estimated	Actual	Difference
Pointer	12	9	25%
Dragon Eye	8.4	5.8	30%
Raven	6.2	4.5	27%

5.3.3 Surveillance Area

The remotely-powered systems and battery-powered systems can also be compared by the area that they can cover. Since remotely powered systems can operate anywhere within the range of the transmitter, they area they can cover is a circle around the transmitter, where the down range sizing distance is the radius. For a battery powered vehicle, it is a more complex. For this work, it is assumed that the area a battery powered UAV can cover, is the area that it can provide footage of. This way, the area covered is dependent upon the endurance of the vehicle, and the camera on board.

As an example we'll use the same mission parameters as in Figure 56. An endurance requirement of 1 hour, and down range distance requirement of 2 miles, will be used so that the both battery-powered and laser-powered UAVs will be about the same weight. From this it is possible to say that the laser-powered vehicle can cover an area of 12.6 miles^2.

For the battery-powered UAV, the area covered determined from the endurance, 1 hour, the cruise velocity, which was 57 ft/s, and the camera field of view. Multiplying the endurance and the cruise velocity, gives a possible distance travelled of about 39 miles. Using the altitude of 1000 ft, it can be calculated that the battery-powered UAV needs a

camera with a horizontal field of view of 81° in order to cover an area of 12.6 miles^2. If the camera has a horizontal field of view greater than 81°, the battery-powered UAV can cover more area than the laser powered UAV, or if it's less than 81°, the laser-powered UAV covers more area.

5.4 Hybrid Systems

5.4.1 Augmented versus Non-Augmented systems

Now we will take a look at the second and third scenario in Figure 41. These involve hybrid systems, in that they are powered remotely and with batteries. For analyzing these, the down range distance, R, is a set point, and the sizing distance ℓ, is varied. Choosing a R value of 7 miles, and still using the output power of 20 kW, results in a nonconvergent system, for a purely remotely powered system. This is due to not enough power being output. The system was not able to converge until an output power of 600 kW was used, and this resulted in a takeoff weight of around 80 lbs. Figure 59 shows a plot of the two scenarios for hybrid systems.

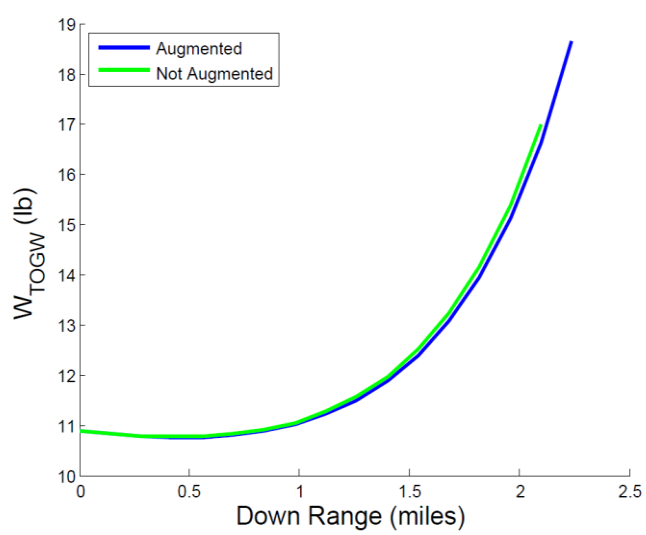

Figure 59. Plot of hybrid remote-battery powered systems, with a down range requirement of 7 miles.

Figure 59 shows that, while there is a slight weight benefit, there is not a significant difference between a system that continues to augment the battery power with the laser power, and one that just relies on pure battery power after the sizing distance ℓ. This is because after the sizing distance ℓ, the beam spot area continues to grow but the receiver is no longer able to capture the entire area. This dramatically reduces the power received, and was illustrated in Figure 41 (c). With the hybrid systems, there is an optimal point where the weight is a minimum. This occurs when the receiver sizing distance is around 0.5 miles.

5.4.2 Comparison of Hybrid, Battery, and Remote Systems

Understanding that there is an optimal sizing distance for hybrid systems, allows for better comparisons of with battery-powered systems and remote-powered systems. By creating a range of values R and a matrix of values ℓ, where each row is a range of distances between 0 and $R(i)$, we can get a matrix of takeoff weight values. With this, we can determine the optimal weight for each value of R, and then compare these with battery and remote power systems for the same range of R. This is depicted below in Figure 60.

Similar to before, the battery-powered system will weigh less than either the remote powered system or the hybrid system, as long the endurance requirement is below 0.7 hours. The weight of the optimized hybrid system does not increase as rapidly as either the battery-powered system or the remotely-powered system. This allows it to reach much further distances, while still maintaining a reasonable weight. This plot clearly shows that there are significant benefits to using a hybrid system.

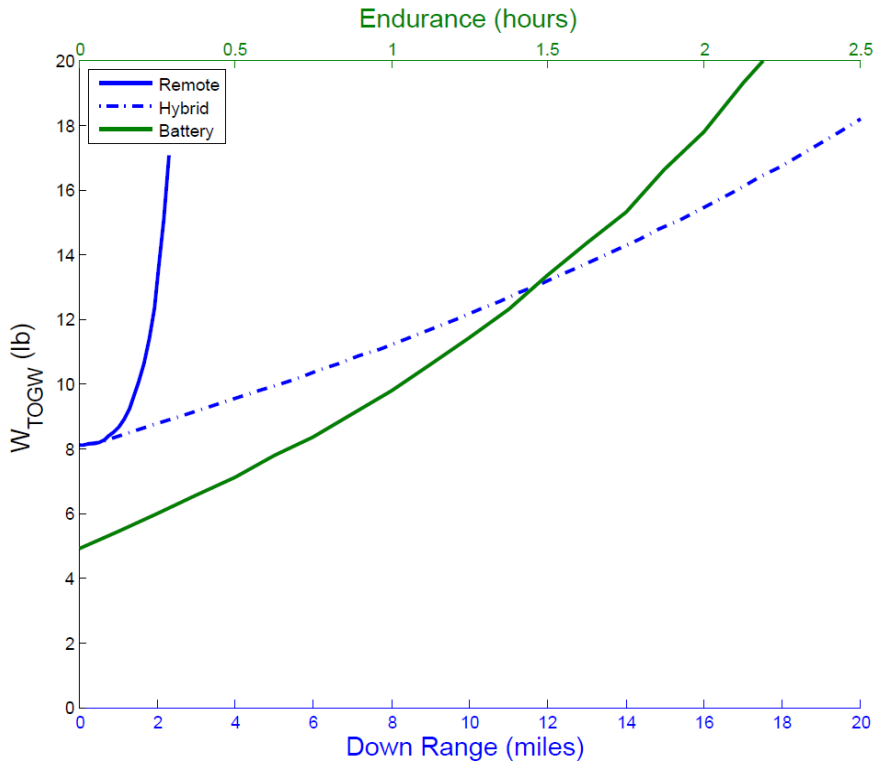

Figure 60. Comparison of remotely powered, hybrid, and battery powered system.

When comparing the estimated area these systems could cover, the hybrid systems would be similar to the remote powered system, in that the area they can cover is a circle around the transmitter. A battery powered system with and endurance of 1 hour weighs about the same as a hybrid system with a maximum range value of 7 miles. This results in an estimated area of about 150 miles^2 for the hybrid system. In order for the battery powered system to compete with that, it would have to have a camera with a horizontal field of view of about 170°.

A good thing to understand about the sizing results is the growth factor. The growth factor is how much the takeoff gross weight will increases per pound of payload, and is found by dividing the resulting takeoff weight by the payload weight. Some typical growth factor values are: 12-13 for hypersonic vehicles, 4-5 for supersonic transports, and 2 for

subsonic aircraft. [41] The higher the growth factor is, the more sensitive the system is. For a hypersonic vehicle, for each extra pound of payload, the takeoff weight will increase by 12 lbs. So hypersonic vehicles are very sensitive. On the other hand, for a subsonic vehicle, for each extra pound of payload, the takeoff weight will only increase by 2 lbs.

Figure 61 depicts contours of the growth factor for various ranges and payload weights. This plot shows that as the payload weight increases, the growth factor decreases. With a payload weight greater than 12 lbs, and for a range up to 2 miles, a remotely powered vehicle is very similar to a supersonic transport with a growth factor value between 4 and 5. As the payload weight decreases, remote powered systems become more sensitive. As the range increases, the vehicle also becomes more sensitive. For low payload weights and high ranges, a remotely powered vehicle can have a growth factor of up to 180. This shows that remotely powered vehicles can be very sensitive systems.

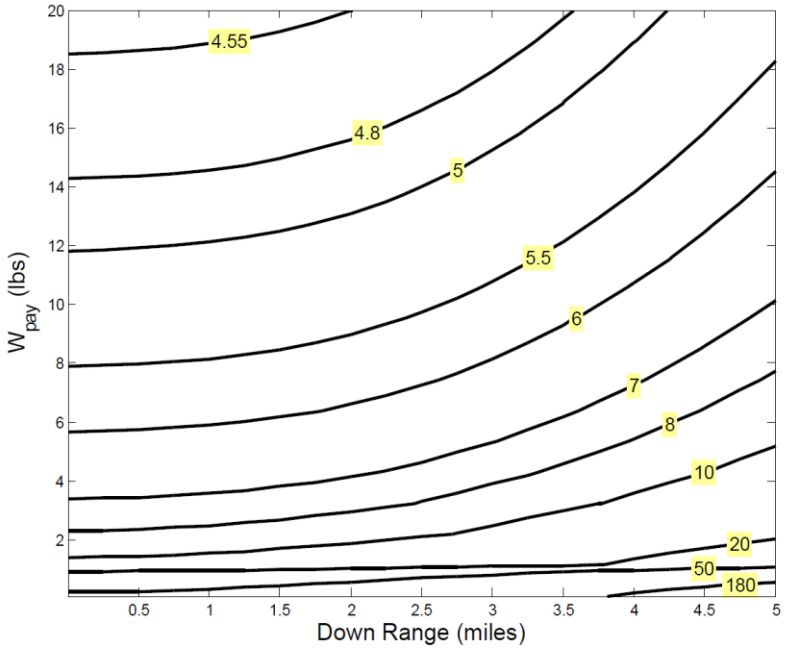

Figure 61. Contours of the growth factor while varying the downrange sizing value and the payload weight.

6. Conclusion

6.1 Design Methods in Use

To analyze the results of the methods developed, the design of a small UAV is considered. Currently, the Raven is the most widely used small UAV within the US military. The purpose of the example UAV will be to perform the same mission characteristics as the Raven, but with an increased endurance. These next sections will show how the requirements work with the design matrix.

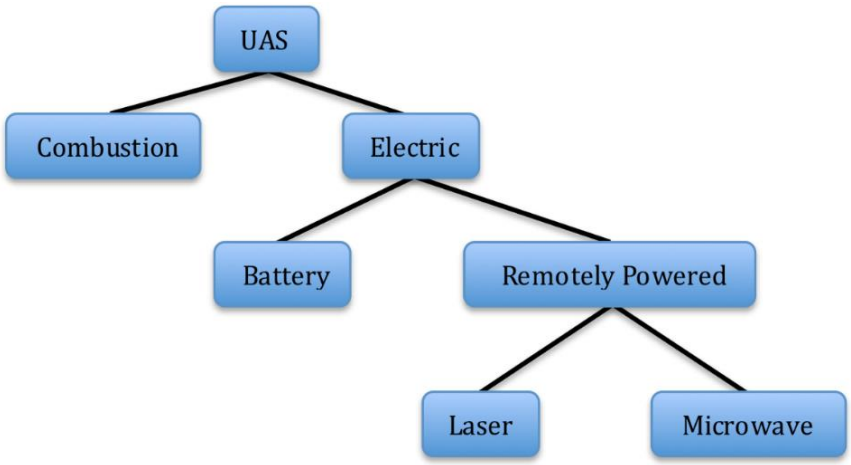

Figure 62. The design process flow.

6.1.1 Concept of Operations

Unmanned aerial systems are used differently within the army hierarchy, depending on the on the size of the UAV and its range. In descending order, the army is broken up into corps, divisions, brigades, battalions, companies, platoons, and finally squads. UAVs are only broken into three groups: long range, mid-range, and short range. A depiction of the different ranges is shown in Figure 63. The short range is considered to be less than 25 km. The UAVs of this class are used to provide a direct support role to the brigades and anything below. This is where the Raven is used. Mid-range is considered to be less than 125 km. These usually provide a general support, and sometimes direct, support role to the

divisions. The Shadow is the most commonly used UAV in this class. The long-range class is anything above 125 km. These provide support to the division and above. The Hunter, Gnat, and Global Hawk are all used as in this class. Figure 63 shows an outline of Iraq in each sub picture. The ranges for each class of vehicle are depicted by the circles. In (a), the class range capabilities just appear to be dots. The mid-range vehicles in (b) cover a fair amount of area, and then (c) shows how a long range vehicle can cover the entirety of Iraq by itself.

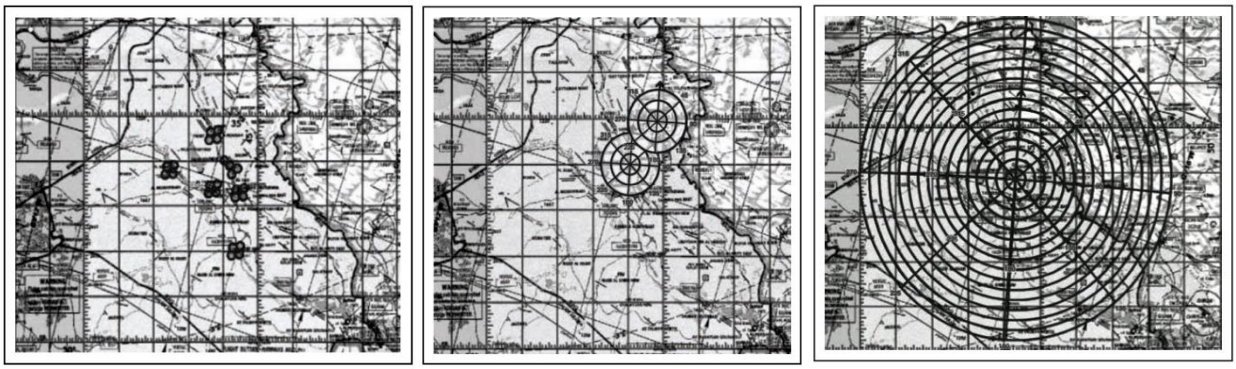

(a) (b) (c)

Figure 63. Range of different unmanned aerial systems over a map of Iraq: (a) short range (b) mid-range and (c) long range. [11]

The UAV to be designed must fit within the current Army architecture. The goal of designing a short range UAV means it will be used within the brigades. Because it is to be remotely powered, it needs a ground station and therefore needs some type of vehicle for transportation. The brigades are broken into three categories: the Infantry Brigade, the Stryker Brigade, and the Armored Brigade. Within these separate brigades exist the Mounted Reconnaissance, the Stryker Reconnaissance Troop, and the Armored Reconnaissance Troop respectively. Each of these groups contains vehicles capable of transporting a ground station. In order to fulfill the mission of the Raven, the RPUAV has to achieve the requirements in Table 4.

Table 4. Requirements of Raven's mission.

Range	7.5 miles
Airspeed	23 kt loiter, 34 kt cruise, 70 kt dash
Climb	11 ft/s
Payload	EO and IR sensors
Launch	Hand launch

There is also the derived requirement that the ground station has to be portable. This means that the power supplied to the laser must also be portable. The infantries Mounted Reconnaissance use HMMWVs for transportation. Recent upgrades allow the alternator of the M1123 HMMWV to output 35 kW. [42] The Stryker vehicles and Abram tanks used by the other two troops allow for greater power. Using the minimum, results in 35 kW as the maximum available power to be transmitted.

The first step for designing the UAV is to consider whether it should have a combustion propulsion system or an electric propulsion system. In order to do this, it is necessary to know the required range and power. The range is simply found in Table 4. In order to estimate the power required for the vehicle, a simple back-of-the-hand calculation using the lift-to-drag ratio should suffice.

$$P = \frac{1}{(L/D)} \frac{v}{\eta_{prop}} \mathrm{W_{TOGW}} \tag{93}$$

For this estimation, it is assumed that the UAV is in steady-level flight. Using a conservative lift to drag estimate of 3, a propeller efficiency of 50%, a takeoff gross weight of 5 lbs, and the dash speed gives a power requirement of 550 W. This a very conservative estimate, as the Raven itself has a 200 W motor. Even when doubling the takeoff gross weight, the power requirement estimate still stays below 1 kW line. So because the design requirements fall below 1 kW and 30 mile markers, an electric propulsion system should be used. This is summed up in Table 5.

Table 5. Determining factors for a combustion vs. electric system

	Power	Range
Deciding Factor	1 kW	30 miles
Requirements	0.55 kW	7.5 miles

6.1.2 Constraints

The requirements from Table 4 are used to form Figure 64. The constraints are formed using the specific excess power equation found in Eq. (5) Since the UAV does not change weight throughout the duration of the mission, the weight fraction is equal to one. The coefficient of drag is estimated using

$$C_D = C_{D,0} + \frac{C_L^2}{\pi e AR} \tag{94}$$

where $C_{D,0}$ is the parasitic coefficient of drag, e is the Oswald efficiency factor, and AR is the aspect ratio. Usually the Oswald efficiency is estimated to be between 0.7 and 0.9. These values of e only hold for high Reynolds numbers, $Re > 5 \times 10^6$. It has been shown that values of e can be as low as 0.22 for $Re \approx 2 \times 10^4$. [43] Since the Reynolds number for the above mission and requirements will be between 2×10^5 and 3×10^5, a moderate value of 0.5 was used for the Oswald efficiency. The parasitic drag coefficient is found by summing up the skin friction coefficients for each part of the vehicle. [44] The estimate for the parasitic drag was broken up into four parts: the fuselage, the wing, the horizontal tail, and the vertical tail. The equations for the wing, horizontal tail, and vertical tail are the same.

$$\mathrm{C_{D,0_{w/ht/vt}}} = \mathrm{C_f f_{tc}} \left(\frac{\mathrm{S_{wet_{w/ht/vt}}}}{\mathrm{S}}\right) \left(\frac{\mathrm{C_{d,min_{w/ht/vt}}}}{0.004}\right)^{0.4} \tag{95}$$

where S_{wet} is the wetted surface are of the part, S is the planform area, $C_{d,min}$ is the two-dimensional minimum drag coefficient of the airfoil used, f_{tc} is a function of the maximum thickness ratio, and C_f is the skin friction coefficient. The function of the thickness ratio is found with

$$\mathrm{f_{tc}} = 1 + 2.7\left(\frac{\mathrm{t}}{\mathrm{c}}\right)_{\mathrm{max}} + 100\left(\frac{\mathrm{t}}{\mathrm{c}}\right)^4_{\mathrm{max}} \tag{96}$$

where $\left(\frac{t}{c}\right)_{max}$ is the maximum thickenss ratio. The coefficient of friction is

$$\mathrm{C_f} = \frac{0.455}{[\log_{10}(\mathrm{Re})]^{2.58}} \tag{97}$$

for turbulent flow or

$$\mathrm{C_f} = \frac{1.327}{\sqrt{\mathrm{Re}}} \tag{98}$$

for laminar flow. Due to the low Reynolds number, the flow was considered to be mostly laminar.

The equation for the parasitic drag due to the fuselage is slightly different from that of the wing and tails. The coefficient is now a function of the length to diameter ratio and there is no minimum drag term,

$$\mathrm{C_{D,0_f}} = \mathrm{C_f f_{LD}}\left(\frac{\mathrm{S_{wet_f}}}{\mathrm{S}}\right) \tag{99}$$

where f_{LD} is a function of the length to diameter ratio.

$$\mathrm{f_{LD}} = 1 + \frac{60}{(\mathrm{L/D})^3} + 0.0025\left(\frac{\mathrm{L}}{\mathrm{D}}\right) \tag{100}$$

The total parasitic drag coefficient comes from summing all the parts together.

$$\mathrm{C_{D,0}} = \left(\mathrm{C_{D,0_f}} + \mathrm{C_{D,0_w}} + \mathrm{C_{D,0_{ht}}} + \mathrm{C_{D,0_{vt}}}\right)\mathrm{C_{D,crud}} \tag{101}$$

The entire thing is multiplied by a factor deemed the crud drag factor. This is due to the fact that, for small vehicles, there is an increased drag effect caused by not having a perfectly smooth vehicle surface. This is usually not taken into account because the effect of a bolt, gap between materials, or antenna is insignificant in comparison to the total drag for a large vehicle. There is not much literature on this subject because small UAVs are relatively new, so the crud drag factor was estimated.

$$C_{D,crud} = \frac{S + 4}{S} \tag{102}$$

This equation was developed so that, as the span increased, the crud factor would approach 1. For a small vehicle with a planform area of 4 ft^2, the crud drag would double the parasitic drag coefficient.

In order to size the vertical and horizontal tails, the dimensions of the UAV need to be known. Since the size of the vehicle changes depending on the parameters, the dimensions are determined based on payload weight and propulsion system power requirements. The required power for the propulsion system is used in Eq. (24) or Eq. (25) to find the volume an electric or internal combustion system respectively. Using a payload density, the volume of the payload can be found from the weight of the payload. Using the estimated volume of the fuselage, the fuselage length was found with

$$l_f = \left(\frac{3}{0.3 \times 4}\pi V_f\right)^{1/3} \tag{103}$$

and the diameter of the fuselage was found with the following.

$$d_f = 2 \times 0.3 \times l_f \tag{104}$$

The distance from the aerodynamic center of the tails was assumed to be 1.5 times the length of the fuselage. These equations were developed so that a vehicle with the same approximate payload weight and volume, would have dimensions similar to the Raven.

To get the hand-launch requirement, the coefficient of lift needs to be determined. The coefficient of lift is estimated with

$$C_L = \frac{n\vartheta}{q}\left(\frac{W_{TOGW}}{S}\right) \tag{105}$$

where n is the g-loading. To get the hand launch requirement, it is assumed that the UAV can be thrown at 10 ft/s. This velocity is used to solve for the specific excess power. By assuming that after being thrown, it needs to have a climb rate of 5 ft/s, a constraint contour is made.

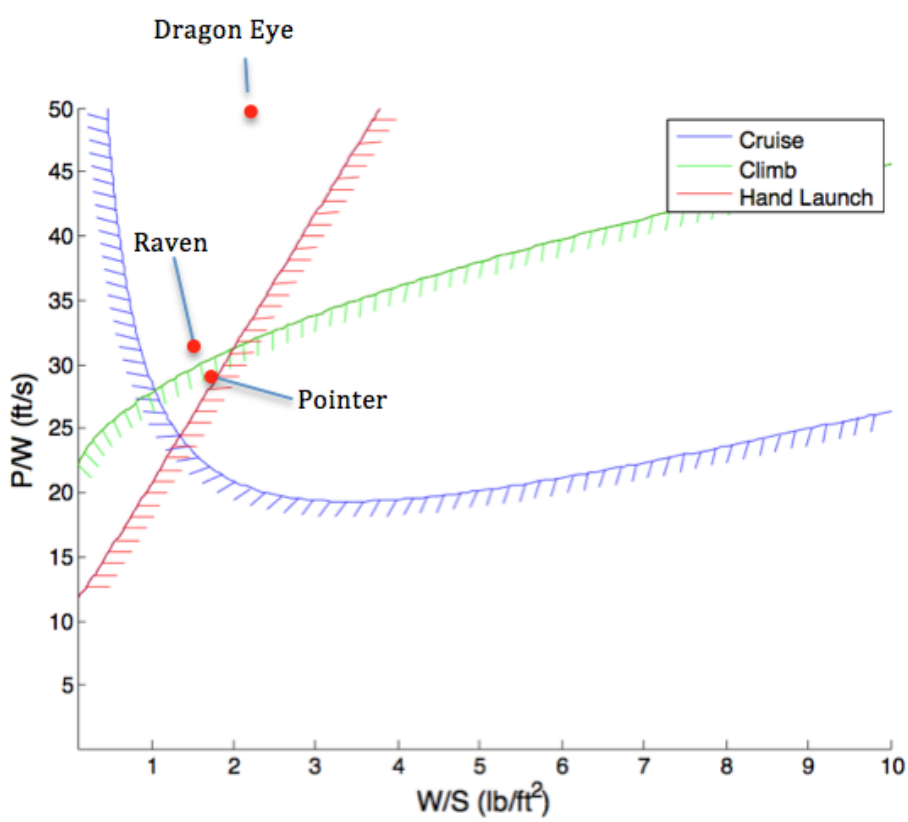

Figure 64. Constrain diagram using Raven requirements.

This figure shows that the design space has a power to weight ratio of roughly 30 ft/s, with a wing load between 1 and 2 lb/ft^2. Three small UAVs currently in production are shown. The all have a wing loading of around 2 lb/ft^2. The Raven and the Pointer have power to weight ratios around 30 ft/s, but the Dragon Eye has a much higher power to weight ratio at about 50 ft/s. From this constraint diagram, and taking into account working UAVs, a power to weight ratio of 30 ft/s and a wing loading of 2 lb/ft^2 was decided upon.

6.1.3 Example Sizing

With the requirements and design space known, it is possible to actually estimate the takeoff weight of the vehicle. A flow diagram of the code used to estimate the takeoff weight can be seen in Figure 65. Information from the laser model is only input into the battery weight model if the battery is being augmented after distance ℓ. The requirements, conditions, along with an initial weight guess are input into the system and takeoff weight is found. The new takeoff weight is used to determine the next guess. This is iterated until the input takeoff weight and output takeoff weight are the same.

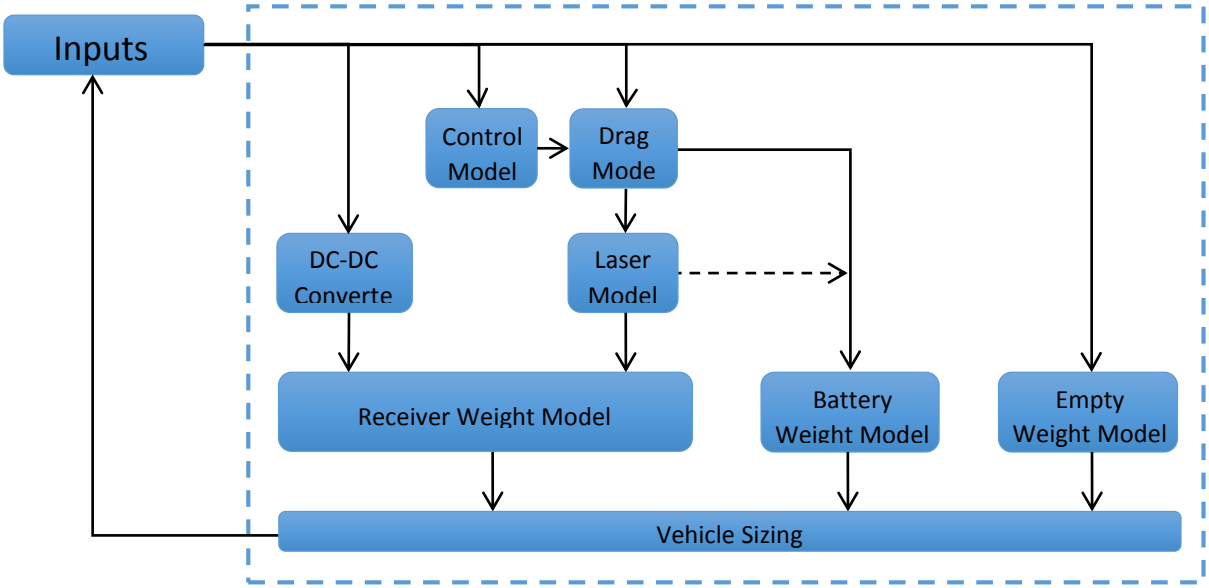

Figure 65. Information flow diagram of sizing code.

The control model is used to estimate the size of the horizontal and vertical tails. This was done by using historical values of tail volume coefficients to find the required surface area for the tails. A value of 0.5 is used for the horizontal tail and 0.04 for the vertical tail. [44] These values correspond to that of a home-built aircraft. Because of the low Reynolds numbers expected, a S1223 airfoil was used for the model. This airfoil was designed to have high lift characteristics at low Reynolds numbers. The cross section can be seen below in Figure 66 and the lift and drag characteristics are shown in Figure 67.

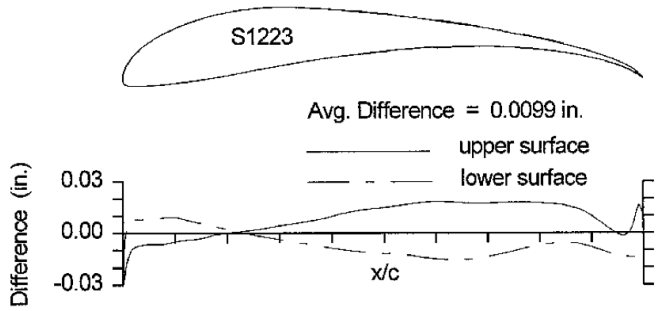

Figure 66. Cross section of the S1223 airfoil. [45]

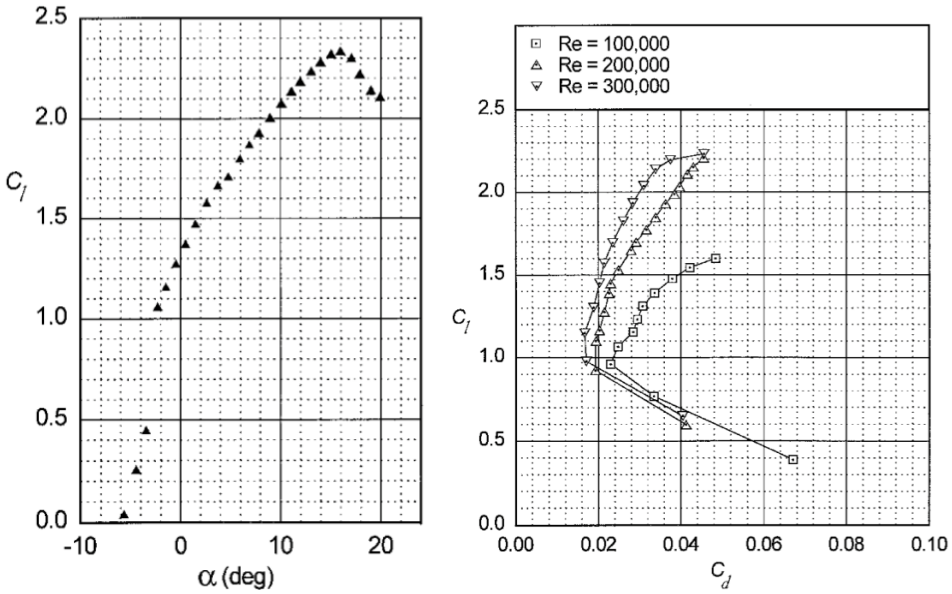

Figure 67. Lift curve and drag polar of the S1223 airfoil.

Three lasers from Table 2 were chosen to be used with the sizing code. The lasers chosen were the 10 kW fiber laser, the 25 kW thin disk laser, and the 10 kW diode Laser. These were chosen for their high power outputs and relatively good quality. Using an efficiency of 50% for converting energy to light, means that the power in to the laser needs to be 20 kW for the diode and fiber Lasers, and 50 kW for the thin disk laser. Since the maximum output from the alternator of the HMMWV is 35 kW, it was assumed that the thin disk laser would be pulsed such that the resulting power output was 17.5 kW. Results from the sizing code are shown in Figure 68.

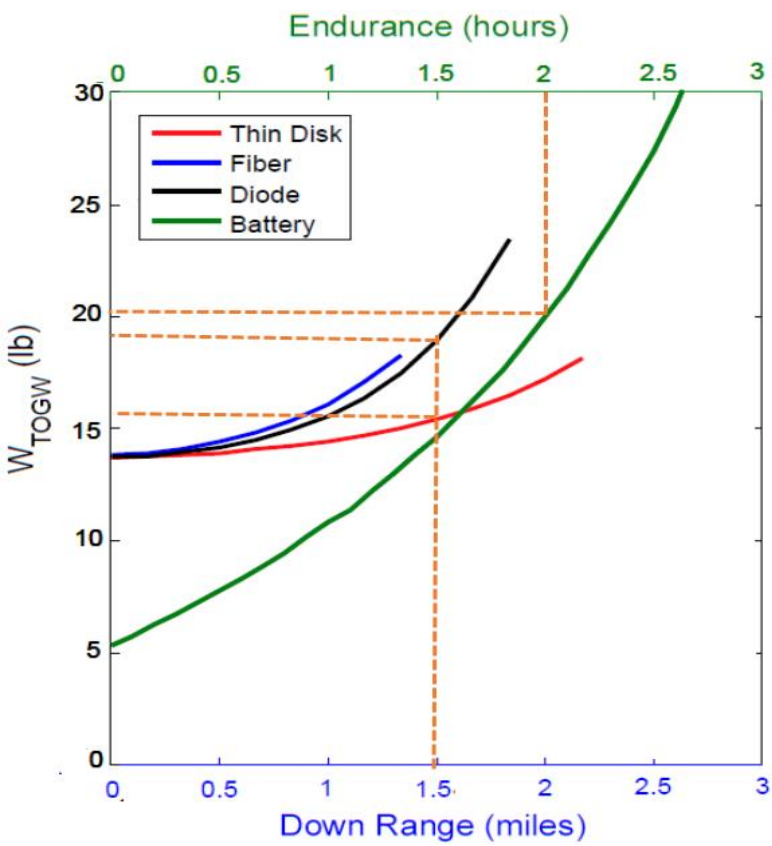

Figure 68. Comparing battery powered system, with different laser powered systems.

Figure 68 shows that, no matter what laser you use, if the endurance requirement is less than about 1.5 hours, the battery system will be the lighter option. If the endurance

requirement is greater than 1.5 hours, then the range requirement comes into play. For example, if the endurance requirement was 2 hours and the range requirement was 1.5 miles, the either a thin disk or diode laser powered UAV would give greater endurance, for less takeoff weight than the battery system. The Fiber laser would not be a viable option for this range requirement.

Recalling from Table 4, the range requirement is 7.5 miles. Figure 68 shows that a UAV completely powered by a laser is not possible with these mission parameters. As discussed in section *2.2 Mission Profile,* it is possible to have a UAV that is only partially powered by a laser. The issue with this is determining what distance the receiver should be sized to. In Figure 69, the down range distance is the distance to which the receiver is sized to, however, now there is a battery added, with the capacity to take the UAV out to the max range, 7.5 miles, and back at cruise speed.

Each of these vehicles can reach a range of 7.5 miles, and do not actually need to land as the batteries can be powered in flight, as long as they are in range of the laser. If the endurance requirement is 2 hours or greater, then a vehicle utilizing both a battery and laser power can be lighter than that of the equivalent using just a battery. The sizing range at which it will have a lower takeoff weight, is dependent upon the type of laser used. For the Thin Disk laser, as long as the sizing range is less than 1.5 miles, then it will be lighter. It is the same way when using a Diode laser and a receiver sized to around 0.7 miles, and a Fiber laser and a receiver sized to around 0.5 miles. For the Thin Disk laser, there is an optimum sizing range at around 0.5 miles, where the takeoff weight is the least. For the Diode laser there is one around 0.25 miles. Due to the characteristics of the Fiber laser, there isn’t really an optimum point.

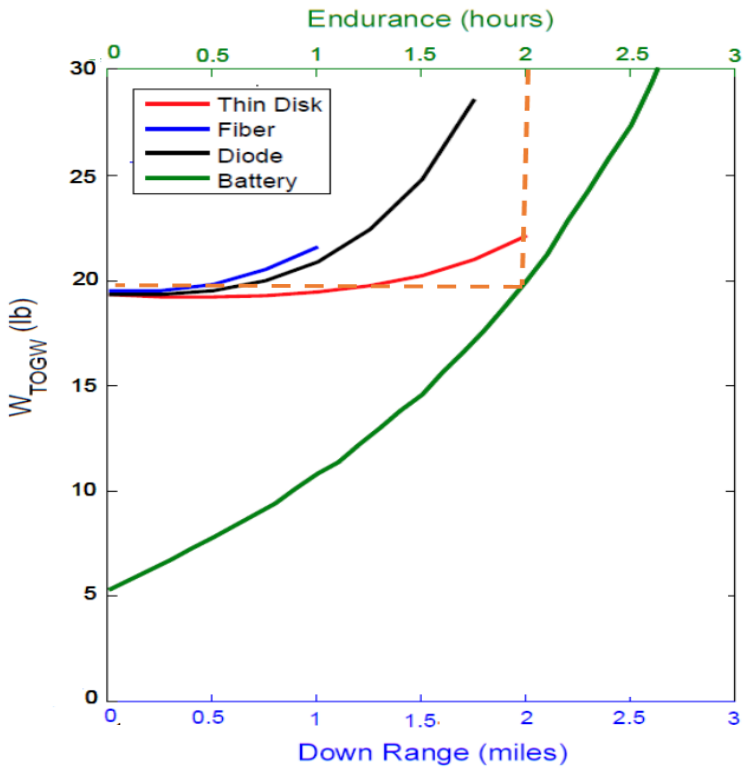

Figure 69. Comparison of battery powered system and system using both batteries and lasers.

The purpose of this paper was to develop the methods for designing a remotely powered UAV, and to determine the design space that it falls within. With the advance of technology, it is possible to create aircraft that do not fall within traditional design methods. This paper provides a platform with which a remotely powered UAV can be designed. It also provides the way with which to determine if a remotely powered UAV is actually a viable solution to the specific mission requirements.

6.2 Process Overview

The first step to developing a method to design a remotely powered vehicle was to take the conventional sizing method and convert it so that it was dependent upon on the weight of the onboard energy source, instead of specific fuel weight. Defining this term as an onboard energy source allows for this method to account for battery source that is

actually located on the vehicle, and a receiving panel that gets its power from another location. Since these are both electrical powering methods, the specific energy for each leg was derived from the specific excess power equation.

With the basic sizing method established, it was then necessary to determine how the power would be transmitted. From research, it was determined that the best methods were either microwave power or laser power. Models from previous papers were used to establish how both methods propagated through the atmosphere. This allowed for the loss of power to be calculated depending on the distance and orientation of the UAV, with respect to the transmitter. Receiving methods were also researched, and it showed that the best method for receiving the transmitted power was with a flat panel for the laser, and patch antenna for the microwaves.

An equation for the weight fraction of the receiving apparatus was derived from the way in which the energy propagated. By finding the energy needed to completely power the vehicle at a given distance, the size of the receiving apparatus was determined. This was then converted into a weight fraction. Using this weight fraction, it was shown how the takeoff gross weight was affected by changing the different parameters of the respective transmitter. With the complete sizing method developed, a design matrix was developed.

6.3 Conclusion

A design flow was developed to determine when to use a specific type of vehicle. This was done by starting with the overall systems, and breaking it down within each system, as shown in Figure 5. It first compares combustion systems and electric systems. Using historical data, it was shown that if the power requirement is less than 1 kW and the

range requirement is less than 30 miles, then it is likely that an electrical system is the better option.

The electrical system was broken into subcategories of battery powered and remotely powered. In order to compare these, it was necessary to understand the capabilities of both the microwave and laser powered systems. By plotting the takeoff gross weight versus range for the laser/microwave powered system, and takeoff gross weight versus endurance for the battery powered system, it can be shown when the specific type of vehicle should be chosen. This is dependent upon both the mission requirements and the transmitter/receiver parameters. This plot, such as Figure 56, shows at what endurance requirement remote power become a viable option, and the limit on the range requirement.

The efficiencies of the microwave and laser systems were also compared. This showed that, except at very close ranges, the laser system is the better option. This is due to the fact that it is much more focused than microwave system. The laser receiving options were then compared and it was found that the turret just added too much weight. The best option was just a flat panel. Hybrid missions, where the UAV is both battery powered and remotely powered, where also analyzed by varying the range at which the receiver was sized to. This showed that there was an optimal point at which the receiver could be sized to, in order to minimize the weight. This was around 0.5 miles for the parameters used. The hybrid system's weight was also less affected by the range than a pure remotely powered system.

There are three major area of work within this paper: the historical data, the drag buildup, and laser propagation. The first part that can be enhanced upon is the historical data. Historical data was used to determine multiple different things throughout this paper

such as: the break between combustion and electric systems, the weight of the motors, and more. By gather more data, it would create more accuracy in the conclusions that are being draw.

The next part for more work would be to include a better drag estimation. Data on drag estimation on small UAVs is very limited, so it is not possible to really determine how accurate this buildup is. The next step would be to create a sizing code that determined the drag from a CFD model that was generated using the payload weight and volume requirements.

The equations for the propagation of microwaves are well established. Lasers are another matter. It is affected by many different conditions, such as temperature, turbulence, and particulate matter in the air. Using localized data for the mission requirements would allow for better results to be determined.

Billions of dollars are being put into the development of UAVs and their requirements are becoming more and more complex. Remote powering offers the chance to have a UAV with theoretically unlimited endurance. This paper provides the method with which to design these vehicles. It also creates a step by step process, given a set of requirements, to determine if they are a viable option.

REFERENCES

[1] A. Bomber, "Wireless Power Transmission: An Obscure History, Possibly a Bright Future," Portland State College, 2006.

[2] G. Sato, "A Secret Story About the Yagi Antenna," *IEEE Antennas & Propagation Magazine,* pp. 7-18, 1991.

[3] I. A. Shcherbakov, "Development History of the Laser," *Physics-Uspekhi,* vol. 54, pp. 56-71, 2011.

[4] D. S. Abraham, "A Demonstration Plan for Laser-Bearmer Power," Jet Propulsion Laboratory, 1993.

[5] L. Krock, "Pre-Aviation UAVs: Eddy's Surveillance Kite (USA)," Nova, November 2002. [Online]. Available: http://www.pbs.org/wgbh/nova/spiesfly/uavs_02.html. [Accessed June 2011].

[6] L. Krock, "1940s: V-1 (Germany)," Nova, November 2002. [Online]. [Accessed April 2011].

[7] J. R. Iwaszko, "History of Wireless Electormagnetic Powered Flight Timeline & Replications," Academia.edu, 2001.

[8] G. Jull, "An Overview of SHARP," Ottowa, 1997.

[9] L. Myrabo, "Approaching Warp Speed: Advanced Space Propulsion," in *NewSpace*, Troy, 2010.

[10] Lockheed Martin Skunkworks, "Lockheed martin Performs First Ever Outdoor Flight Test of Laser Powered UAS," 7 August 2012.

[11] J. Gertler, "U.S. Unmanned Aerial Systems," Congressional Research Service, 2012.

[12] ""Raven Small UAV demonstrates Persisten Surveillance Capability on a 30 Hour Mission," Defense Update, 19 November 2001. [Online]. Available: http://defense-update.com/features/2009/april/persistent_suav_raven_020409.html.

[13] J. Fehrenbacher, S. L. David, J. E. Mary and J. Honchell, "Electric Motor & Power Source Selection for Small Aircraft Propulsion," Purdue University, Purdue, 2011.

[14] J. Newman, "Pushing Lithium-Ion's Limits," *Time,* 1 April 2013.

[15] K. Willcox, "Aircraft Systems Engineering Cost Analysis," MIT, 2004.

[16] "Northrop Grumman X-47B Design & Build," May 2014. [Online]. Available: Flite Test Weblog. [Accessed August 2014].

[17] A. Sobester, A. J. Keane, J. Scanlan and N. W. Bressloff, "Conceptual Design of UAV airframes Using a Generic Geometry Sevice," *AIAA*, vol. 7079, 2005.

[18] G. Thomas, "Overveiw of Storage Development: DOE Hydrogen Program," Sandia National Laboratories, San Ramon, 2000.

[19] Wester Lithium, "Hybrid/Electric Vehicles," Western Lithium, 2012.

[20] C. Burt, Z. Piao, F. Gaudi and B. Busch, "Electric Motor Efficiency under Variable Frequencies and Loads," ITRC, San Luis Obispo, 2006.

[21] R. Ashwin, "UAV Power Plant Performance Evaluation," Oklahoma State University, Oklahoma, 2010.

[22] O.S. Engines, "FT-160 Twin Cylinder Ringed Engine," O.S. Engines, 2012.

[23] MAXX Products International, "Himax Brushelss Outrunner Motor," MAXX Products International, Lake Zurich, 2006.

[24] University of Hawaii, Antenna Introductions/Basics, Antarctic Impulse Transient Antenna.

[25] C. M. Ho, W. Charles, K. Angkasa and G. Kelly, "Estimation of Microwave Power Margin Losses Due to Earth's Atmosphere and Weather in the Frequency Range of 3-30 GHz," Jet Propulsion Laboratory, 2004.

[26] R. K. Yadav, S. Das and R. L. Yadava, "Rectennas Design, Development and Application," *International Journal of Engineering Science and Technology,* vol. 3, no. 10, pp. 823-824, 2011.

[27] Pattern Magus, "Antenna Pattern Information," 12 April 2013. [Online]. Available: http://www.patternmagus.com/database/patterns/pattern_page.php?dir=8.

[28] P. P. Viezbicke, "Yagi Antenna Design," *Boulder: National Buerau of Standards,* vol. 688, 1976.

[29] Cisco, "Antenna Patterns and Their Meaning," 10 March 2013. [Online]. Available: http://www.cisco.com/en/US/prod/collateral/wireless/ps7183/ps469/prod_white_paper0900aecd806a1a3e.html.

[30] R. Mason, "Feasibility of Laser Power Transmission to a High-Altitude Unmanned Aerial Vehicle," RAND, 2011.

[31] A. Prokes, "Atmospheric Effects on Availability of Free Space Optics Systems," *Optical Engineering,* vol. 48, no. 6, 2009.

[32] S. Bergeson, "Gaussian Laser Beams," Brigham Young University, Provo, 2012.

[33] H. Breaux, W. Evers, R. Sepucha and C. Whitney, "Algebraic Model for CW Thermal-Blooming Effects," *Applied Optics,* vol. 18, no. 15, pp. 638-644.

[34] E. Friedman and J. L. Miller, Photonics Rules of Thumb: Optics, Electro-Optics, Fiber Optics, and Lasers, McGraw Hill Professional, 2003.

[35] J. K. Lawson and C. J. Carrano, "Using Historic Models of Cn2 to Predict R0 and Regimes Affected by Atmospheric Turbulence for Horizontal, Slant and Topological Paths," in *SPIE Optics & Photonics* , San Diego.

[36] W. R. Wilson, "SLODAR: measuring optical turbulence altitude with a Shack-Hartmann wavefront sensor," *Astronomical Insturmentation Group,* vol. 337, pp. 103-108, 2002.

[37] D. C. Smith, "High-power laser propagation: Thermal blooming," *IEEE,* vol. 65, no. 12, pp. 1679-1714, 1977.

[38] R. Z. Yahel, "Trubulence Effects on High Energy Laser Beam Propagation in the Atmosphere," *Tel Aviv: Open University of Israel,* vol. 29, no. 21, 1990.

[39] M. K. Masten, "Inertially Stabilized Platforms for Optical Imaging Systems," *IEEE Control Systems Magazine,* vol. 28, no. 1, pp. 47-64, 2008.

[40] R. Sabatini and M. A. Richardson, "Laser System Performance," *Airborne Laser Systems Testing and Analysis,* vol. 29, 2010.

[41] D. G. Brewer, "Hydrogen Aircraft Technology," CRC, Boca Raton, 1991.

[42] M. Marcel, "DRS-TEM On-Board Vehicle Power System," DRS Technologies, Huntsville.

[43] J. J. Guglielmo and M. S. Selig, "Spanwise Variations in Profile Drag for Airfoils at Low Reynolds Numbers," *Journal of Aircraft,* vol. 33, no. 4, pp. 669-707, 1996.

[44] M. Sadraey, Aircraft Performance Analysis, VDM Verlag.

[45] M. S. Selig and J. J. Guglielmo, "High-Lift Low Reynolds Number Airfoil Design," *Journal of Aircraft,* vol. 34, no. 1, 1997.

A: UAV Data

Engine Type	Launch Weight(lb)	Payload weight (lb)	Body Diameter	Wing Span	Length (ft)	Mission	
1 x UAV Engines Ltd. AR 741 rotary	337	56	0.9	12.8	11.2	Multimission	**Shadow 200 (RQ-7A)**
1 x UAV Engines Ltd. AR 741 rotary	450	75	1.4	16.9	12.5	Multimission	**Shadow 400**
1 x UAV Engine Ltd. AR 801 rotary	585	91	1.4	22.4	13.5	Multimission	**Shadow 600**
1 x AT-1700 tj.	150	50	0.8	4.8	8	Multimission	**ALAMM**
1 x diesel rotary	40		0.4	4.7	3	Recon./surveillance	**GLOV**
1 x TTL-WAE 342	276	1000	2.3	17.1	10.2	Multimission	**Vulture**
1 x Aerosonde H-Type, 1.2 kw.	30	10	0.6 x 0.75	9.5	5.6		**Aerosonde**
1 x 4W d.c. electric	0.2	0.015	—	0.5	0.5	Micro-AV demonstrator	**Black Widow**
14 x Aerovironment, brushless	1,801	600	—	206	12	High alt.	**Centurion**
2 x 200W d.c. electric	5.8	1	0.3	4	3	Recon./surveillance	**Dragon Eye**
14 x Aerovironment, brushless	1,669	730	—	247	12	High alt., long-endur.	**Helios**
1 x Akkerman eng. recip.	770		—	50	19	High alt., long-end. recon.	**HILINE**
1 x 10W d.c. electric	0.3	0.033	—	1.3	0.8	Micro-AV demonstrator	**Hornet**
8 x Aerovironment electric	700	25	—	120	12	High alt., long-end. recon.	**Pathfinder Plus**
1 x 300W d.c. electric	8	2	0.4	9	6	Multipurpose/recon.	**Pointer FQM-151A**
1 x 600W d.c. electric	11	2.2	0.4	9	6	Multipurpose/recon.	**Puma**
1 x 200W d.c. electric	4.5	0.4	0.3	4.4	3	Recon./surveillance	**Raven**
Ballistic launch/glide or electric	1		0.2	1.5	1	Recon./targeting	**SOAR**
1 x 10W d.c. electric	0.4	0.03	—	1.2	0.7	Micro-AV demonstrator	**Wasp**
1 x TTL WAE 342-30A	242.5		1.2	11.2	10.6	—	**Mart Mk. 2**
1 x Alvis 731	317		1.4	11.2	9.9	Surveillance, EW	**S-Mart**
2 x Con. IO360	5,000	700	3.6 x 5.5	38	31.5	Marine/atmospheric science	**Chiron**
1 x 3W d.c electric	16	2.2	1.5	5	2.25	Multipurpose	**Golden Eye 50**
1 x UAV Engines Ltd. AR 741 rotary	150	22	3	10	5.5	Multipurpose	**Golden Eye 100**
1xArion2B	2,400	260	2.6 x 2.4	71.5	25	Atmospheric science	**Perseus B**

	Production	Altitude(ft)	Range (mi)	Endurance	Speed (MPH or NO)	Type	Manufacture
Theseus	In production for US Army.	16,500		6hr.	131	EO/IR-SAR	—
Skyeye R4E	In production.	12,000		5hr.	131	EO/IR-SAR	—
BQM-147A Dragon Drone/Exdrone	In production.	17,000		14hr.	138	EO/IR-SAR	—
Dragon Eye/Snake Eye/Evolution	In development.	40,000	1000	2 hr.	M 0.95	EW, munition	Accurate Automation
Isis	Entering production. Three prototypes tested.	20,000	365	4 hr.	91	EO/IR	Accurate Automation
Javelin	In production for South African army.	16,400	125	3 hr.	100	Optronic day sight	M-Tek
Tern	Also for remote sensing, radio relay.	21,000	2000	30 hr.	50-80	Meteorological	Aerosonde
HV-911 Eagle Eye	Under development for DARPA.	800	2	30 min.	30-40	Color video	Aerovironment
Scythe	Under development for NASA ERAST.	100,000		16hr.	M 0.2	Turbulence measuring	Aerovironment
Kestrel 2	Under development for US Marines.	1,000	3	0.8 hr.	40-50	EO/B&W lowlight	Various
Neptune	NASA ERAST. Earth science or telecommunications.	96,863	120	96 hr.	M 0.2	Weather monitoring	Aerovironment, JPL
Sentry	200 lb. payload, autonomous flight, highly mobile.	40,000		1-2 days	120 loiter	Autop.data link,nav.comp.	S-Tec, Tracor, AACOMS
Sentry HP		200	0.2	6 min.	15-20	Fuel cell	Lynntech
Eagle 1	NASA ERAST. Experimental science payloads.	80,201		16hr.	20	Environ. sensing	AACOMS
FOX AT	Procured by US forces. Cooperation with EADS.	12,500	5	2 hr.	25-50	EO/IR, Chem. sensing	Aerovironment, various
POINTER	Under development for US military.	12,500	15	4 hr.	25-60	EO/IR, Chem. sensing	Aerovironment, various
Hermes 180	Under development for US Army.	10,000	0.5	1 hr.	25-60	EO/IR	EO/IR
Hermes 450	Under development for US Army.	10,000	16	0.4 hr.	45	EO	EO
Hermes 1500	Under development for DARPA.	300	0.2	107 min.	25-30	—	—
Mini-V	In production.	9,850		4hr.	119	TV	Altec
Seagull	In development.	9,850		7hr.	119	TV, ECM, ESM	Altec or other
Skylark	Can be flown as UAV or manned.	20,000		10hr.	115	Scientific	Various
Aladin	Maritime law enforcement, homeland security.	5,000		45 min.	115	EO, Chem. sensing	Various
Luna	Intelligence, surveillance, recon. payload.	10,000		4hr.	184	Imaging	Various
Falco	Flown to 60,000 ft., June, 1998.	65,000		24hr.	60-220	Atmospheric sampling	Various

Type	Manufacture	Engine Type	Launch Weight(lb)	Payload weight (lb)	Body Diameter	Wing Span	Length (ft)	Mission
—	Various	1 x ASE TPE331	7,800	4500	3.5	117	29	Multipurpose
EO/IR, EW, IRLS	Various	1 x UAV Engines Ltd. 52 hp. rotary	1,250	175	—	24	13.4	Multipurpose
Various	BAI, various	1 x 100 cc, 2-stroke or heavy fuel	100	25	0.75	8	6	Multipurpose/recon.
TV,IR	BAI, Indigo	2 x Aveox electric	6.5	1.125	0.25	4	2	Multipurpose/recon.
Various	BAI, various	1 x UAE Engines Ltd. rotary, 38 hp.	350	34	2	24	14	Multipurpose/recon.
TV	BAI, various	1 x 2-stroke, 2 hp.	18	6	0.5	8	6	Recon.
Various	BAI, various	1 x 100 cc, 2-stroke	125	22	1	10	8	Multipurpose/recon.
Radar, EO/IR	Various	1 x PWC PW200	2,600	300	2.8	15.3	17.3	Multipurpose
—	Brandebury Tool	1 x 10 cc. heavyfuel or 2-stroke	17		0.4	6	5	Multipurpose/recon.
Flir/TV	—	—	264	65	—	16.4	13.1	Multipurpose
EO/IR/various	Various	1xLAE150,14hp.	116	20	4.8 x 2.3	7	6	Recon./surv./target
EO/IR/various	Various	1 x Herbrandson 290, 28 hp.	250	65	3.4 x 2.5	11	8	Recon./surv./target
EO/IR/various	Various	1 x Herbrandson 290, 28 hp.	325	75	4.4 x 4.5	12.8	8.4	Recon./surv./target
Various	EADS	1 x Rotax 914	2,700	550	—	49	28	Reconnaissance
CCD, IR	CAC Systemes/various	1 x Limbach 22 hp. recip.	1250	25	1.5	12	9.1	Recon./surv./target
CCD/IR/various	CAC/Aerovironment/various	Electric	8	2	0.5	9	6	Recon./surv./target
EO, various	Various	1x UEL AR-74-1000 38 hp. rotary	430	70	1.7	19.7	14.5	ISTAR
EO, SAR	Various	1x UEL AR-80-1010 52 hp. rotary	990	330	1.7	34.5	20	Multipurpose
EO, SAR	Various	2 x Rotax 914, 100 hp. (ea.), rotary	3,640	880	2.4x3	49.2	30.8	Recon./surv./target
EO	Various	2 x 5.5 hp., 2-stroke	110	100	0.7 x 0.7	12	9	Recon./surveillance
—	Various	Electric	12	2.5	—	7	—	Recon./surveillance
—	Various	Electric	12	2.5	—	7	—	Recon./surveillance
EO/IR	Various	Electric	7	0.66	—	5	5	Recon./surv./target
EO, IO, SAR	Various	1x8hp.	66	12	—	13.9	7.4	Recon./surv./target
EO/IR/SAR	—	1x75hp.	1,122	155	1.9	23.7	18	Multipurpose

Wing Span	Length (ft)	Mission		Production	Altitude(ft)	Range (mi)	Endurance	Speed (MPH or NO)
15.5	12.4	Surv./target/acq.	**Mirach 26**	In development.	65,000	6000	24 hr.	60-290
12	10.5	Recon./surveillance	**Raven**	Procured by US Army and others. In production.	15,000	238	8-12 hr.	125
9.8	6.8	Multipurpose	**Scorpion 60**	Several hundred produced since 1985.	5,000	30	2.5 hr.	80
14.8	17.4	Surveillance	**FFOS**	In production.	500		1 hr./5 mi.	45
86	36	High alt. research	**Altair**	Production-ready.	15,000	2000	24 hr.	120
55.3	23.6	High alt. research	**Altus 1**	Production-ready.	3,000	5	2.5 hr.	55
55.3	23.6	High alt. research	**Altus 2**	In production.	10,000	30	4 hr.	75
35	18	Recon./surveillance	**GNAT 750**	Tiltrotor.	20,000	127	6 hr.	253
42.2	20.8	Recon./surveillance	**IGNAT**	Airframe in production; payload in development.	12,000	1000	12 hr.	100
48.7	27	Recon./surv./target	**Predator (MQ-1)**	—	12,000		8hr.	80-115
66	36	Recon./surv./target	**Predator B (MQ-9)**	Maritime vehicle. Pneumatic launch; skid or chute recovery.	8,000	40	3hr.	98
24	14	Tactical surveillance	**Prowler 2**	Pneumatic or wheeled launch. Skid or wheeled recovery.	10,000	62	6hr.	110
4	10	Recon./surveillance	**Seascan**	Pneumatic or wheeled launch. Wheeled recovery.	10,000	62	5hr.	139
16	11	Recon., research	**LEARS 4**	Under development. Operational in 2003.	30,000	2050	39 hr.	120
50.5	24.7	Multipurpose	**E-Hunter**	In service.	10,000		3hr.	60-120
54.5	28.2	Multipurpose	**Heron**	In service. Joint with Aerovironment.	3,000		1hr.	20-40
75.5	39.4	Multipurpose	**Heron TP**	Runway/catapult launch, runway/parachute/airbag, recovery.	15,000	95	10 hr.	70-105
29.2	22.6	Recon./surv./target acq.	**Hunter**	Operational.	18,000	125	20 hr.	70-95
18.7	15.1	Recon./surv./target acq.	**Ranger**	Multi-payload UAV.	30,000	125	26 hr.	80-130
28.1	19.2	Recon./surv./target acq.	**Searcher Mk. 2**	Catapult launch, parachute, recovery.	12,000	30	5 hr.	60-85
—	17.4	Multipurpose	**Ka-137**	Expendable, air-launched mini UAV.	—		—	20-40
10.7	8.9	Surveillance, EW	**Spectre 2**	Hand, bungee-launched mini UAV.	—		—	20-40
10.9	11.9	Target/surveillance	**Voodoo**	In service.	12,000	3	45 min.	—
4	3.3	Recon./surveillance	**Buster**	In service.	10,000	50	2 hr.	37-75
11	10	Multimission	**Hellfox**	Radio-controlled and autonomous navigation. In flight trials.	21,000		14hr.	130

Altitude(ft)	Range (mi)	Endurance	Speed (MPH or NO)	Type	Manufacture	Engine Type	Launch Weight(lb)	Payload weight (lb)	Body Diameter
13,000		5hr.	140	TV, LLTV, Flir, Elint	Various	1x28hp.	440	110	1.2
15,000	60	3 hr.	75 (cruise)	TV, Flir	Various	1 x Aerrow Quadra 200 cc	185	40	—
5,000		2hr.	125	Various 25 lb.	—	1 x 12 hp. recip.	83	25	1
—		3hr.	84	—	Fuji	1xMG6	606		3.9
52,000		32hr.	220	Scientific	Various	1 x Honeywell TPE331-10	7,500	660	3.7
45,000		40hr.+	115	Scientific	Various	1 x Rotax turbo, gasoline	1,800		2.5
65,000		40hr.+	115	Scientific	Various	1 x Rotax twin turbo, gasoline	1,800	330	2.5
20,000		40hr.	100	Day TV or Flir	Wescam	1 x Rotax 582	1,130	140	2.5
25,000		40hr.+	140	EO/IR or SAR	Various	1 x Rotax 914 turbo, gasoline	1,400	450	3.7
25,000		40hr.+	140	EO/IR, SAR, weapons	Various	1 x Rotax 914 turbo, gasoline	2,250	450	3.7
50,000		28hr.	220	EO/IR, SAR, weapons	Various	1 x Honeywell TPE331-10	10,500	800	3.7
18,000		14hr.	115	EO/IR	Wescam	1 x Rotax 582 (heavy fuel options)	800		2.4
16,000	1100	15 hr.	78	TV	Hood Tech	1 x 3W d.c. electric	40	2.2	0.7
14,000	700	14 hr.	100	Various	Various	1 x 70 cc, recip.	120		1
20,000	175	25 hr.	122	TV, IR, custom	IAI Tamam	2x64hp.Dual	2,100		—
30,000	620	50 hr.	138	TV, IR, custom	IAI Tamam	1x100hp.	2,420	550	2.8
45,000	620	24 hr.	242	TV, IR, custom	IAI Tamam, various	1 x 1,200 hp. turboprop	7,720	2200	—
15,000	175	12 hr.	127	TV,IR	IAI Tamam	2x64hp.Dual	1,600	250	—
15,000	62	5 hr.	137	TV,IR	IAI Tamam	1 x 40 hp. recip.	550	100	—
18,500	155	16 hr.	124	TV, Flir	IAI Tamam	1 x 73 hp. rotary	939	265	—
16,400		4hr.	95	Various	Various	1 x Hirth 2706 P05, 65 hp.	615	390	3.9
23,000		3-6hr.	77-150	IR camera, EW	Meggitt	1xMDS342cc	350	80	1.5
20,000		1.5hr.	90-350	EO/IR countermeasures	Meggitt	1xMDS955cc	440		1.6
10,000		4hr.	35-80	EO/IR	DRS	1 x 1.6 hp. recip.	10	3	—
18,000		8hr.	60-120	CCD camera, Flir, SAR	Various	1 x 38 hp. recip.	350	70	—

Launch Weight(lb)	Payload weight (lb)	Body Diameter	Wing Span	Length (ft)	Mission		Production
105	25	—	7.1	6.6	Multimission/surveillance	**Mini-Vanguard**	In service. Booster launch, parachute recovery (Italian army).
25,600	2000	4.8	116.2	44.4	Recon.	**Global Hawk (RQ-4A)**	Catapult launch, parachute recovery.
488.4	110	—	19.7	12.5	Recon./surveillance	**ASN-206**	Thrust vectoring. No launcher or parachute.
1000	440	1.2	16.8	13.9	Recon./surv./target	**RQ-2B Pioneer**	Rotary-winged vehicle.
605	100	—	18.7	15.1	Recon./surv./target	**Ranger**	First flight 2003.
265	80	—	10.8	9.02	Recon./surv./target	**Crecerelle**	—
265		—	10.8	9.02	Comm. jamming	**Crecerelle-EW**	Customer: NASA.
770	220	—	21	11.05	Recon./multipurpose	**Sperwer-EC/LE**	Exported to Turkey.
660	100	—	14.2	11.5	Recon./target	**Sperwer/Ugglan**	In production.
12,500	3000	3.75	95	58	Recon./scientific	**Proteus**	In production for US Air Force.
355	80	1.2	11.2	7.4	Recon./surv./target	**KZO**	In production for US Air Force.
419		1.2	11.9	8	EW	**Tucan/Mucke**	First flight June, 1998.
304		1	10.7	9.1	Recon.	**Pchela 1**	—
216		1	7.8	8.8	Recon./EW	**Yak-060**	GPS autopilot. 60-lb. payload.
							Runway t.o./landing. Upgrade kit to Hunter.
							Demonstrator.
							—
							In production. US Army, French army operation.
							—
							In production. In use in Israel.
							R/c helo. Programmable. In development.
							In service in France as Crecerelle.
							High speed, sea-skimming capability.
							Launch from elastic-powered rail.
							Short takeoff and landing.

Altitude(ft)	Range (mi)	Endurance	Speed (MPH or NO)	Type	Manufacture	Engine Type
15,000		4hr.	50-110	EO/IR, CCD camera	Various	1 x 17 hp. recip.
65,000	16566	42 hr.	454	SAR/MTI, EO, IR	Northrop Grumman	1 x RR AE3007H tf.
—	80	4-8 hr.	113	—	—	1 x HS-700, recip.
15,000	115	5.5 hr.	115	IR&TV	IAI-Tamam, Wescam	1 x Sachs SF-350
18,000	97	8 hr.	60-130	EO	IAI/Taman	1 x Goebler-Hirth 42 hp., 2-stroke
15,000		5hr.	155	Flir	SAGEM	1 x recip. engine
15,000		3.5hr.	155	EW	Thales	1 x rotary engine
20,000	125	12 hr.	95	Day TV, Flir, SAR, Airborne relay	SAGEM	1 x 70 hp., 2-stroke
17,000	125	6 hr.	130	Day TV, Flir, EW, SAR	SAGEM	1 x 70 hp., 2-stroke
63,500	18 hr./500 mi., 6 hr./3,000 mi.		M 0.4	Various	Various	2 x Williams-Rolls FJ44-2E tf.
13,000		3.5 hr. +	95	Flir	STN Atlas	1 x 30 hp. recip.
13,000		5hr.	95	Jammer	EADS	1 x 45 hp. recip.
8,200		8,202	97	TV	—	1 x Kuznetsov, 32 hp.
8,200		8,202	76	TV or EW jammer	—	1 x Kuznetsov, 20 hp.

Production
For Swedish forces.
In production.
Made by Xian ASN Technology Group.
Joint AAI/IAI project. In service with US Marines.
Operational with Finnish and Swiss forces.
Real-time video downlink. Deployed w/French army.
EW version is for comm. jamming.
In production. In development for recon./target and radar jamming.
In production for Dutch, Swedish (UGGLAN), Danish, French and Greek armies.
Piloted version. UAV systems testbed.
In production for German army.
Based on KZO.
Entered service in 1997 as part of Stroy-PM system.
Limited production in 1982 as part of Stroy-PM system.

B: Plots of Electric and Combustion Systems

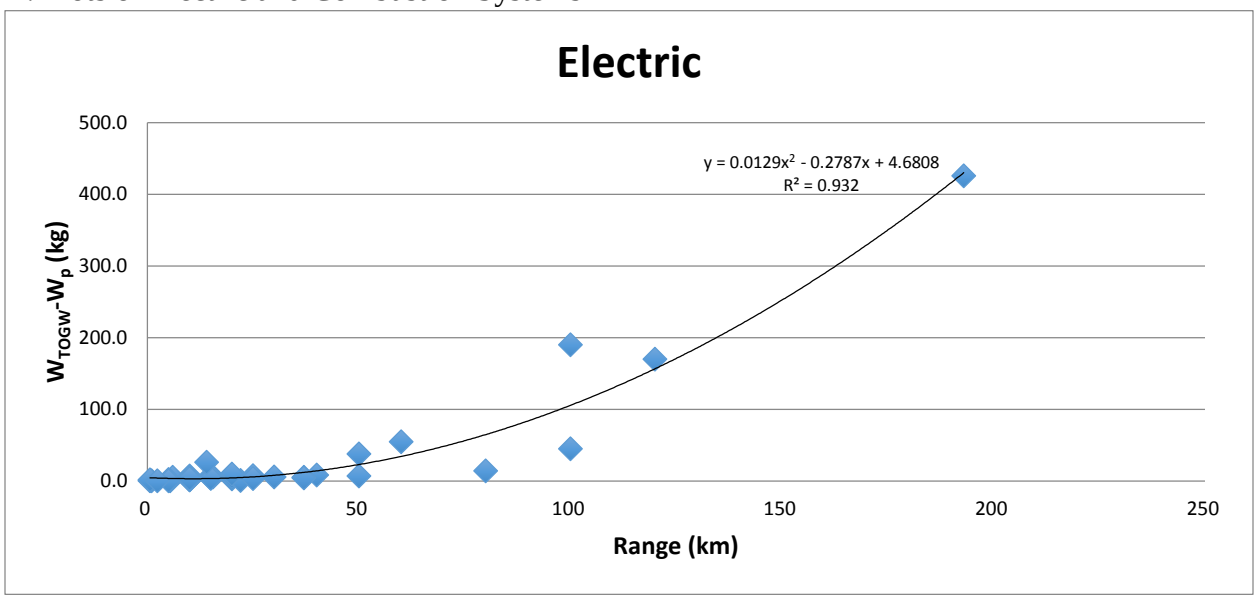

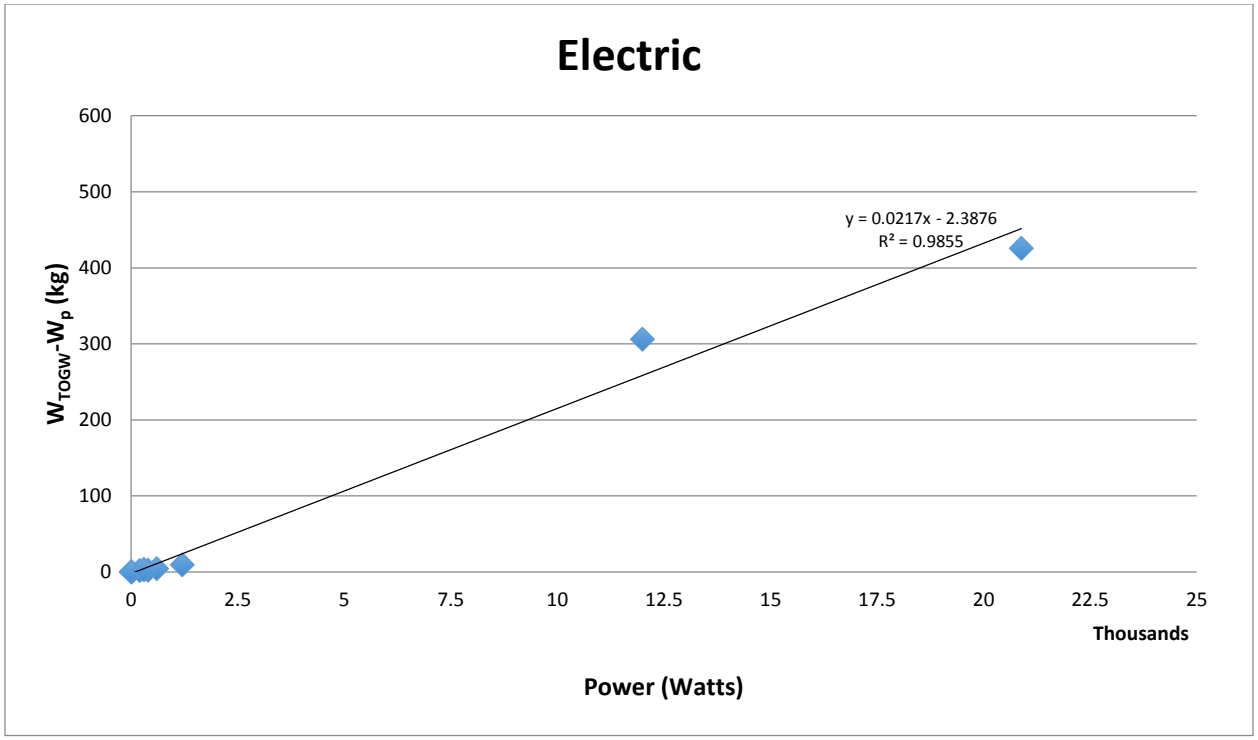

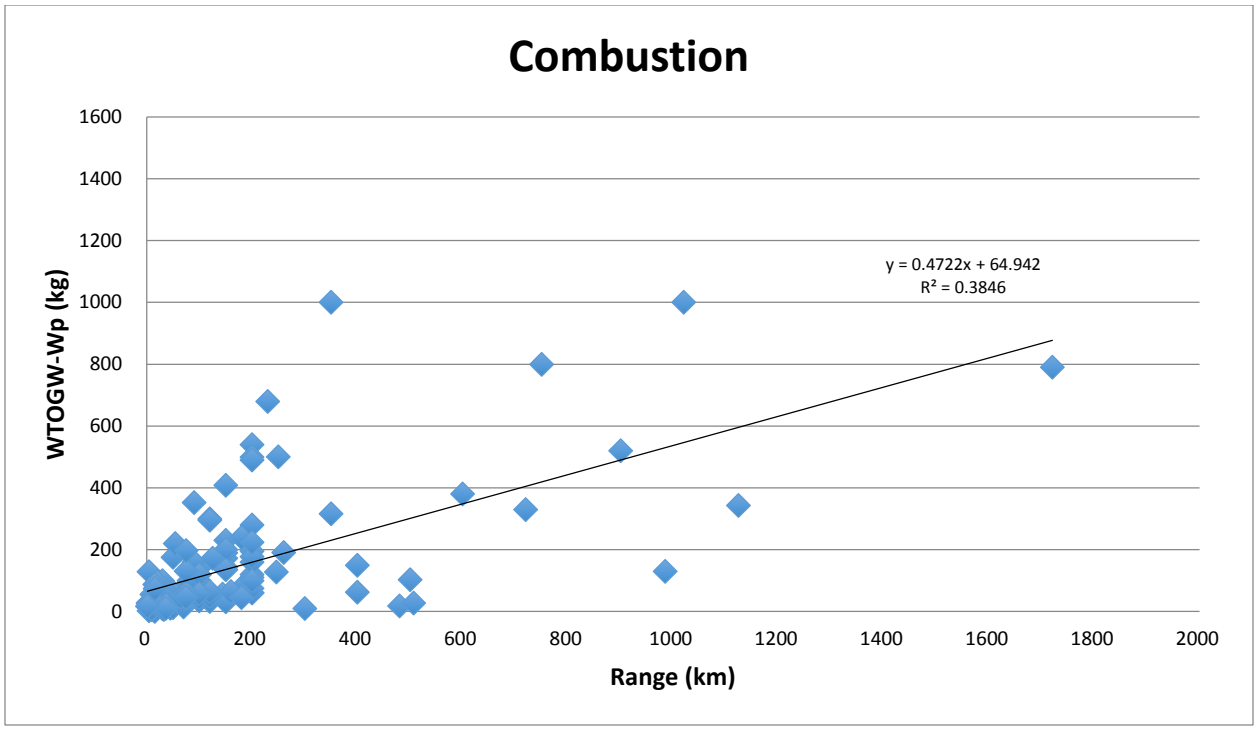
Combustion
y = 0.4722x + 64.942
R² = 0.3846
WTOGW-Wp (kg)
Range (km)
0
200
400
600
800
1000
1200
1400
1600
1800
2000

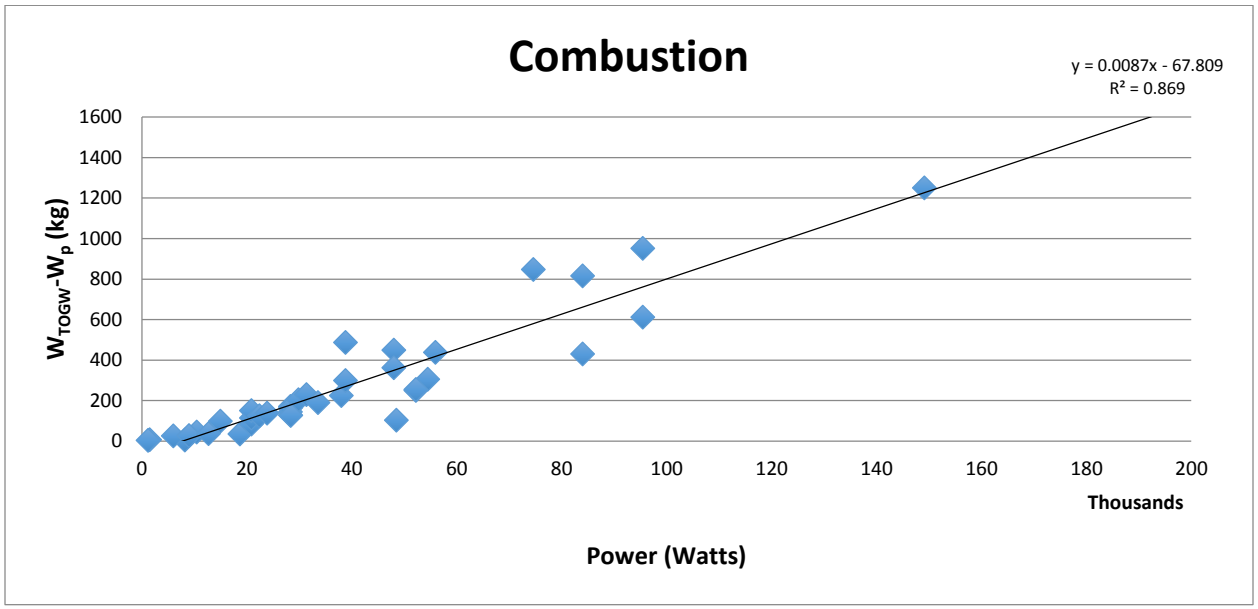
Combustion
y = 0.0087x - 67.809
R² = 0.869
W_TOGW-W_p (kg)
Power (Watts)
Thousands
0
20
40
60
80
100
120
140
160
180
200